THEORETICAL STUDIES ON THREE MEMBERED RINGS AND ORGANOMETALLIC COMPLEXES

A Thesis

Submitted for the Degree of

DOCTOR OF PHILOSOPHY

By

Pattiyil Parameswaran

School of Chemistry

University of Hyderabad

Hyderabad 500 046

INDIA

August 2006

Dedicated to My Parents

CONTENTS

Statement		ix
Certificate		xi
Acknowledgements		xiii
CHAPTER 1: Introduction to Computational Chemistry and Outline of the Thesis		**1**
[1.1]	Introduction	3
[1.2]	Electronic Structure Methods	4
[1.2.1]	*Ab initio* Methods	4
i.	The Born-Oppenheimer Approximation	5
ii.	Variation Theorem	6
iii.	The LCAO-MO Approximation	7
iv.	The Hartree-Fock Self Consistent Field Method	9
v.	Basis Functions	12
[1.2.2]	Electron Correlation	14
i.	Configuration Interaction	15
ii.	Møller-Plesset Perturbation Theory	15
[1.2.3]	Semiempirical Methods	16
i.	Extended Hückel Method	17
[1.2.4]	Density Functional Theory	19
i.	Local Density Approximation	21
ii.	Local Spin Density Approximation	22
iii.	Generalized Gradient Approximation	22
[1.3]	Outline of the Thesis	24
[1.3.1]	Structure and Bonding in Cyclic Isomers of $BAl_2H_n^m$ (n = 3 - 6, m = -2 - +1): Preference for Planar Tetra-coordination, Pyramidal Tri-coordination and Divalency	24
[1.3.2]	The Effect of Metal Complexation on Ring Opening of Bowl Shaped Hydrocarbons: A Theoretical Study	26

[1.3.3] Binuclear Organometallic Compounds Containing Planar Tetra-coordinated Carbon Atoms: Theoretical Study on Geometrical and Bonding Patterns 27

[1.3.4] Theoretical Study on the Insertion of Heteroallenes (CO_2, COS and CS_2) to Metal-metal Polar Bond of Early-late Bimetallic Complexes 29

[1.4] References 31

CHAPTER 2: Structure and Bonding in Cyclic Isomers of $BAl_2H_n^m$ (n = 3 - 6, m = -2 - +1): Preference for Planar Tetra-coordination, Pyramidal Tri-coordination and Divalency **35**

[2.0] Abstract 37

[2.1] Introduction 38

[2.2] Computational Details 40

[2.3] Results and Discussion 41

[2.3.1] Structure and Bonding in the Isomers of $BAl_2H_3^{2-}$ 42

[2.3.2] Protonation Pathways of $BAl_2H_3^{2-}$ to $BAl_2H_4^-$, BAl_2H_5 and BAl_2H_6 50

[2.4] Conclusions 67

[2.5] References 68

CHAPTER 3: The Effect of Metal Complexation on Ring Opening of Bowl Shaped Hydrocarbons: A Theoretical Study **75**

[3.0] Abstract 77

[3.1] Introduction 78

[3.2] Computational Details 81

[3.3] Results and Discussion 84

[3.3.1] Complexation of Metal Fragments (CrC_6H_6, MnC_5H_5, FeC_4H_4, CoC_3H_3 and RhC_3H_3) on Benzene and Tris-acetylenes 85

[3.3.2] Benzenoid and Tris–acetylenic Model Metal Complexes (FeC_4H_4, CoC_3H_3) of Fullerene and Its Fragments (C_{60}, $C_{36}H_{12}$, $C_{21}H_9$, $C_{12}H_6$ and $C_{12}H_{12}$) 86

[3.3.3] Relative Stability of Benzene and Tris–acetylenic Model Metal Complexes 89

[3.4] Conclusions 91

[3.5] References 92

CHAPTER 4: Binuclear Organometallic Compounds Containing Planar Tetra-coordinated Carbon Atoms: Theoretical Study on Geometrical and Bonding Patterns **95**

[4.0] Abstract 97

[4.1] Introduction 98

[4.2] Computational Details 100

[4.3] Results and Discussion 100

[4.3.1] Metal-acetylene Complexes 101

[4.3.2] Metallacyclocumulenic Complexes 102

[4.3.3] Organobimetallic Compounds Containing Planar Tetra-coordinated Carbon Atoms 105

[4.4] Conclusions 109

[4.5] References 111

CHAPTER 5: Theoretical Study on the Insertion of Heteroallenes (CO_2, COS and CS_2) to Metal-metal Polar Bond of Early-late Bimetallic Complexes **115**

[5.0] Abstract 117

[5.1] Introduction 118

[5.2] Computational Details 120

[5.3] Results and Discussion 121

[5.3.1] Bimetallic Complexes (**9p**) and Heteroallenes (XCY) 122

[5.3.2] Bimetallic Complexes (**10pq**) 125

[5.3.3] Bimetallic Complexes (**12pq**) 129

[5.3.4] Transition States (**11pq**) 133

[5.4] Conclusions 136

[5.5] References 137

List of Publications 143

STATEMENT

I do hereby declare that the work embodied in this thesis is the result of investigations carried out by me in the **School of Chemistry, University of Hyderabad, Hyderabad, India,** under the supervision of **Prof. Eluvathingal D. Jemmis**.

In keeping with the general practice of reporting scientific observations, due acknowledgements have been made whenever the work described is based on the findings of other investigators.

P. Parameswaran

CERTIFICATE

Certified that the work embodied in the thesis entitled "**Theoretical Studies on Three Membered Rings and Organometallic Complexes"** has been carried out by **Mr. Pattiyil Parameswaran** under my supervision and the same has not been submitted elsewhere for any degree.

Eluvathingal D. Jemmis
Thesis Supervisor

M. Durga Prasad
Co-supervisor

Dean
School of Chemistry

ACKNOWLEDGEMENTS

It is a pleasant aspect that I have now the opportunity to express my gratitude for all who have been accompanied and supported me throughout the course of my doctoral research carrier. First of all, I wish to express my sincere gratitude to Prof. E. D. Jemmis for having introduced me to the interesting area of computational chemistry. This work would not be possible without his patient guidance, encouragement and excellent advice. I am grateful to him for his kindness, concern and care extended to me, both academically and personally.

Next, I would like to thank my co-supervisor Prof. M. Durga Prasad for his valuable support. I also owe a huge debt of gratitude to Prof. M. A. Anto because of whom I am here today.

I avail this opportunity to thank our collaborator, Prof. Uwe Rosenthal. I thank CSIR, New Delhi and BRNS, Mumbai for the financial assistance. Computational facilities of the Centre for Modeling Simulation and Design (CMSD), University of Hyderabad and Supercomputer Education and Research Centre (SERC), Indian Institute of Science are greatly acknowledged.

I express my sincere thanks to Dean and all the faculty members of the School of Chemistry, University of Hyderabad and Department of Inorganic and Physical Chemistry, Indian Institute of Science. Special thanks to Prof. K. L. Sebastian.

My sincere thanks to all the non-teaching staffs in the School of Chemistry as well as Department of Inorganic and Physical Chemistry for providing their valuable services at the appropriate time.

I would like to thank all my lab mates, both past and present, for their help at one point or another. The critical assessment of each chapter by Shameema, Susmita and Usha helped me to rectify many errors in this thesis.

I thank all my friends at School of Chemistry and NRS hostel especially Pradeep, Varghese, Rajesh, Jayasree, Panchu, Bishu and Anoop who made my stay most memorable in Hyderabad. The help from Debojyoti and Rakhi in the initial days at Indian Institute of Science are appreciable. I also thank my friends from IPC. I would like to thank Neenu, Pradeep, Anshita, Paromita, Thomas and Shijo, making my stay more comfortable and enjoyable in the IISc campus.

Finally, I take this opportunity to express my profound gratitude to my beloved parents, brothers and sister for their love, encouragement and moral support.

Parameswaran

CHAPTER 1

INTRODUCTION TO COMPUTATIONAL CHEMISTRY AND OUTLINE OF THE THESIS

[1.1] Introduction

Computational chemistry has evolved as a supplement to experiments in studying problems in chemistry and can generate information which complements the experimental data on the structures, properties and reactions of substances. The tremendous progress in the development of faster computer chips and the availability of various computational chemistry software have made it possible to carry out the computations on reasonably large size molecules to obtain accurate and reliable information in a relatively short time. There are different areas in computational chemistry, depending on the formalism of the theory employed. The basis of the computational methodology used in the thesis is quantum mechanics.[1] Main approaches in computational qunatum chemistry are (a) *Ab initio* methods (b) Semiempirical methods and (c) Density functional methods. Brief descriptions of these three electronic structure methods used to compute the chemical properties described in this thesis are given in the following sections. This is followed by an overview of the remaining chapters.

[1.2] Electronic Structure Methods[1,2]

Electronic structure methods are based upon the basic laws of quantum mechanics and employ a variety of mathematical techniques to solve the fundamental equations. *Ab initio* (from the beginning) methods do not use any experimental parameters other than the fundamental constants such as mass and charges of electron and nuclei, the Planck's constant and the speed of light. Semiempirical methods on the other hand simplify the computation either by approximating the different integrals using parameters derived from the experimental data of atoms and molecules or by neglecting some of them. In contrast to these wave function based methods, density functional methods calculate the molecular electron probability density ρ and subsequently the molecular electronic energy from the density.

[1.2.1] *Ab initio* Methods

The time independent Schrödinger equation used to solve the chemical problems in this thesis which can be expressed in its succinct form,

$$\mathrm{H}\Psi = \mathrm{E}\Psi \tag{1.1}$$

where, H is Hamiltonian operator, which is the sum of the kinetic and potential energy operators, E is the total energy and Ψ is the exact wave function which define the system. The Hamiltonian for any molecule having M nuclei and N electrons, assuming the nuclei and electrons to be point masses is

$$\mathrm{H} = -\frac{\hbar^2}{2}\sum_{\alpha}^{M}\frac{1}{m_\alpha}\nabla_\alpha^2 - \frac{\hbar^2}{2m_e}\sum_{i}^{N}\nabla_i^2 - \sum_{\alpha}^{M}\sum_{i}^{N}\frac{Z_\alpha e^2}{r_{i\alpha}} + \sum_{\alpha}^{M}\sum_{\beta>\alpha}^{M}\frac{Z_\alpha Z_\beta e^2}{r_{\alpha\beta}} + \sum_{j}^{N}\sum_{i>j}^{N}\frac{e^2}{r_{ij}} \tag{1.2}$$

where, α and β refer to the nuclei and i and j to the electrons. Here, m is the mass of the particle, e is the electronic charge, Z is the atomic number and r is the distance between the particles. The first and second terms are the nuclear and electronic kinetic energy operators. The third, fourth and fifth terms represent the potential energy for the nuclear-electron attraction, nuclear-nuclear repulsion and electron-electron repulsion respectively.

Ab initio molecular orbital methods are the most accurate and consistent because they provide the best mathematical approximation to the actual system. Even though *ab initio* methods are computationally quite expensive as compared to the semiempirical methods, the results obtained from the *ab initio* calculations are highly reliable. The limitations of *ab initio* calculations are in the approximation in defining Hamiltonian and using a finite wave function in solving the Schrödinger equation. The following approximations are used for solving the Schrödinger equation.

(i) The Born-Oppenheimer Approximation[3]

The Born-Oppenheimer approximation is the assumption that the electronic motion and the nuclear motion in molecules are independent of each other which can be separated.

As the nuclei are much heavier than the electrons, $m_\alpha >> m_e$, the electrons move much faster than the nuclei. To a good approximation, one can consider the nuclei as fixed during the electronic motion. Thus, the nuclear kinetic energy term can be omitted from the Hamiltonian and the Schrödinger equation 1.1. will take the form of

$$(H_{el} + V_{NN})\Psi_{el} = (E_{el} + V_{NN})\Psi_{el} \tag{1.3}$$

where the purely electronic Hamiltonian,

$$H_{el} = -\frac{\hbar^2}{2m_e}\sum_i^N \nabla_i^2 - \sum_\alpha^M \sum_i^N \frac{Z_\alpha e^2}{r_{i\alpha}} + \sum_j^N \sum_{i>j}^N \frac{e^2}{r_{ij}} \tag{1.4}$$

and

$$V_{NN} = \sum_\alpha^M \sum_{\beta>\alpha}^M \frac{Z_\alpha Z_\beta e^2}{r_{\alpha\beta}} \tag{1.5}$$

The quantity V_{NN} is independent of the electronic coordinates and constant for a given nuclear configuration. Hence, Schrödinger equation for the electronic motion can be written as

$$H_{el}\Psi_{el} = E_{el}\Psi_{el} \tag{1.6}$$

The electronic energy, E_{el} depends parametrically on the nuclear coordinates and is related to the electronic energy including internuclear repulsion by

$$U = E_{el} + V_{NN} \tag{1.7}$$

This approximation of separating electronic motion from the nuclear motion is called the Born-Oppenheimer approximation. This approximation gets support from the spectral studies and it fails when nontrivial coupling of electronic and nuclear motion occurs in cases such as Jahn-Teller and Renner effects. Further approximations are required to get reliable information on the electronic structure for large molecules.

(ii) Variation Theorem

For dealing with time independent Schrödinger equation for systems such as atoms or molecules containing interacting particles, methods based on variation

principle give the approximate ground state energy without solving the exact Schrödinger equation.

For a given system with time independent Hamiltonian H and energy E, variation theorem states that energy calculated using a trial function is always greater than or equal to the exact ground state energy E_0.

$$E_\Psi = \frac{\int \Psi^* H \Psi d\tau}{\int \Psi^* \Psi d\tau} \geq E_0 \tag{1.8}$$

Ground state energy is obtained by minimizing E_Ψ with respect to parameters which define the trial function. For getting good approximate value of the ground state energy, E_0 many trial functions have to be tried and the lowest value of the variational integral gives the closest approximation to E_0.

(iii) The LCAO-MO Approximation

The Linear Combination of Atomic Orbital Molecular Orbital (LCAO-MO) is the most common trial function for calculating molecular orbitals in quantum chemistry. The trial function (Ψ) needed to solve the Schrödinger equation can be considered as a combination of atomic orbitals (ϕ) which form an orthonormal basis.

$$\Psi = \sum_{i=1}^{n} c_i \phi_i \tag{1.9}$$

Where, c_i is the coefficient of each atomic orbitals.

The energy calculated using this trial function is

$$E_{\Psi} = \frac{\int (\sum_{i}^{n} c_i \phi_i)^* H (\sum_{i}^{n} c_i \phi_i) d\tau}{\int (\sum_{i}^{n} c_i \phi_i)^* (\sum_{i}^{n} c_i \phi_i) d\tau} \geq E_0 \qquad (1.10)$$

Minimization of energy using the variation theorem leads to n linear and homogeneous equations known as Secular equations. The corresponding determinant is called Secular Determinant which can be written as

$$H_{ij} - ES_{ij} = \begin{vmatrix} H_{11} - ES_{11} & H_{12} - ES_{12} & \ldots & H_{1n} - ES_{1n} \\ H_{21} - ES_{21} & H_{22} - ES_{22} & \ldots & H_{2n} - ES_{2n} \\ \ldots & & & \\ H_{n1} - ES_{n1} & H_{n2} - ES_{n2} & \ldots & H_{nn} - ES_{nn} \end{vmatrix} = 0 \qquad (1.11)$$

Where, $$H_{ii} = \int \phi_i^* H \phi_i d\tau \qquad (1.12)$$

$$H_{ij} = \int \phi_i^* H \phi_j d\tau \qquad (1.13)$$

$$S_{ij} = \int \phi_i^* \phi_j d\tau \qquad (1.14)$$

The integrals H_{ii} and H_{ij} are called coulomb integral and bond (or resonance) integral respectively. The integral S_{ij} represents the extent to which the two functions ϕ_i and ϕ_j can interact each other and is called the overlap integral. The solution of this n^{th} order determinant will give n roots i.e., a set of n energy values, $E_1, E_2, E_3, \ldots, E_n$ and a set of n wave functions, $\Psi_1, \Psi_2, ..., \Psi_n$ for each molecule.

Antisymmetric nature of complete wave function Ψ leads to the following Slater Determinantal form of the wave function,

$$\Psi = \begin{vmatrix} \Psi_1(1) & \Psi_2(1) & \ldots & \Psi_n(1) \\ \Psi_1(2) & \Psi_2(2) & \ldots & \Psi_n(2) \\ \ldots & & & \\ \Psi_1(n) & \Psi_2(n) & \ldots & \Psi_n(n) \end{vmatrix} = 0 \qquad (1.15)$$

where, $\Psi_n(i)$ is the spin orbital of i^{th} particle.

Thus, by applying the LCAO-MO, one can generate several molecular orbitals for each molecule.

(iv) The Hartree-Fock Self Consistent Field Method[4]

The Hartree-Fock theory is a landmark in the development of quantum chemistry. It is useful to calculate an approximate wave function in case of many electron systems. The Hamiltonian for any molecule having M nuclei and N electrons (equation (1.4)), assuming the nuclei and electrons to be point masses is

$$\mathrm{H}_{el} = -\frac{\hbar^2}{2m_e}\sum_{i}^{N}\nabla_i^2 - \sum_{\alpha}^{M}\sum_{i}^{N}\frac{Z_\alpha e^2}{r_{i\alpha}} + \sum_{j}^{N}\sum_{i>j}^{N}\frac{e^2}{r_{ij}}$$

The inter-electronic repulsion terms make the Schrödinger equation non-separable. A zeroth order wave function can be obtained by neglecting these repulsions and the wave function thus obtained is a product of N one electron orbitals.

$$\Psi^{(0)} = f_1(r_1,\varphi_1,\theta_1)f_2(r_2,\varphi_2,\theta_2)...f_n(r_n,\varphi_n,\theta_n) \qquad (1.16)$$

The one electron orbital can be expressed as $f = \mathrm{R}_{nl}(r)\mathrm{Y}_l^m(\varphi,\theta)$ (1.17)

Where r,φ,θ are spherical polar coordinates; R_{nl} is radial part and Y_l^m is spherical harmonics of the electronic wave function.

Even though it is qualitatively advantageous to use the approximate wave function represented by the equation (1.15), the wave function is devoid of any quantitative accuracy. The accuracy of the wave function can be improved by considering different effective quantum numbers for different orbitals, which will

take care of the screening effect of electrons. In order to further improve the quality of the wave function, a variational function like ϕ is considered. This leads to the following trial function for variation.

$$\phi = g_1(r_1,\varphi_1,\theta_1)g_2(r_2,\varphi_2,\theta_2)...g_n(r_n,\varphi_n,\theta_n) \tag{1.18}$$

The wave function can be made more accurate by considering a function g_i that minimizes the variational integral,

$$\frac{\int \phi^* \mathrm{H} \phi d\tau}{\int \phi^* \phi d\tau}$$

and g_i is represented by a product of radial function and spherical harmonics

$$g_i = \mathrm{h_i}\left(r_i\right)\mathrm{Y}_{li}^{mi}\left(\varphi_i,\theta_i\right) \tag{1.19}$$

This is the basis of Hartree Self Consistent Field (SCF) method. Fock modified it and includes the antisymmetric function in the form of Slater determinants. Thus, the SCF calculation that uses antisymmetrized spin orbitals is called Hartree-Fock method. The differential equation for finding Hartree-Fock orbitals is

$$\mathrm{F}\mu_i = \varepsilon_i \mu_i \qquad i = 1,2,.....,n \tag{1.20}$$

μ_i is i^{th} spin-orbital. F is called Hartree-Fock operator and the eigen value ε_i is the energy of spin orbital.

$$\mathrm{F} = -\frac{1}{2}\nabla_i^2 - \sum_i^N \frac{Z_\alpha}{r_{i\alpha}} + \sum_i^{N/2}\sum_j^{N/2} 2J_{ij} - K_{ij} \tag{1.21}$$

$$= \mathrm{H}^{\text{core}} + \sum_i^{N/2}\sum_j^{N/2} 2J_{ij} - K_{ij} \tag{1.22}$$

The one electron core Hamiltonian,

$$\mathrm{H}^{\mathrm{core}} = \int \phi_i \left(-\frac{1}{2}\nabla_i^2 - \sum_i^N \frac{Z_\alpha}{r_{i\alpha}} \right) \phi_i^* d\tau \tag{1.23}$$

$$J_{ij} = \int \phi_i(1)\phi_j(2) \left(\frac{1}{r_{12}} \right) \phi_i^*(1)\phi_j^*(2) d\tau \tag{1.24}$$

$$K_{ij} = \int \phi_i(1)\phi_j(2) \left(\frac{1}{r_{12}} \right) \phi_i^*(2)\phi_j^*(1) d\tau \tag{1.25}$$

J_{ij} and K_{ij} are called Coulomb and Exchange integrals respectively. Both of these integral together give a measure of the energy of interaction of electron i with all the other electrons. The equation (1.20) is not linear and must be solved iteratively. The procedure which does so is called Hartree-Fock Self Consistent Field (SCF) method.

The interactions between the electrons are taken into account only an average way in HF wave function. If we consider instantaneous electron correlation into wave function, we can say that at a particular region near one electron, the probability of finding another electron will be small or large. This is known as electron correlation.

The correlation energy (E_{corr}) is given by,

$$\mathrm{E}_{corr} = \mathrm{E}_{nonrel} - \mathrm{E}_{HF} \tag{1.26}$$

E_{nonrel} is the exact non-relativistic energy and E_{HF} is HF energy.

From the set of occupied and virtual spin orbitals obtained from a HF calculation, several antisymmetric many electron functions having different occupancies can be formulated. These different open shell functions are called configuration state functions or configuration functions.

(v) Basis Functions

The HF orbitals can be represented as linear combinations of a set of functions called basis functions. The commonly used set of basis functions for HF calculations is the set of Slater Type Orbitals (STO).[5] The actual representation of many electron atomic orbitals requires a linear combination of several STOs.

For performing any quantum mechanical calculation according to any method, a set of basis function χ_r is used to express the orbitals ϕ_i as

$$\phi_i = \sum_r^n C_{ri}\chi_r \tag{1.27}$$

When, the χ_r are STOs[5], the molecular orbitals are called Linear Combination of Slater Type Orbitals (LCSTO) MOs.

The atomic orbitals (AO) can be always represented by Slater type functions which have exponential radial parts. Thus, a STO with principal quantum number n,

$$\chi(r,\varphi,\theta) \propto r^{n-1}e^{(-\xi r)}\mathrm{Y}_m^l(\varphi,\theta) \tag{1.28}$$

where, ξ is the orbital exponent. $\mathrm{Y}_m^l(\varphi,\theta)$ contains all the angular information needed to describe the wave function (spherical harmonics). STOs can be used as basis functions for more accurate solutions for small atoms and linear molecules. The many-centre two-electron integrals involving STOs are rather difficult to evaluate, require numerical integration techniques and are very time consuming. This problem can be overcome to some extent by the use of Gaussian type functions to the MO computations as introduced by Boys.[6] It has the important advantage that all integrals in the computation can be evaluated explicitly without recourse to

numerical integration and has proved extremely useful in *ab initio* calculations of polyatomic molecules. The Cartesian Gaussian Type Orbital (GTO) has the form:

$$\chi(x,y,z) \propto x^l y^m z^n e^{(-\alpha r^2)} \tag{1.29}$$

where, l, m and n are positive integers or zero and α is the orbital exponent. The main disadvantage of the Gaussian function is that it does not resemble very closely the form of real atomic orbitals. In particular, the Gaussian function lacks a cusp at the nucleus and hence the region near the nucleus is described rather poorly. In practice, the functional behavior of an STO is simulated by a number of GTOs with different orbital exponents. These GTOs are then referred as primitives and the resulting STO as the contracted Gaussians functions. There are different types of basis sets which are commonly employed. The basis set which consists of one STO for each inner shell and each valence shell AO of each atom is called a minimal basis set. A double zeta (DZ) basis set contains two STOs that differ in the orbital exponent for each AO. Similarly, triple zeta (TZ) basis set uses three STOs for construction of basis set. Since only valence orbitals are involved in chemical bonding, the efficiency can be enhanced without excessive computing time by doubling only the valence orbitals. This results in split valence basis. The basis sets which add basis function STO's whose angular quantum number is greater than the maximum angular quantum number of the valence shell of the ground state atom is called polarized basis set. For anions, compounds with lone pairs and H-bonded dimers where electron density has a significant value at a large distance from nuclei, highly diffuse function with very small orbital exponent are used for better agreement with experiment.

Computations involving heavier atoms are relatively difficult than those involving first and second row atoms of the periodic table. This is related to the increasing number of two electron integrals to be evaluated and the relativistic effects. This can be overcome by the use of pseudo potentials. Since the core orbitals are not affected by the changes in chemical bonding, one can treat them as an average potential. The state of valence electrons can be described by appropriate basis functions. A commonly used pseudo potential is the Effective Core Potential (ECP)[7] and is of the general form,

$$\text{ECP(r)} = \sum_{i}^{k} C_i r^{n_i} e^{(-\alpha_i r^2)} \tag{1.30}$$

where, k is the number of terms in the expansion, C_i is a coefficient characteristic of each term, r is the distance from the nucleus, n_i and α_i is an exponent for i^{th} term. The use of ECP is found to be computationally very efficient, particularly for transition metals, because it reduces the number of basis functions. ECP also makes room for the incorporation of relativistic effects.

[1.2.2] Electron Correlation

One of the limitations of HF calculations is that they do not include exact electron correlation.[8] HF takes into account an average effect of electron repulsion, but not the explicit electron-electron interactions. Within HF theory the probability of finding an electron at some location around an atom is determined by the distance from the nucleus but not the distance from the other electrons. There are three common methods which incorporate electron correlation viz. Configuration

Interaction,[9] Møller-Plesset Perturbation theory,[10] and Coupled Cluster Theory.[11] These calculations begin with a HF calculation and then correct for correlation.

(i) Configuration Interaction

A configuration interaction wave function is a multiple Slater determinant wave function. It is constructed from the HF wave function and making new determinants by promoting electrons from the occupied to unoccupied orbitals. Configuration interaction methods are classified by the number of excitations used to make each determinant. If only one electron has been excited for each determinant, it is called a configuration interaction single-excitation (CIS) calculation. CIS calculations give an approximation to the excited states of the molecule, but do not change the ground state energy. Single and double excitation (CISD) calculations yield a ground state energy that has been corrected for correlation. The configuration interaction calculation with all possible excitations is called full CI. The full CI calculation using an infinitely large basis set will give an exact quantum mechanical energy. However, full CI calculations are rarely done due to the immense amount of computer power required.

(ii) Møller-Plesset Perturbation Theory

Correlation can be treated as a perturbation to HF wave function. This method takes the sum of the one electron HF operator as the unperturbed Hamiltonian (H^0).

$$H^0 = \sum_{m}^{n} F(m) \qquad (1.31)$$

The perturbation H' is the difference between the true inter-electronic repulsions and the HF inter-electronic potential.

$$H' = H - H^0 \tag{1.32}$$

In mapping the HF wave function in a perturbation theory for formulation, HF becomes a first order perturbation. The energy correction in MP theory can be taken as various orders like 1st order (HF), 2nd order (MP2), 3rd order (MP3) and so on. The accuracy of an MP4 calculation is roughly equivalent to the accuracy of a CISD calculation.

[1.2.3] Semiempirical Methods[1,2]

Semiempirical methods use empirically determined parameters and parameterized functions to approximate the different integrals in the Hamiltonian. The earlier semiempirical methods treated the π-electrons of conjugated molecules separately from the σ-electrons. These are known as π-electron approximation. The simplest semiempirical π-electron theory is free electron molecular orbital (FEMO).[1,2] Here, the interatomic repulsions are ignored. The most celebrated semiempirical theory is the Hückel Molecular Orbital theory (HMO)[12] developed in 1930's. Here, the π-electron Hamiltonian is approximated by the simpler form,

$$H_\pi = \sum_i^{n_\pi} H_{eff}(i) \tag{1.33}$$

$H_{eff}(i)$ incorporates the effects of the π-electrons repulsion in the average way. The next approximation in the HMO method is to approximate the π-MOs as LCAOs.

A semiempirical π-electrons theory that takes electron repulsion into account and there by improves on Hückel method is Pariser-Parr-Pople (PPP) method,[13] developed in 1953. Here, the π-electrons Hamiltonian including electrons repulsion is used along with zero differential overlap (ZDO) approximation.[14] This is known as 2-electron theory.

(i) Extended Hückel Method[15]

The semiempirical theories discussed so far applies only to planar conjugated molecules and treats only π-electrons. But the extended Hückel theory can be applied to all molecules as it includes all the valence electrons. The extended Hückel method begins with the approximation of treating the valence electrons separately from the rest. The valence electron Hamiltonian is taken as the sum of one electron Hamiltonian.

$$\mathrm{H}_{val}=\sum_{i}^{n}\mathrm{H}_{eff}(i) \tag{1.34}$$

The MOs are approximated as linear combinations of the valence atomic orbitals of the atoms and are represented as.

$$\phi_i=\sum_{r}^{n}C_{ri}f_r \tag{1.35}$$

This method usually uses atomic orbitals comprised of Slater type orbitals (STO) with fixed orbital exponents determined from Slater's rules. Thus, the many electrons Hamiltonian separates into several one electron Hamiltonian as

$$\mathrm{H}_{eff}(i)\phi_i=\varepsilon_i\phi_i \tag{1.36}$$

$$E_{val} = \sum_{i}^{n} \varepsilon_i \tag{1.37}$$

If the variation theorem is applied on the trial function, the secular equation and the equation for the MO coefficients become

$$\left| H_{rs}^{eff} - \varepsilon_i S_{rs} \right| = 0 \tag{1.38}$$

$$\sum_{s}^{n} (H_{rs}^{eff} - \varepsilon_i S_{rs}) = 0 \qquad r = 1,2,\ldots \tag{1.39}$$

Unlike simple Hückel theory, EH theory does not neglect overlap integrals, S_{rs}.

for $r = s$,

$$H_{rs}^{eff} = H_{rr}^{eff} = \left\langle f_r \left| H_{eff} \right| f_r \right\rangle \tag{1.40}$$

when $r \neq s$,

$$H_{rs}^{eff} = \frac{1}{2} k (H_{rs}^{eff} + H_{rr}^{eff}) S_{rs} \tag{1.41}$$

where, k is a numerical constant. Since H_{rs}^{eff} and H_{rr}^{eff} are usually negative, the value of H_{rs}^{eff} in equation (1.39) is also negative. The difference of EH with simple Hückel theory is that, H_{rs}^{eff} is non-zero for all pairs of orbitals unless S_{rs} vanishes for symmetry reasons.

Equation (1.37) gives the total energy as the sum of orbital energies. Though equation (1.36) omits both electron-electron and nuclear-nuclear repulsions, EH method gives the geometric parameters which are rather accurate in case of not highly polar bonds, but fails for molecules having very polar bonds. EH does not give reliable quantitative results but provides good qualitative results and which

helps in understanding many chemical problems. Walsh diagram and fragment molecular orbital (FMO) analysis can be done qualitatively using EH calculations.

There are several other semiempirical methods like CNDO,[1,2] INDO,[1,2] NDDO,[1,2] MINDO,[16] MNDO,[17] AM1[18] etc, which includes overlap and electron-electron repulsion integrals to different extent.

[1.2.4] Density Functional Theory[19]

Traditional methods like Hartree-Fock theory in electronic structure calculations are based on the complicated many-electron wavefunction. The main objective of density functional theory (DFT) is to replace the many-body electronic wavefunction with the electronic density as the basic quantity. Whereas the many-body wavefunction is dependent on $3N$ spatial coordinates and N spin coordinates for each of the N electrons, the density is only a function of three variables and is a simpler quantity to deal with both conceptually and practically. The basic form of the DFT is that ground state energy is a functional of ground state electron probability density ρ_0.

$$E_0 = E_0[\rho_0] \tag{1.42}$$

where, the zero subscript indicates ground state. DFT calculates the energy and other molecular properties from the electron probability density in contrast to *ab initio* theory where wave function is considered as the basis for all calculations. All DFT calculation are based on Hohenberg-Kohn (HK) theorems.[19c,e] The first theorem (HK-I) states that there is one to one correspondence between ground state energy and ground state density. The Hamiltonian in this case is

$$\mathrm{H}=-\frac{1}{2}\sum_{i}^{N}\nabla_i^2+\sum_{i}^{N}\upsilon(\vec{r}_i)+\sum_{j}^{N}\sum_{i>j}^{N}\frac{1}{r_{ij}} \tag{1.43}$$

where, $\upsilon(\vec{r}_i)$ is the potential energy of interaction between electron and nuclei, called as external potential and expressed as

$$\upsilon(\vec{r}_i)=-\sum_{\alpha}^{N}\frac{Z_\alpha}{r_{i\alpha}} \tag{1.44}$$

The number of electrons, (n) can be determined from $\rho_0(r)$ as

$$\int \rho_0(r)dr = n \tag{1.45}$$

The HK-II theorem states that for every trial density function $\rho_{tr}(r)$ that satisfies the equation (1.45) and $\rho_{tr}(r)\geq 0$ for all r, the following inequality holds. $\mathrm{E}_0 \leq \mathrm{E}_\upsilon\left[\rho_{tr}(r)\right]$, where, E_υ is energy functional. Since, $\mathrm{E}_0=\mathrm{E}_0\left[\rho_0\right]$ where ρ_0 is true ground state electron density, the true ground state electron density minimizes the energy functional, $\mathrm{E}_\upsilon\left[\rho_{tr}(r)\right]$.

Later this method is improved by Kohn and Sham to yield the exact result and known as Kohn-Sham (KS) method.[19f] KS method also can not give the accurate result as the equation of KS method contains an unknown functional that must be approximated. This method considers a reference system of non-interacting electrons.

The accuracy of KS method depends on the quality of the exchange-correlation functional, $\mathrm{E}_{xc}\left[\rho_0\right]$.

$$\mathrm{E}_{xc}\left[\rho_0\right]=\Delta\overline{T}\left[\rho_0\right]+\Delta\overline{V}_{ee}\left[\rho_0\right] \tag{1.46}$$

$\Delta\overline{T}$ and $\Delta\overline{V}_{ee}$ are the difference in average electronic kinetic energy and electron-electron repulsion terms in comparison to non-interacting reference system. The functional derivatives of E_{xc} is the exchange-correlation potential

$$V_{xc}(r)=\frac{\delta \mathrm{E}_{xc}\left[\rho_0(r)\right]}{\delta\rho_0(r)} \tag{1.47}$$

Inclusion of variational principle in HK-I theorem yields HK-II theorem

$$\mathrm{E}_{v(r)}\left[\rho(r)\right]=T\left[\rho(r)\right]+V_{ee}\left[\rho(r)\right]+\int\rho_0(r)\upsilon(r)dr\geq \mathrm{E}_{v(r)}\left[\rho_0(r)\right] \tag{1.48}$$

Considering the effect of external potential V_s, the energy become

$$\mathrm{E}_s\left[\rho(r)\right]=\int\Psi_s\left[\rho(r)\right](T+V_s)\Psi\left[\rho(r)\right]d\tau+T_s\left[\rho(r)\right]+\int\Psi_s\left[\rho(r)\right]V_s\Psi\left[\rho(r)\right]d\tau\geq \mathrm{E}_{v(r)}\left[\rho_0(r)\right] \tag{1.49}$$

(i) Local Density Approximation (LDA)

In LDA, the contribution of each volume element to the total exchange correlation energy is taken to be that of an element of homogenous electron gas density at that point,

When ρ_0 varies with position extremely slowly, then $\mathrm{E}_0\left[\rho_0\right]$ can be expressed as,

$$\mathrm{E}_{xc}^{LDA}\left[\rho_0\right]=\int\rho_0(r)\varepsilon_{xc}^{LDA}[\rho_0]d\tau \tag{1.50}$$

$\varepsilon_{xc}[\rho_0]$ is the exchange and correlation energy per electron in a homogenous electron gas with electron density ρ_0. The functional derivative of $\mathrm{E}_{xc}^{LDA}\left[\rho_0\right]$ gives

$$V_{xc}^{LDA}=\frac{\delta \mathrm{E}_{xc}^{LDA}\left[\rho_0\right]}{\delta\rho}=\varepsilon_{xc}^{LDA}[\rho_0(r)]+\rho_0(r)\frac{\partial\varepsilon_{xc}^{LDA}(\rho)}{\partial\rho} \tag{1.51}$$

Here, ε_{xc} can be written as the sum of exchange and correlation energy

$$\varepsilon_{xc}^{LDA}(\rho_0) = \varepsilon_x^{LDA}(\rho_0) + \varepsilon_c^{LDA}(\rho_0) \tag{1.52}$$

Similarly,

$$E_{xc}^{LDA} = E_x^{LDA} + E_c^{LDA} \tag{1.53}$$

(ii) Local Spin-Density Approximation (LSDA)

LSDA allows electrons with different spins to occupy different spatial KS orbitals unlike LDA where electrons with opposite spin paired with each other occupy same spatial KS orbital. Hence, for open-shell molecules and molecular geometries near dissociation LSDA works better than LDA.

(iii) Generalized Gradient Approximation (GGA)

GGA estimates the contribution of each volume element based on the magnitude and gradient of the electron density within that element. In other words, in addition to LDA and LSDA, this method considers the variation of the electron density with varying position. Here, the exchange correlation energy is given by

$$E_{xc}^{GGA}\left[\rho_0^{\alpha}, \rho_0^{\beta}\right] = \int f(\rho_0^{\alpha}(r), \rho_0^{\beta}(r), \nabla\rho_0^{\alpha}(r), \nabla\rho_0^{\beta}(r))d\tau \tag{1.54}$$

where, f is a function of spin densities of electrons and their gradients. Here, the exchange correlation energy is expressed as

$$E_{xc}^{GGA} = E_x^{GGA} + E_c^{GGA} \tag{1.55}$$

The commonly used gradient-correlated functional are Lee-Yang-Parr (LYP)[20] functional, Perdew-Burke-Ernzerhof (PBE)[21] exchange and correlation functional, Vosko-Wilk-Nusani functional (VWN),[22] Becke[23] correlation functional. The method like B3LYP uses Hartree-Fock and gradient-corrected functionals.

Several other hybrid functionals (HF-DFT) are also known which define the exchange functional as a linear combination of HF, local and gradient-corrected exchange terms. This exchange functional is then combined with a local or a gradient-corrected correlation functional. Different levels of theory are available based on the approximations to the exchange and correlation functionals.

The computations carried out for the work embedded in the chapters 2, 4 and 5 are done at hybrid HF-DFT method, B3LYP, based on Becke's three-parameter functional including Hartree-Fock exchange contribution with a non-local correction for the exchange potential proposed by Becke together with the non-local correction for the correlation energy suggested by Lee et. al. The density functional calculation using generalized gradient approximation including the Becke's non-local correction to the exchange energy expression and the Perdew's non-local correction to the correlation energy expression is used for the computational calculations in the chapter 3.

[1.3] Outline of the Thesis

The remaining four chapters describe briefly the theoretical studies of 2π-aromatic three membered rings, $BAl_2H_n^m$ (n = 3 - 6, m = -2 - +1) (Chapter 2), stabilization of tris-acetylenic model metal complexes of fullerene and its fragments (Chapter 3), stabilization of planar tetra-coordinated carbon in bimetallic complexes (Chapter 4) and the insertion reaction of heteroallenes into metal-metal bond in early-late heterobimetallic (ELHB) complexes (Chapter 5).

[1.3.1] Chapter 2: Structure and Bonding in Cyclic Isomers of $BAl_2H_n^m$ (n = 3 - 6, m = -2 - +1): Preference for Planar Tetra-coordination, Pyramidal Tri-coordination and Divalency

The group 13 hydrides play a dominant role in chemistry in many ways: applications in organic synthesis, organometallic catalysis, materials chemistry and possible hydrogen storage materials are among them. Availability of a variety of coordination numbers and geometries contribute to this versatile chemistry. In view of the unusual structures encountered experimentally and theoretically of mixed compounds from the group 13 elements, we have studied the three membered system involving one boron and two aluminum atoms, starting with the 2π-aromatic $BAl_2H_3^{2-}$ and structures obtained by its sequential protonation, $BAl_2H_4^-$, BAl_2H_5 and $BAl_2H_6^+$.

The structure and energetics of cyclic $BAl_2H_n^m$ (n =3 - 6, m = -2 - +1) obtained at B3LYP/6-311+G** and QCISD(T)/6-311++G** levels are compared with corresponding homocyclic boron and aluminum analogues. Structures having varying number of coordination mode on boron and aluminum atoms are found to be

minima (scheme 1.1). There are several unusual geometrical and bonding patterns such as planar tetra-coordinate boron and aluminum atoms in the same ring in $BAl_2H_4^-$ and divalent boron containing lone pair are common among them. There is a parallel between the structure and bonding in the isomers of $BAl_2H_3^{2-}$ and BSi_2H_3. The number of structures having hydrogens out of the BAl_2 ring plane is found to increase from $BAl_2H_3^{2-}$ to $BAl_2H_6^+$. Double bridging at one bond is common in BAl_2H_5 and $BAl_2H_6^+$. Similarly, species with lone pairs on divalent boron and aluminum atom are found to be minima on the potential energy surface of $BAl_2H_3^{2-}$. Bridging hydrogen atoms on B-Al bond prefers not to be in the BAl_2 plane so that π-MO is stabilized by π-σ mixing. This stabilization of the π-MO is a major contributor for the preference of non-planar structures with H-bridging. As the number of bridging hydrogen atoms increases, the stabilization of the π-MO also increases. Stability order of structures is decided by optimizing the preference for lower coordination at aluminum, higher coordination at boron and more bridging hydrogen atoms between B-Al bonds. The stabilization energy for the minimum energy structures of $BAl_2H_n^m$ which contain π-delocalization are compared with the corresponding homocyclic aluminum and boron analogues.

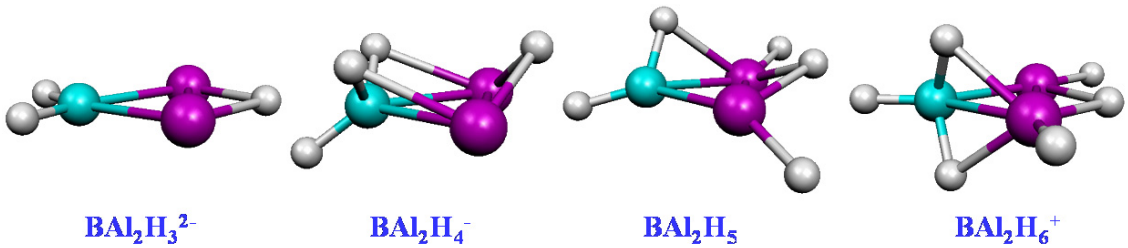

Scheme 1.1: Most stable structures of $BAl_2H_3^{2-}$, $BAl_2H_4^-$, BAl_2H_5 and $BAl_2H_6^+$ at B3LYP/6-311+G** level of theory have several unusual coordination modes around boron and aluminum.

[1.3.2] Chapter 3: The Effect of Metal Complexation on Ring Opening of Bowl Shaped Hydrocarbons: A Theoretical Study

The organometallic chemistry of fullerenes and bowl shaped hydrocarbons was triggered by the synthesis of the organometallic compounds, η^2-$C_{60}Pt(PPh_3)_2$. It led to further development in exohedral organometallic chemistry of these molecules. Another fascinating aspect is endohedral chemistry of fullerenes. One of the approaches to achieve endohedral fullerene is by the reversible breaking of bonds or rings and opening a "window" large enough for entry of atoms. The ring opening of C_{60} and its fragments is compared with the reverse process of the well-known catalytic conversion of acetylene into benzene (scheme 1.2).

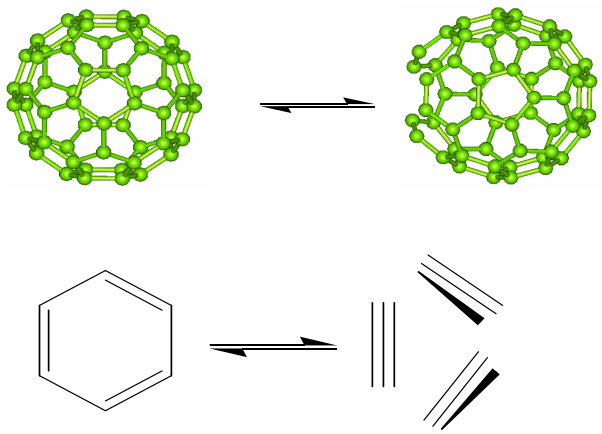

Scheme 1.2: Benzene-acetylene equilibrium and benzeniod and tris-acetylenic structure of fullerene.

A DFT study on benzenoid and tris-acetylenic structure of fullerene and its fragments are described in this chapter. The results show that tris-acetylenic model structures lead to benzenoid structure, due to the proximity of π-orbitals in the former. The tris-acetylenic model structures are stabilized on metal complexation in comparison to the parent benzene-acetylene equilibrium. The acetylenic metal complex becomes more stabilized in going from CrC_6H_6 to CoC_3H_3, than benzene-

metal complex. The curved surface of the tris-acetylenic fullerene fragments causes one set of π-orbital of the tris-acetylenic groups to rehybridize so as to reorient towards the metal fragments than found in the parent acetylene complexes (scheme 1.3). This leads to the increased overlap between metal fragments and tris-acetylenic model structures. The benzenoid and tris-acetylenic model complexes of $C_{12}H_6$ and $C_{12}H_{12}$ where five membered rings are replaced with more strained four membered rings are also studied.

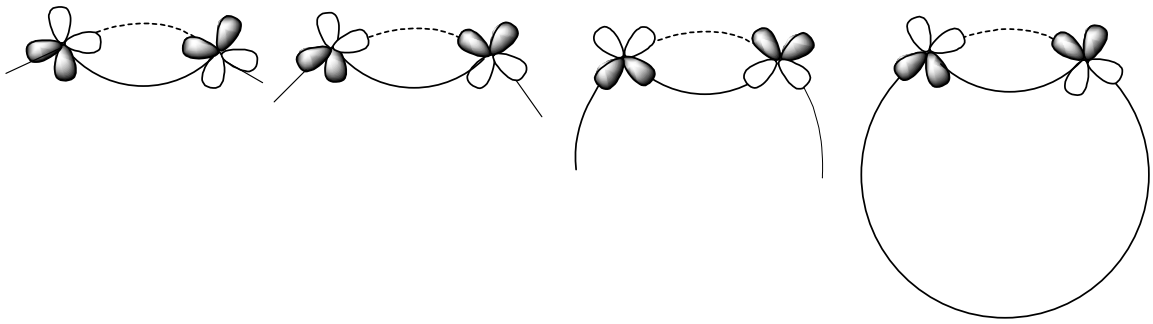

Scheme 1.3: Schematic representation of the inclinations of π-orbitals of six membered rings in bowl shaped hydrocarbons as a function of curvature.

[1.3.3] Chapter 4: Binuclear Organometallic Compounds Containing Planar Tetra-coordinated Carbon Atoms: Theoretical Study on Geometrical and Bonding Patterns

The chemistry of unstable 14-electron titanocene (Cp_2Ti) and zirconocene (Cp_2Zr) has been playing a vital role in structural and catalytical chemistry. These metallocenes are important in the stoichiometric C-C coupling and cleavage reactions of unsaturated molecules such as alkynes, olefins, acetylides and vinylides. The carbene type frontier orbital of Cp_2M help in the reaction with unsaturated compounds to form metallacycles. It undergoes further reactions with metallocenes and other substrates. The cyclization of the 1,2,3-butatrienes and 1,3-butadiynes

lead to highly strained carbocycles, which are not viable. Such, geometry can be realized by the metallocenes derivatives, metallacyclopentynes and metallacyclocumulenes. The metallacycles occupy a special place in the chemistry of transition metal organometallics as they are involved in important reactions such as the synthesis of carbocyclic and heterocyclic compounds and their unusual ability to stabilize highly reactive organic entities.

In this chapter, the density functional theory studies on the structure and bonding in the binuclear complex **1**, which has two planar tetra-coordinate carbons adjacent to each other are discussed (scheme 1.4). This is compared with that of the metallacyclocumulene**, 2** and the metal-acetylene complex, **3** (scheme 1.4). The geometrical pattern on metal-acetylene complex shows that the diffuseness of the orbitals of the metal atom and the extent of back bonding are the main reasons for the elongation on the C-C bond length in metal-acetylene complexes. Since the C1-C2-C3 angle in **2** changes to get effective overlap as the size of metal is changed, the central C-C bond length of the cumulene remains nearly constant. In many ways the ML_2 fragments dictate the bond angles C1-C2-C3 and C4-C3-C2 and the distance C2-C3 to have effective overlap with the C_4H_2 frame. The central C-C bond length in **1** increases with an increase in the size of the metal M′ as in the case of metal-acetylene complex, **3**. The planar tetra-coordinate arrangements around two adjacent carbons are stabilized through the four in-plane delocalized molecular orbitals resulting from the interaction with the metal fragment orbitals and two π molecular orbitals perpendicular to the MC_4M' plane. When the C1-C2-C3 bond angle of **2** comes closer to the C-C-H bond angle of **3**, the stability of the complex, **1**, increases.

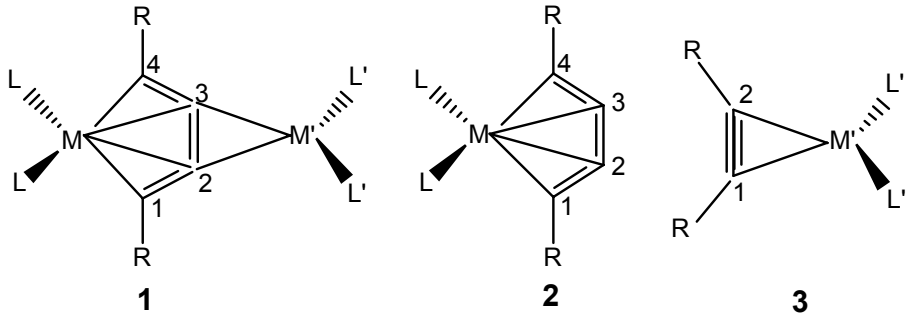

Scheme 1.4: Schematic diagram of the binuclear complex (**1**), the metallacyclocumulene (**2**) and the metal-acetylene complex (**3**). The lines here meant to imply the nature of bonding in the ligands and do not represent the numbering of bonds.

[1.3.4] Chapter 5: Theoretical Study on the Insertion of Heteroallenes (CO_2, COS and CS_2) to Metal-metal Polar Bond of Early-late Bimetallic Complexes

Early-late heterobimetallic (ELHB) complexes have widespread interest in catalytic reactions, synthetic organometallic chemistry and materials science. Interest in these complexes arises from the possibility of utilizing the complementary reactivities of the electron-poor early transition metal and the electron-rich late transition metal. The synergetic effect of the two metals plays a key role in their reactivity such as insertion of polar substrate like CO_2, COS and CS_2 into metal-metal bonds and their functionalization.

In this chapter, the mechanism of the insertion of heteroallenes, XCY (CO_2, COS, and CS_2,) into metal-metal polar bond of early-late heterobimetallic (ELHB) complexes, $(NH_2)_3$M-M′$(CO)_2$Cp (where M= Ti, Zr and M′= Fe, Ru) is studied using Density Functional Theory. The reactions of CO_2 and COS with M-M′ bond of ELHB complexes (**9p**) give the initial intermediates, **10pq** which undergo isomerization to the four membered metallacycles, **12pq** through transition states, **11pq** (scheme 1.5).

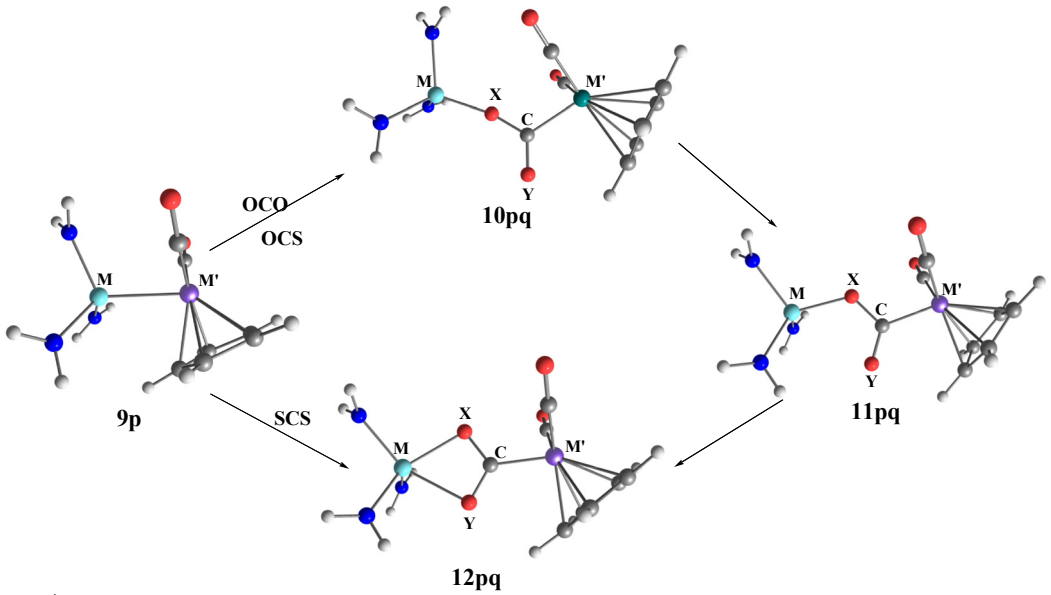

pq	aa	ab	ac	ba	bb	bc	ca	cb	cc	da	db	dc
M	Ti	Ti	Ti	Ti	Ti	Ti	Zr	Zr	Zr	Zr	Zr	Zr
M'	Fe	Fe	Fe	Ru	Ru	Ru	Fe	Fe	Fe	Ru	Ru	Ru
XCY	OCO	OCS	SCS	OCO	OCS	SCS	OCO	OCS	SCS	OCO	OCS	SCS

Scheme 1.5: Mechanistic scheme for the insertion of heteroallenes (XCY) into ELHB complexes, **9p**. **10pq** and **12pq** are the complexes resulting from XCY insertions and **11pq** is the transition state for the interconversions. Here, **p** stands for **a-d** indicating the M-M′ complexes and **q** for **a-c** indicating the heteroallenes, XCY.

The synergetic effect of both transition metals plays a key role in the reactivity towards the heteroallenes. The greater strain arising from the smaller size of titanium and oxygen rules out the formation of the metallacycles, **12aa** and **12ba**. On the other hand, larger size of sulphur averts the formation of **10pc**. The first row late transition metal stabilizes the LUMO of XCY which favors the bending more effectively than the second row. This reflects in the more stability of the complexes, **10pq** which have the late transition metal from the first row. The smaller atomic size of Ti and hence more strain in the OCS angle destabilize the complexes, **12ab** and **12bb** more than **10ab** and **10bb**.

[1.4] References

(1) (a) Levine, I. N. *Quantum Chemistry*, 5th Edition, Prentice Hall, NJ, 2000. (b) McQuarrie, D. A. *Quantum Chemistry*, Oxford University Press, California, 1983. (c) Pilar, F. L. *Elementary Quantum Chemistry*, Mc-Graw Hill Publishing Co., NewYork, 1968. (d) Chandra, A. K. *Introductory Quantum Chemistry*, Tata Mc-Graw Hill Publishing Co., New Delhi, 1988. (e) Szabo, A.; Ostlund, N. S. *Modern Quantum Chemistry*, Mc-Graw Hill Publishing Co., NewYork, 1982.

(2) (a) Hehre, W. J.; Radom, L.; Schleyer, P. v. R.; Pople, J. A. *Ab-initio Molecular Orbital Theory*, John Wiley & Sons, Inc., New York, 1986. (b) Pople, J. A.; Beveridge, D. L. *Approximate Molecular Orbital Theory*, Mc-Graw Hill Publishing Co., NewYork, 1970. (c) Lowe, J. P. *Quantum Chemistry*, Academic Press, New York, 1978. (d) Schaefer III, H. F. *The Electronic Structure of Atoms and Molecules*, Addison-Wesley, Massachusetts, USA, 1972. (e) Foresman, J. B.; Frisch, A. *Exploring Chemistry with Electronic Structure Methods,* Gaussian Inc. Pittsburgh, USA. 2004 (f) Richards, W. G.; Cooper, D. L. *Ab initio Molecular Orbital Calculations for Chemists*, Clarendon Press, Oxford, 1983. (g) Jensen, F. *Introduction to Computational Chemistry*, John Wiley & Sons, New York, 1999.

(3) Born, M.; Oppenheimer, J. R. *Ann. Physik* **1927**, *84*, 457.

(4) (a) Hartree, D. R. *Proc. Cambridge Phil. Soc.* **1928**, *24*, 89. (b). Fock, V. *Z. Phys.* **1930***, 61,*126.

(5) Slater, J. C. *Phys. Rev.* **1930**, *36*, 57.

(6) Boys, S. F. *Proc. R. Soc. (London)* **1950**, *A200*, 542.

(7) Frenking, G.; Seijo, L.; Bohme, M.; Dapprich, S.; Ehlers, A. W.; Jonas, V.; Neuhaus, A.; Otto, M.; Stegmann, R.; Veldkamp, A.; Vyboishchikov, S. F.; *Reviews in Computational Chemistry*; Lipkowitz, K. B., Boyd, D. B., Eds.; VCH: New York, 1996, *8*, 63.

(8) McWeeny, R. *Int. J. Quant. Chem.* **1967**, *15*, 351.

(9) (a) Hurley, A. C. *Electron Correlation in Small Molecules* Academic Press, London, 1977. (b) Wilson, S. *Electron Correlation in Molecules* Clarendon Press, Oxford, 1984. (c) Raghavachari, K.; Anderson, J. B. *J. Phys. Chem.* **1996**, *100*, 12960.

(10) Moller, C.; Plesset, M. S. *Phys. Rev.* **1934**, *46*, 618.

(11) Hoffmann, M. R.; Schaefer, H. F. *Adv. Quantum Chem.* **1986***, 18,* 207.

(12) Hückel, E. *Z. Phys.* **1931***, 70,* 204.

(13) Pople, J. A.; Beveridge, D. L.; Dobosh, P. A. *J. Chem. Phys.* **1967**, *47*, 2026.

(14) Pople, J. A.; Santry, D. P.; Segal, G. A. *J. Chem. Phys.* **1965***, 43,* S129.

(15) Hoffmann, R.; Lipscomb, W. N. *J. Chem. Phys.* **1962**, *36*, 2179. (b) Hoffmann, R. *J. Chem. Phys.* **1963**, *39*, 1397; **1964**, *40*, 2474; 2480; 2745. (c) Hoffmann, R. *Angew. Chem., Int. Ed. Engl*. **1982**, *21*, 711.

(16) Bingham, R. C.; Dewar, M. J. S.; Lo, D. H. *J.* Am. *Chem. Soc*. **1975**, *97*, 1285; 1294; 1302; 1307.

(17) Dewar, M. J. S.; Thiel, W. *J. Am. Chem. Soc*. **1977**, *99*, 4899.

(18) Dewar, M. J. S.; Zoebisch, E. G.; Healy, E. F.; Stewart, J. J. P. *J. Am. Chem. Soc*. **1985**, *107*, 3902.

(19) (a) Parr, R. G.; Yang, W. *Density Functional Theory of Atoms and Molecules,* Oxford University Press, Oxford, 1989. (b) Dreisler, R. M.; Gross, E. K. V. *Density Functional Theory: An Approach to the Quantum Many-body Problem*, Springer-Verlag, Berlin, 1990. (c) Hohenberg, P. C.; Kohn, W.; Sham, L. J. *Advances in Quantum Chemistry*, Vol. 21, Academic Press, 1990. (d) Kohn, W.; Becke, A. D.; Parr, R. G. *J. Phys. Chem*. **1996**, *100*, 12974. (e) Hohenberg, P. C.; Kohn, W. *Phy. Rev.* **1964**, *136*, B864. (f) Kohn, W.; Sham, L. *J. Phys. Rev*. **1965**, *A140*, 1133. (g) Geerlings, P.; De Proft, F.; Langenaeker, W. *Chem. Rev*. **2003**, *103*, 1793.

(20) Lee, C.; Yang, W.; Parr, R. G. *Phys. Rev. B* **1988**, *37*, 785.

(21) Perdew, J. P.; Burke, K.; Ernzerhof, M. *Phys. Rev. Lett.* **1996**, *77*, 3865.

(22) Vosko, S. H.; Wilk, L.; Nusair, M. *Can. J. Phys.* **1980**, *58*, 1200.

(23) (a) Becke, A. D. *J. Chem. Phys.* **1993**, *98*, 1372. (b) Becke, A. D. *J. Chem. Phys.* **1993**, *98*, 5648.

CHAPTER 2

STRUCTURE AND BONDING IN CYCLIC ISOMERS OF $BAl_2H_n^m$ (n = 3 - 6, m = -2 - +1): PREFERENCE FOR PLANAR TETRA-COORDINATION, PYRAMIDAL TRI-COORDINATION AND DIVALENCY

[2.0] Abstract

The structure and energetics of cyclic $BAl_2H_n^m$ (n =3 - 6, m = -2 - +1) obtained at B3LYP/6-311+G** and QCISD(T)/6-311++G** levels are compared with corresponding homocyclic boron and aluminum analogues. Structures with coordination numbers of boron and aluminum atoms up to six are found to be minima. There is a parallel between the structure and bonding in the isomers of $BAl_2H_3^{2-}$ and BSi_2H_3. The number of structures having hydrogens out of the BAl_2 ring plane is found to increase from $BAl_2H_3^{2-}$ to $BAl_2H_6^+$. Double bridging at one bond is common in BAl_2H_5 and $BAl_2H_6^+$. Similarly, species with lone pairs on divalent boron and aluminum atom are found to be minima on the potential energy surface of $BAl_2H_3^{2-}$. The first example of a structure with planar tetra-coordinate boron and aluminum atoms in the same structure is found in $BAl_2H_4^-$ (**2b)**. Bridging hydrogen atoms on B-Al bond prefers not to be in the BAl_2 plane so that π-MO is stabilized by π-σ mixing. This stabilization increases with increasing number of bridging hydrogen atoms. Stability order of structures is decided by optimizing the preference for lower coordination at aluminum, higher coordination at boron and more bridging hydrogen atoms between B-Al bonds. The relative stabilization energy (RSE) for the minimum energy structures of $BAl_2H_n^m$ which contain π-delocalization are compared with the corresponding homocyclic aluminum and boron analogues.

[2.1] Introduction

The group 13 hydrides play a dominant role in chemistry in many ways: applications in organic synthesis,[1] organometallic catalysis,[2] materials chemistry[3] and possible hydrogen storage materials[4] are among them. Availability of a variety of coordination numbers and geometries contribute to this versatile chemistry.[2b,5] Binary hydrides of boron and aluminum are especially interesting with their dramatic structural contrasts. For example, global minimum structure of B_2H_2 is linear (scheme 2.1, **i**)[6], while Al_2H_2 prefers a structure with two bridging hydrogens (scheme 2.1, **ii**).[6a,7] Spectroscopically, (Dmp)BB(Dmp) (Dmp=2,6-dimethylpiperidinato) has been shown to have a linear RBBR geometry.[8] Al_2H_2 with double bridging hydrogen geometry has been identified by matrix IR spectra.[9] Mixed hydrides provide even more variety. The global minimum for $AlBH_2$ has a vinylidene type structure[6a,10] similar to $Si{=}CH_2$ (scheme 2.1, **iii**).[6a,11]

The recent revival in the chemistry of aluminum[12] especially with the successful synthesis of compounds such as alumino-cyclopropene[12,13] (scheme 2.1, **iv**) and aluminum analogue of carbene (scheme 2.1, **v**) {$HC(CMeNAr)_2Al$; Ar=2,6-$iPr_2C_6H_3$}[12,14] point to the exciting possibilities for the future. The 2π-aromatic aluminum analogue (AlC_2H_3) of cyclopropenyl cation has been suggested as one of the possible products in the reaction of AlCl monomers with acetylene in a solid argon matrix.[15]

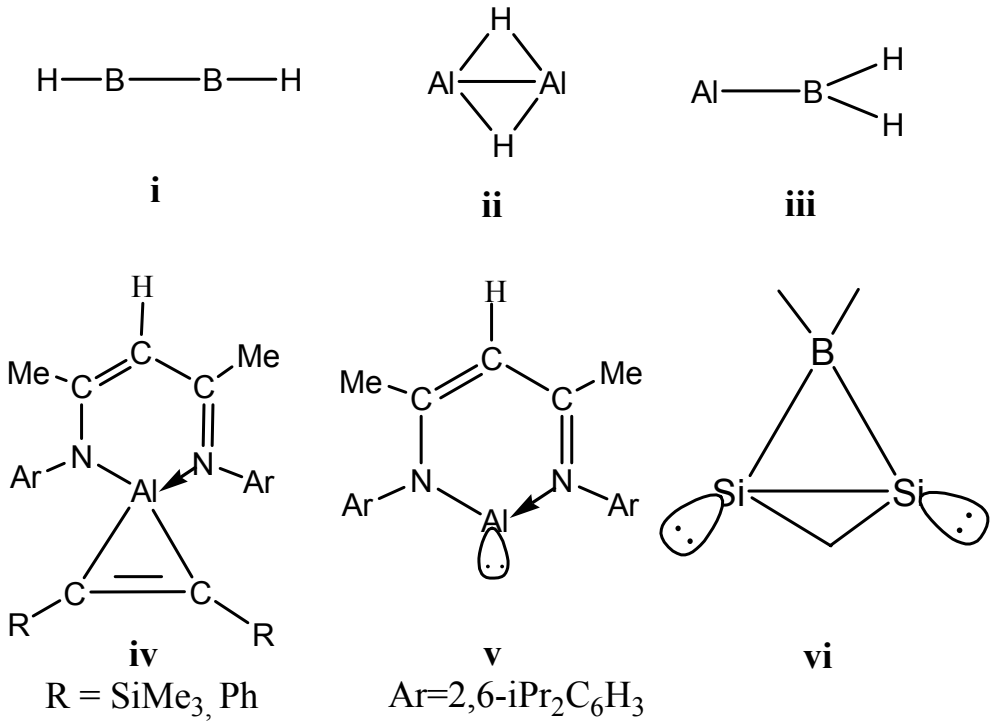

Scheme 2.1

We had studied the structural variety possible for the 2π-systems $B_3H_3^{2-}$, $Al_3H_3^{2-}$ and their protonated species.[16,17] Even more unusual structural variations are expected in heterocyclic rings. For example, the most stable structure of BSi_2H_3[18] which is formally an isoelectronic neutral analogue of cyclopropenyl cation, has a planar tetra-coordinate boron and a bridging hydrogen (scheme 2.1, **vi**). We had proposed an isolobal analogy between divalent silicon and trivalent boron to explain such unusual structures.[18,19] Schaefer and co-workers also reported similarities between silicon and aluminum hydrides (Al_2H_2 and Si_2H_2).[20] In view of the unusual structures encountered experimentally and theoretically of mixed compounds from the group 13 elements,[18-22] we have studied the three membered system involving one boron and two aluminum atoms, starting with the 2π-aromatic $BAl_2H_3^{2-}$. While there is no experimental evidence yet for these species, theoretical

and experimental studies on electronic and geometrical structure of boron doped bare aluminum metal clusters[23] and hydrogenated aluminum clusters [24] are reported.

We present a comprehensive study of all the possible cyclic isomers of $BAl_2H_3^{2-}$ (**1**) and structures obtained by its sequential protonation, $BAl_2H_4^-$ (**2**), BAl_2H_5 (**3**) and $BAl_2H_6^+$ (**4**). The study gives an insight to the structural varieties possible and their interconversions. We also probe the relative stability of these mixed hydrides brought by cooperative effect of one boron and two aluminum atoms.

[2.2] Computational Details

All structures derived as detailed below were optimized using the hybrid HF-DFT method, B3LYP,[25,26] based on Becke's three-parameter functional including Hartree-Fock exchange contribution with a non-local correction for the exchange potential proposed by Becke together with the non-local correction for the correlation energy suggested by Lee et al. The 6-311+G** basis set was used for all calculations.[25] The nature of the stationary points was characterized by vibrational frequency calculations. The Gaussian 03 programme package was used for all calculations.[27] Fragment Molecular Orbital (FMO)[28] and Natural Bond Orbital (NBO)[29] methods were used to analyze the bonding in a given structure. All the structures of the scheme 2.2 are also optimized using the QCISD(T) method using 6-311++G** basis set.[25] The vibrational frequency analysis indicated that the structures were minimum in energy at this level as well. The extent of variations in relative energies and structural parameters was minimal. The energetics of structures of schemes 2.3-2.5 were checked by single point calculations at this level.

[2.3] Results and Discussion

The structures discussed in this chapter are obtained by the isoelectronic replacement of the classical D_{3h} geometry of cyclopropenyl cation by the group 13 elements viz. one CH group by BH and the other two CH groups by AlH groups. The charges and the number of additional hydrogens were adjusted to give two π-electrons. Various starting geometries for $BAl_2H_3^{2-}$ are obtained by considering all possible combinations of bridging and terminal bonding positions. Similarly, the structures of the protonated species, $BAl_2H_4^-$, BAl_2H_5 and $BAl_2H_6^+$ are obtained by considering all possible combination of bridging and terminal hydrogen occupancies. Schemes 2.2, 2.3, 2.4 and 2.5 represent the optimized structures of $BAl_2H_3^{2-}$ and $BAl_2H_4^-$, BAl_2H_5 and $BAl_2H_6^+$ respectively.

A variety of bonding situations exist in these complexes ranging from the standard 2c-2e bonds, 3c-2e bonds involving bridging hydrogen and two heavy atoms, 3c-2e bond involving the three heavy atoms in the sigma plane and the familiar 3c-2e π-delocalization. There are also several structures with lone pairs of electrons and planar tetra-coordinate arrangements. The structural drawings follow the following convention to communicate visually the nature of bonding as much as possible. A 2c-2e bond is represented by a solid line. A 3c-2e bond is represented by dotted lines, except those involving bridging hydrogen. Here, the hydrogen-main group element connection is represented by solid line and the connection between the main group elements is represented by dotted lines. The 2π-electron delocalization is represented by a solid circle inside the three membered ring. These will be discussed once again while specific structures are introduced. Only boron atom of the three membered ring is labeled. The remaining two vertices are

aluminum atoms. The relative energies and number of imaginary vibrational frequencies are given below each structure in the schemes 2.2-2.5. Important geometric parameters of the minimum energy structures are given in figures 2.1-2.4. The discussions begin with the structures of $BAl_2H_3^{2-}$ (**1**). The structures obtained by protonations, $BAl_2H_4^-$ (**2**), BAl_2H_5 (**3**) and $BAl_2H_6^+$ (**4**), are discussed in this order. In view of the large number of minima obtained for **2**, **3** and **4**, these are discussed in relation to the isomers of $BAl_2H_3^{2-}$, **1**. General comparisons are made at the end.

[2.3.1] Structure and Bonding in the Isomers of $BAl_2H_3^{2-}$

A variety of unusual bonding arrangements are noted among the many structures which are characterized as minima in energy. The study started with 28 different structures. Nine of them led to stationary points on the potential energy surface (PES), with six of them characterized as minima and three as transition states. The schematic representations of all the nine isomers of $BAl_2H_3^{2-}$ are shown in the scheme 2.2. The most stable structure **1a** has a planar tetra-coordinate boron atom. The two B-H bonds correspond to conventional 2c-2e bond, the only two of its kind in this structure. These two bonds are represented by solid lines (scheme 2.2). The third hydrogen is bridged between aluminum atoms and is represented by solid lines between hydrogen and aluminum atoms and dotted line between the two aluminum atoms. There is an in-plane 3c-2e bond that binds the three heavier elements together and is represented by dotted lines between the three heavier elements. Thus, there are two dotted lines between the aluminum atoms. There is a lone pair each on aluminum atoms and is indicated by half dumb bell with two dots

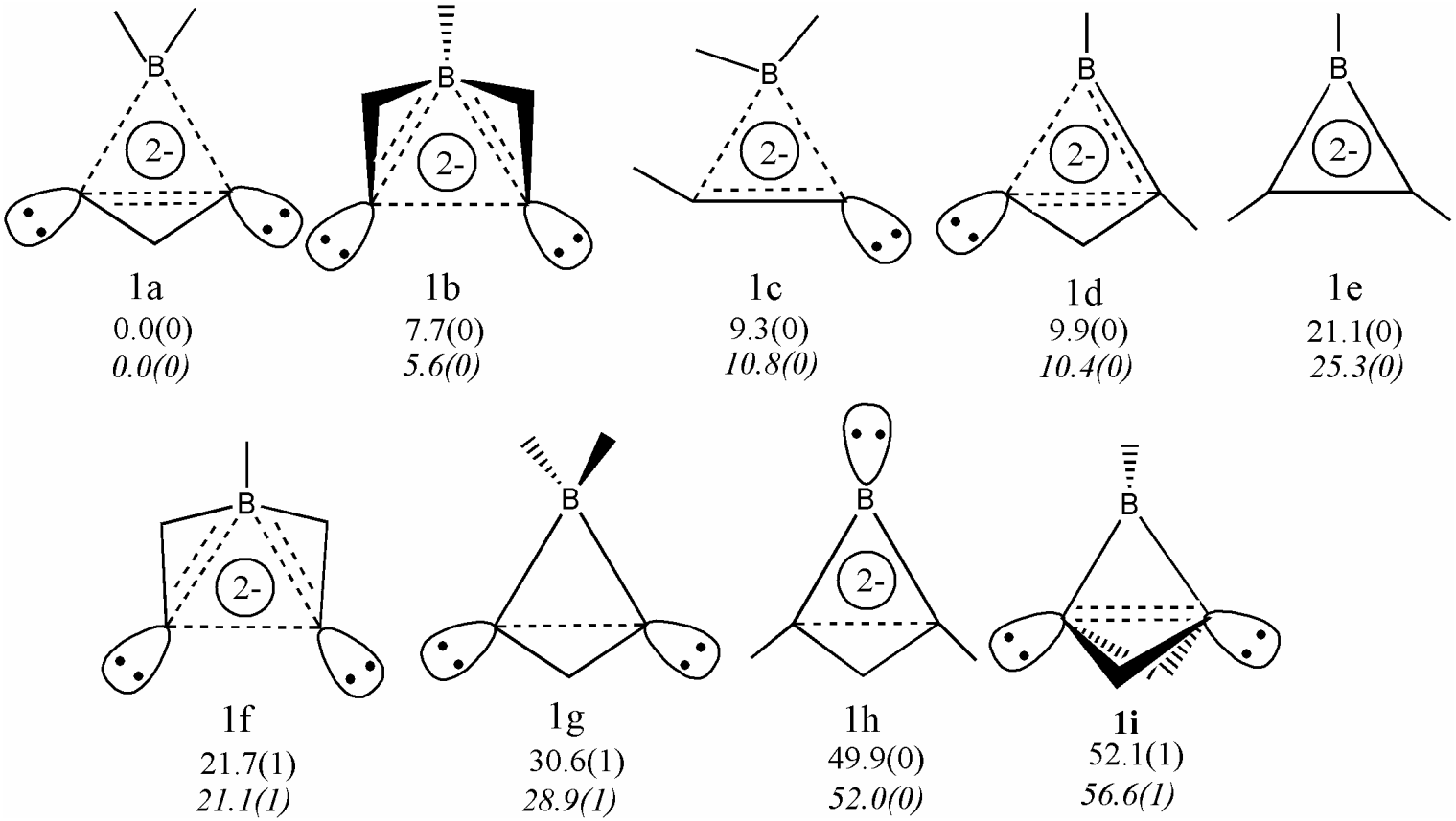

Scheme 2.2: Structures **1a-i**, relative energies (kcal/mol at B3LYP/6-311+G**, values at QCISD(T)/6-311++G** in italics) and the number of imaginary vibrational frequencies (in parentheses) for $BAl_2H_3^{2-}$.

inside. The 2π-electron delocalization is represented by a solid circle and the charge of the molecule (-2) is given inside the solid circle.

An NBO analysis on **1a** supports this description. A similar structure with planar tetra-coordinate aluminum is shown to be the global minimum in $Al_3H_3^{2-}$.[16] The corresponding planar tetra-coordinated homocyclic boron analogue, $B_3H_3^{2-}$ is 58.12 kcal/mol higher in energy than its global minimum structure of symmetry D_{3h}.[16] The reversal of the relative stability of the structure with planar tetra coordination by the replacement of two boron by aluminum is remarkable. An isomer similar to **1a** is the global minimum for the neutral isoelectronic BSi_2H_3.[18] An isolobal analogy that we had proposed between divalent silicon and trivalent boron is extended to make the link between silicon and aluminum and helps in making the connection between **1a** and the isostructural BSi_2H_3.[18,19] A structure with planar tetra-coordination around aluminum leads to **1c** on geometry optimization. This indicates the reluctance of aluminum for sp^n hybridization and higher coordination.

The next stable structure, **1b**, has a penta-coordinated boron atom. It has one terminal B-H bond and bridging hydrogen atoms on each B-Al bond. All the three hydrogen atoms are out of the BAl_2 plane. Following the convention described earlier for structural representation, structure **1b** has one 2c-2e B-H bond, one 3c-2e bond between Al-B-Al, two 3c-2e bonds involving B-H-Al hydrogen bridges and a lone pair each on aluminum atoms. Though there is considerable mixing between the original π-MOs of the planar structure and the bridging hydrogens, it is conceptually better to treat this as a π-MO. The planar alternative, **1f** is a transition state for the conversion of **1b** to the equivalent structure where the direction of the

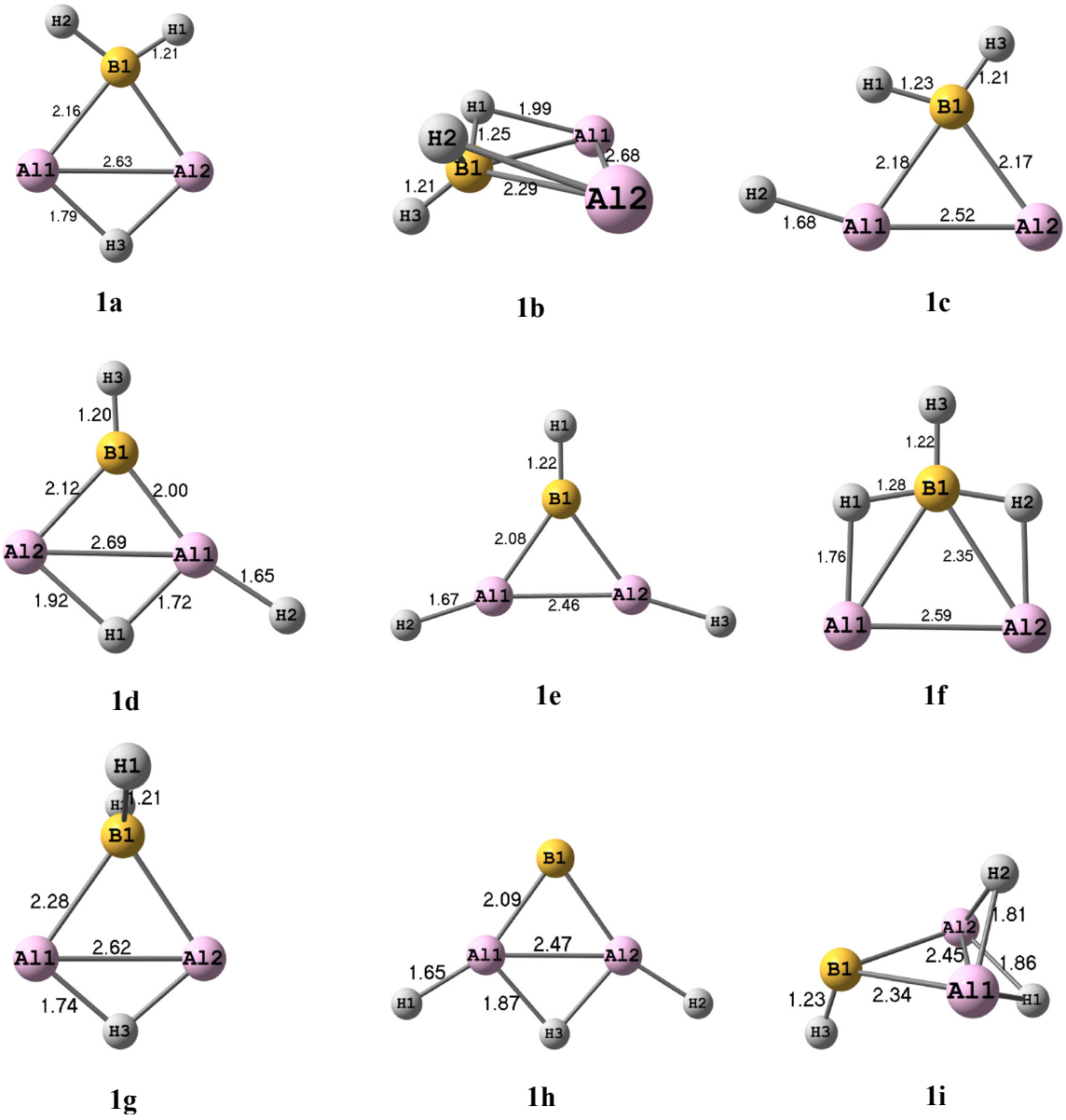

Figure 2.1: Optimized geometries and bond distances of $BAl_2H_3^{2-}$ at B3LYP/6-311+G** level of theory.

bridging and the terminal hydrogens are reversed. Instability of **1f** is mainly due to the non-bonded interaction between bridging hydrogen atoms and terminal hydrogen atom. The distance between these two hydrogen atoms at **1f** is 1.90Å at B3LYP/6-311+G** level of theory. It increases to 2.00Å in **1b**. The H-H distances increase substantially in the homocyclic aluminum analogue of **1f** which is a minimum.[16]

Similar structure is also calculated to be a minimum for the isoelectronic, $Si_3H_3^+$,[30] where the unfavorable H--H interactions are not anticipated. However, similar structures of BSi_2H_3 and $B_3H_3^{2-}$ having penta-coordinate boron have one imaginary frequency. Each of them leads to the minimum energy structure corresponding to **1b**. The structural similarities of $BAl_2H_3^{2-}$ and BSi_2H_3 in **1a**, **1b** and **1f** further illustrate resemblance of silicon and aluminum hydrides (SiH and AlH^-). The bridging hydrogen atoms connected to boron in **1b** and in BSi_2H_3 (similar structure to **1b**) demonstrate the preference of out-of-plane bridging position. Similar several non-planar structures having stabilized π-MOs are unraveled in this study. A comparison of the stabilization of the π-MOs in going from the planar to the non-planar structures and their contribution to the total energies are given at the end.

The structure **1c** is not observed in homocyclic boron and aluminum analogues.[16] It has a planar tetra coordinated boron atom and the BH_2 group is slightly bent towards the aluminum atom having a terminal hydrogen atom. The terminal hydrogen atom of aluminum is also bent towards the BH_2 group. Important bonding interactions in this molecule can be visualized by interacting H-Al-Al and BH_2 fragments. The sp-hybrid lone pair of AlH is donated to the empty in-plane p-orbital of bare aluminum atom (scheme 2.6a). This results in 2c-2e bond between aluminum atoms. NBO analysis also supports this description. The second interaction (scheme 2.6b) is the hyperconjugative donation from the pseudo in-plane π-MO of BH_2 to the empty antibonding Al-H σ^* orbital. This explains the elongation of B-H (1.23Å) and Al-H bond lengths (1.68Å) and tilting of the BH_2 group towards the aluminum having the hydrogen atom. NBO analysis shows that

the stabilization energy due to hyperconjugation is 4.5kcal/mol. In addition, there is a delocalized π-MO, two 2c-2e B-H and one 2c-2e Al-H bond.

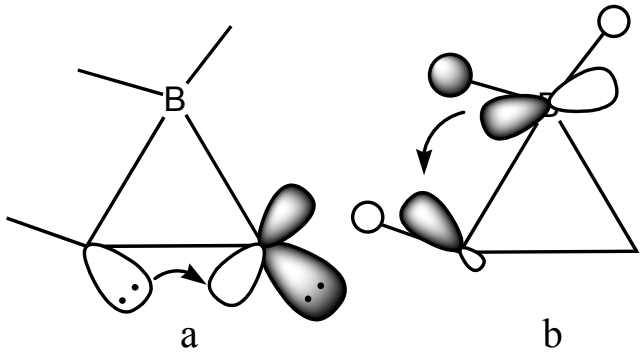

Scheme 2.6: Representations of (a) 2c-2e Al-Al bond and a lone pair on Al and (b) a hyperconjugative B-H and Al-H interaction in **1c**.

The structure **1d** has a bridging hydrogen atom between two aluminum atoms and one B-H and one Al-H terminal bonds. Homocyclic aluminum and boron analogues of **1d** are not stable.[16] A structure similar to **1d** in which hydrogen bridges between boron and silicon is a minima for BSi_2H_3.[18] Structure **1d** has an elongated Al-Al bond (2.69Å) and the shortest HB-AlH bond (2.00Å) among all structures studied here. This molecule can be considered as a combination of two fragments such as HAl-H-Al and BH. The mono bridged HAl-H-Al and its silicon analogues are characterized as minima.[20] The HAl-H-Al fragment donates its sigma lone pair to the in-plane empty p-orbital of the BH fragment (scheme 2.7a**)**. This forms a bend bond and results in short HB-AlH bond length (2.00Å).[31] A noteworthy feature in the HAl-H-Al fragment is the hyperconjugative donation from the pseudo in-plane π-orbital of the AlH_2 fragment into the empty p-orbital of the aluminum atom which forms a weak 3c-2e Al-H-AlH bond. It results in the elongation of Al-H bond lengths (1.92Å, 1.72Å) (figure 2.1). In addition, it has 2c-2e B-H and Al-H bonds and a delocalized π-MO over the ring.

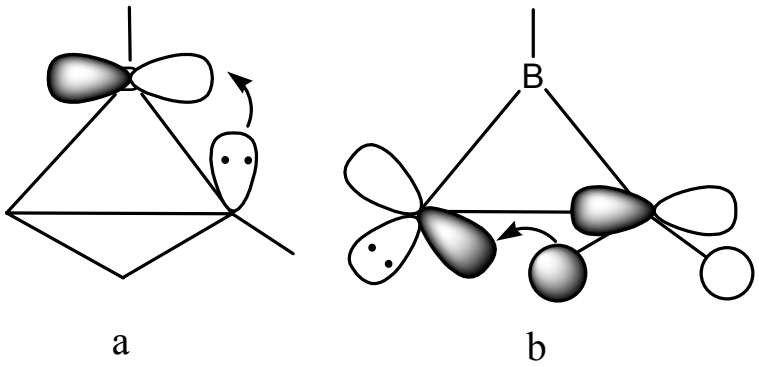

Scheme 2.7: Representations of (a) a 2c-2e bend B-Al bond and (b) a hyperconjugative 3c-2e Al-H-Al bond and a lone pair on Al in **1d**.

Classical structure **1e** has three terminal hydrogen atoms on each atom of three membered ring. It is 21.0 kcal/mol higher in energy than the global minima structure, **1a**. Corresponding aluminum analogue is 1.8 kcal/mol higher in energy than its global minimum structure.[16] The Al-Al and B-Al distances are shorter than their corresponding single bond distances and longer than the double bonds. The MOs of **1e** are similar to the classical Walsh orbitals of cyclopropenyl cation and a delocalized π-MO over the ring.

Structure **1g** is non-planar with a tetrahedral arrangement around boron and a bridging hydrogen atom between Al-Al bond. It is obtained by twisting of BH_2 group of **1a** by 90º. This structure is a first order saddle point and 30.6 kcal/mol higher in energy than **1a**. The imaginary vibrational frequency vector of **1g** leads to ring opened structure.

Structure **1h** is the highest energy minimum that we have obtained on the PES of $BAl_2H_3^{2-}$; 49.9 kcal/mol higher in energy than **1a**. A similar structure is a first order saddle point for homocyclic boron analogue, but second most stable structure for the aluminum analogue.[16] Both the B-Al and H-bridged Al-Al bond distances in **1h** are shorter compared to those in **1a**, with the exception of the Al-H_b

(bridging hydrogen). The electronic structure of **1h** has one 3c-2e Al-H-Al bridge to bind the two Al-Al atoms. As shown in scheme 2.8b, Al-H-Al bridge has a direct radial overlap between aluminum atoms and as a result Al-Al bond is shorter (2.47Å). Similarly, **1h** has two 2c-2e B-Al bonds. It is formed by the donation of lone pair of electron from the aluminum atom to the empty sp^2-hybrid orbital of boron as shown in the scheme 2.8a and results in shortening of B-Al bonds (2.09Å). In addition, **1h** has two 2c-2e Al-H bonds, a lone pair on B and a delocalized π-MO over the ring. The lone pair on boron makes the system extremely high in energy. The other structural alternative of **1h**, in which aluminum atom has a lone pair of electrons, on geometry optimization, converges to **1c** which is unusual.

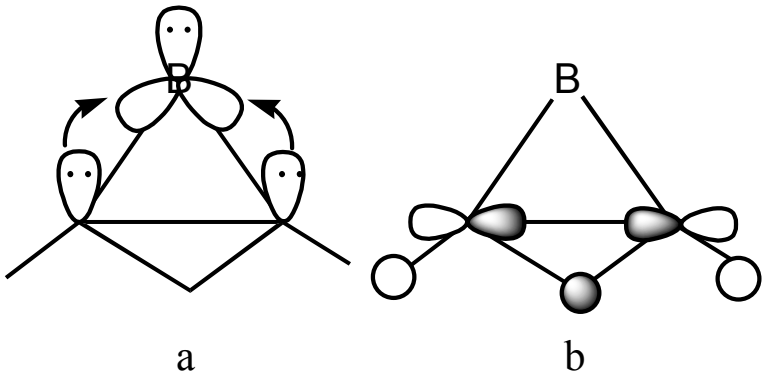

Scheme 2.8: Representations of (a) 2c-2e B-Al bonds and a lone pair on boron and (b) a 3c-2e Al-H-Al bond in **1h**.

The highly unstable cyclic structure of $BAl_2H_3^{2-}$, **1i**, having two hydrogen atoms bridging the Al-Al bond and a pyramidal boron atom is a transition state corresponding to the hydrogen shift from one aluminum atom to another in **1d**. The barrier for the hydrogen shift in **1d** is 42.2 kcal/mol. Similar structure for homocyclic boron and aluminum analogues is second and first order saddle points respectively.[16] It is interesting to note that the isoelectronic, BSi_2H_3, with planar arrangement around boron is a minimum at QCISD(T)/6-31G* level.[18]

In the view of large number of structures within a small range of energy, these structures were also optimized at QCISD(T)/6-311++G** level of theory. There were minimal differences in relative energies. The geometric parameters also did not change dramatically.

The structure and bonding study on various isomers of $BAl_2H_3^{2-}$ shows its similarities to BSi_2H_3 and brings the familiar isolobal analogy between SiH and AlH^-. The relative stabilities of the isomer of $BAl_2H_3^{2-}$ predict the preference of lower co-ordination at aluminum atoms and higher coordination at boron. Generally structures with lone pairs on each aluminum are more preferred over those having less number of lone pairs. Each of the isomers of $BAl_2H_3^{2-}$ provides several sites for protonation. Structures resulting from the sequential protonation of $BAl_2H_3^{2-}$ provide interesting bonding characteristics. Their electronic structure and inter-relationships are discussed next.

[2.3.2] Protonation Pathways of $BAl_2H_3^{2-}$ to $BAl_2H_4^-$, BAl_2H_5 and BAl_2H_6

The relative energy and the number of imaginary frequencies of all the isomers of $BAl_2H_4^-$, BAl_2H_5 and $BAl_2H_6^+$ are represented by schemes 2.3, 2.4 and 2.5. The number of minimum energy structures decreases as one goes from $BAl_2H_3^{2-}$ (six) to $BAl_2H_6^+$ (four). There are several unusual bonding arrangements in these compounds. For example, structures **1a, 1c, 2b** and **4d** have planar tetra-coordinate arrangement on boron. This is due to the electron deficiency of boron and as a result, it becomes more flexible to form multicentre bonding in comparison with carbon.[32] It is important to note that **1a** is the global minimum structure on the PES of $BAl_2H_3^{2-}$. The extra stability of **1a** is due to a combination of effects such as

the tendency for divalent nature of aluminum atoms, 3c-2e σ-Al-B-Al bond and a two π-electron delocalization over the ring.

Structures **1b**, **2a**, **2c**, **3d**, **3i**, **4a** and **4b** have penta-coordinate arrangement around the boron atom. A hexa-coordinate boron is seen in structure **4c**. Planar tetra-coordinate aluminum is present in **1e**, **1h**, **2b**, **2d**, **4a** and **4c**. The planar tetra coordinate boron atom and aluminum in the same structure is observed in **2b**.

The easiest way to understand most of these structures is to treat them as protonated structures obtained from one or the other isomers of $BAl_2H_3^{2-}$ (scheme 2.9). There are six minima available for $BAl_2H_3^{2-}$. Arrows in scheme 2.9 indicate the direct structural relationship that exists between all the minimum energy structures of $BAl_2H_3^{2-}$, $BAl_2H_4^{-}$, BAl_2H_5 and $BAl_2H_6^{+}$ via the protonation route. Several direct connections appear missing. This is because many obvious protonation paths lead to higher order stationary points. Even though these are followed up to their eventual minima, only the minimum energy structures are given here.

Let us for example consider the protonation chain; (**1b-2b(2c)-3d-4b**). Molecular orbital representation of the protonation route is shown in the scheme 2.10. The hydrogen atoms are not represented in the scheme 2.10. As described earlier, **1b** has two 3c-2e Al-H-BH bridges and one 3c-2e Al-B-Al ring and one 2c-2e B-H bond. In addition, it has lone pairs on each Al atoms and a bend π-MO between two aluminum atoms as shown in the scheme 2.10 **(1b)**. Both lone pairs and bend π-MO are out of the plane of the three membered ring and directed opposite to each other.

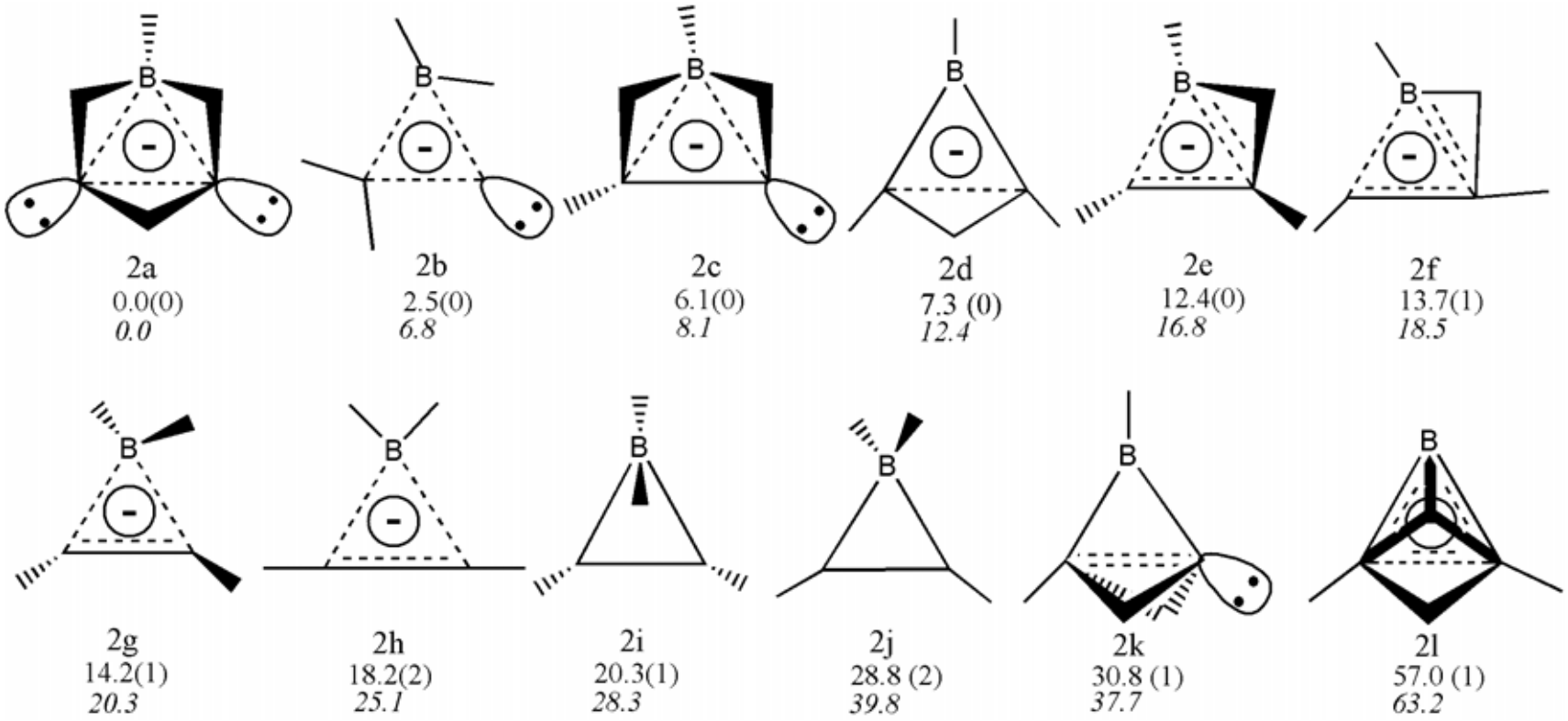

Scheme 2.3: Structures **2a-l**, relative energies (kcal/mol at B3LYP/6-311+G**, in italics at QCISD(T)/6-311++G** (single point energy of B3LYP/6-311+G** optimized geometry)) and the number of imaginary vibrational frequencies (in parentheses) for $BAl_2H_4^-$

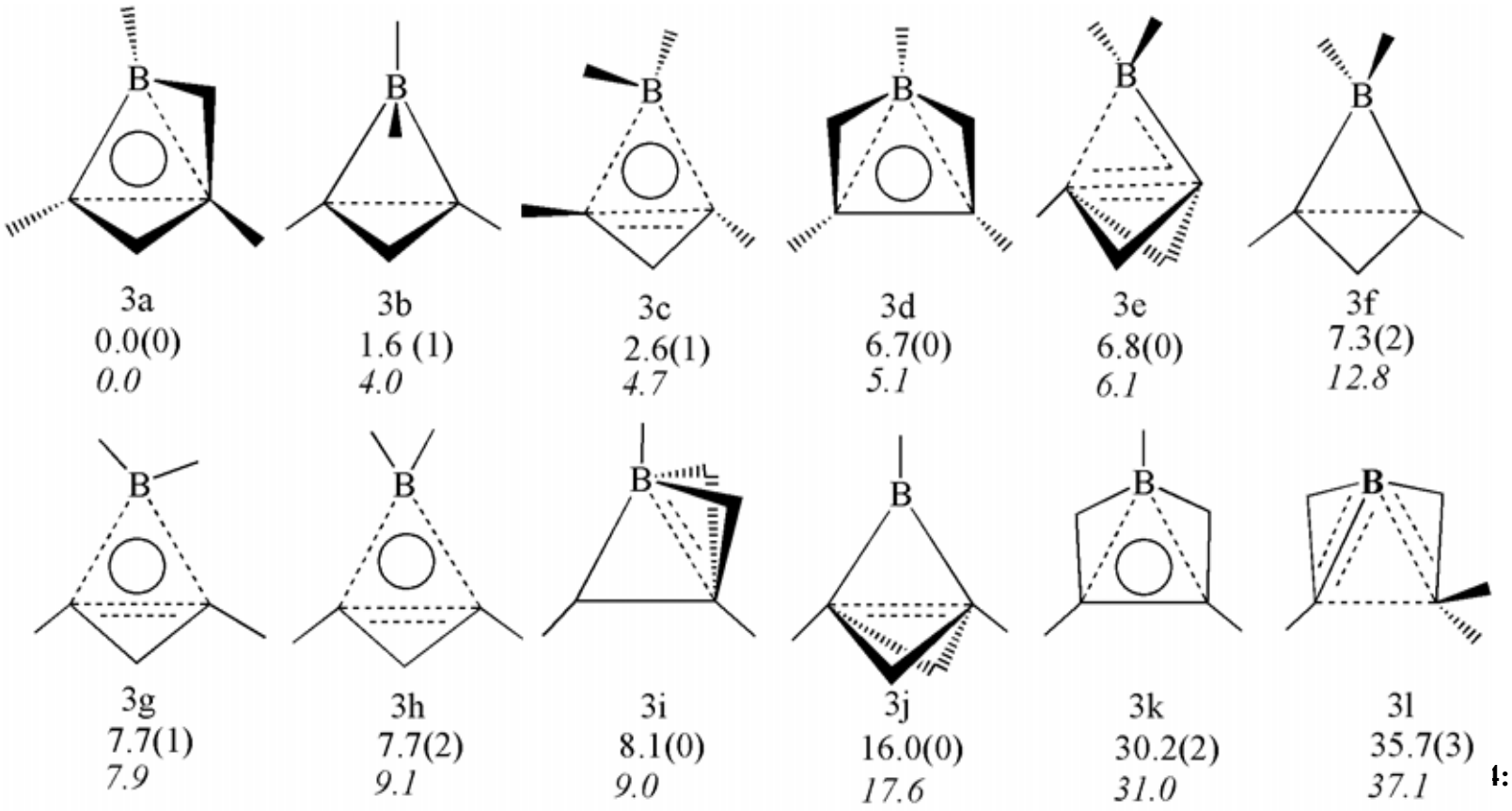

Scheme 2.4: Structures **3a-l,** relative energies (kcal/mol at B3LYP/6-311+G**, in italics at QCISD(T)/6-311++G** (single point energy of B3LYP/6-311+G** optimized geometry)) and the number of imaginary vibrational frequencies (in parentheses) for BAl_2H_5.

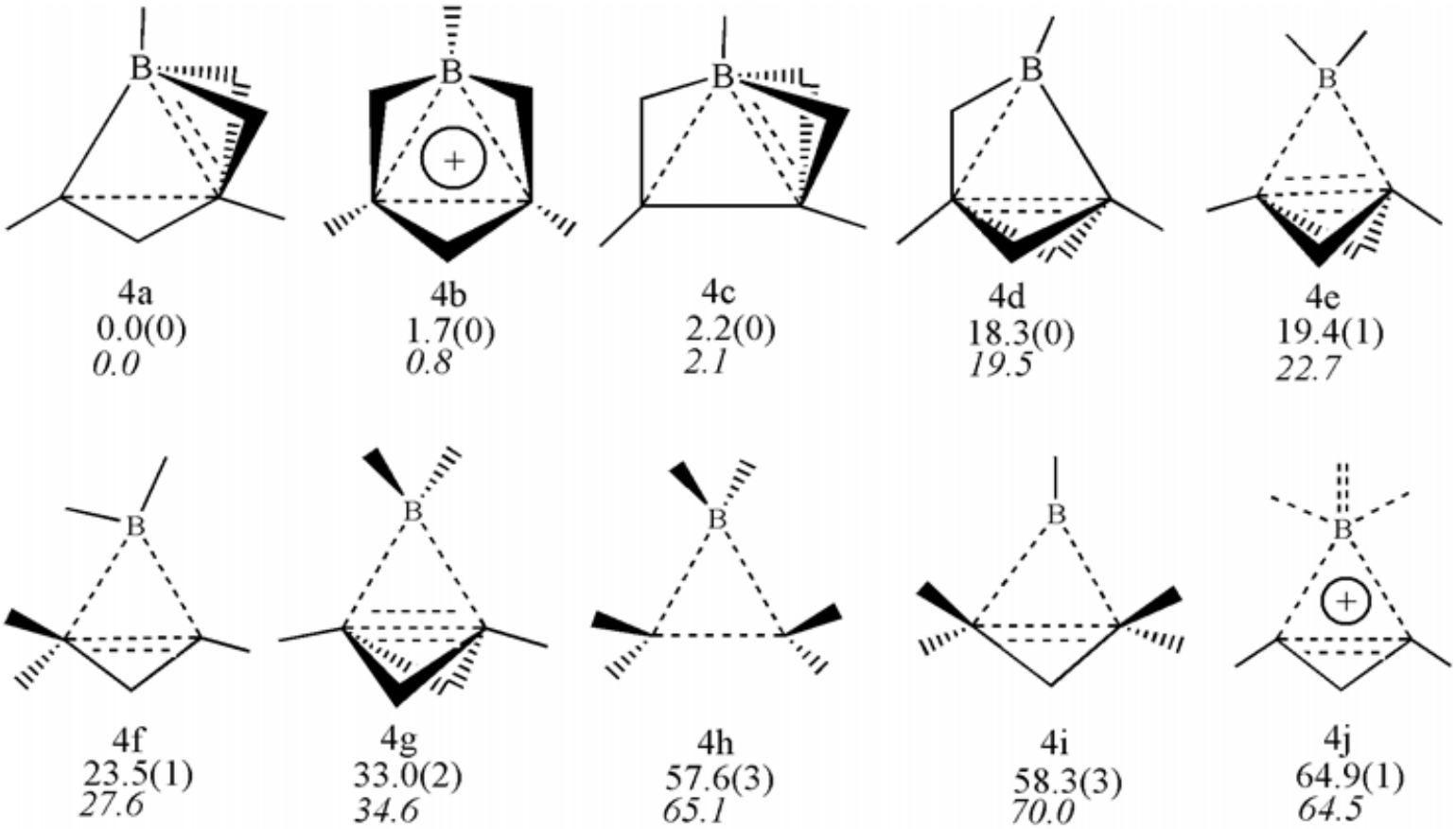

Scheme 2.5: Structures **4a-j,** relative energies (kcal/mol at B3LYP/6-311+G**, in italics at QCISD(T)/6-311++G** (single point energy of B3LYP/6-311+G** optimized geometry)) and the number of imaginary vibrational frequencies (in parentheses) for $BAl_2H_6^+$.

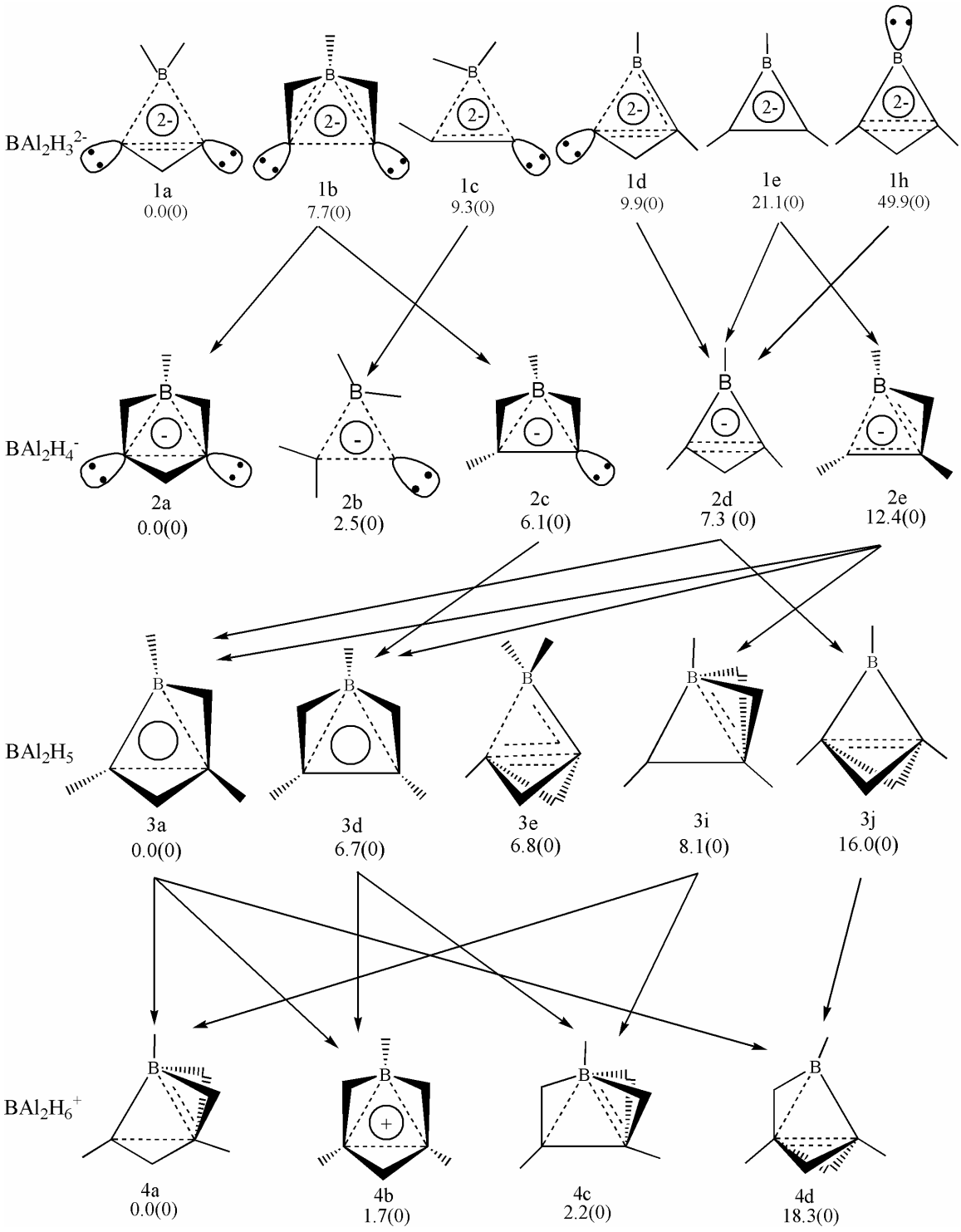

Scheme 2.9: Protonation route of $BAl_2H_n^m$ (n =3 - 6, m = -2 - +1) isomers.

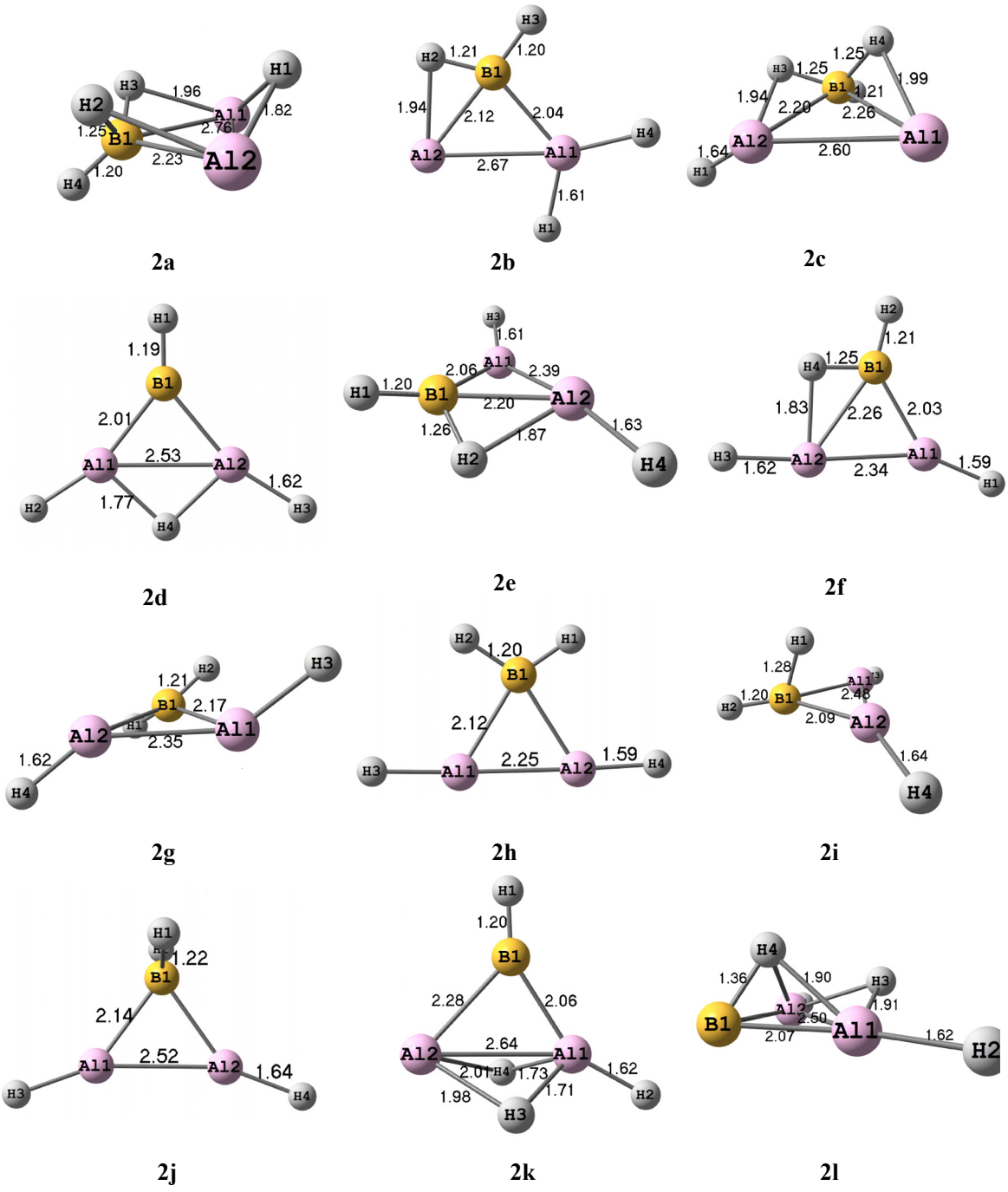

Figure 2.2: Optimized geometries and bond distances of $BAl_2H_4^-$ at B3LYP/6-311+G** level of theory.

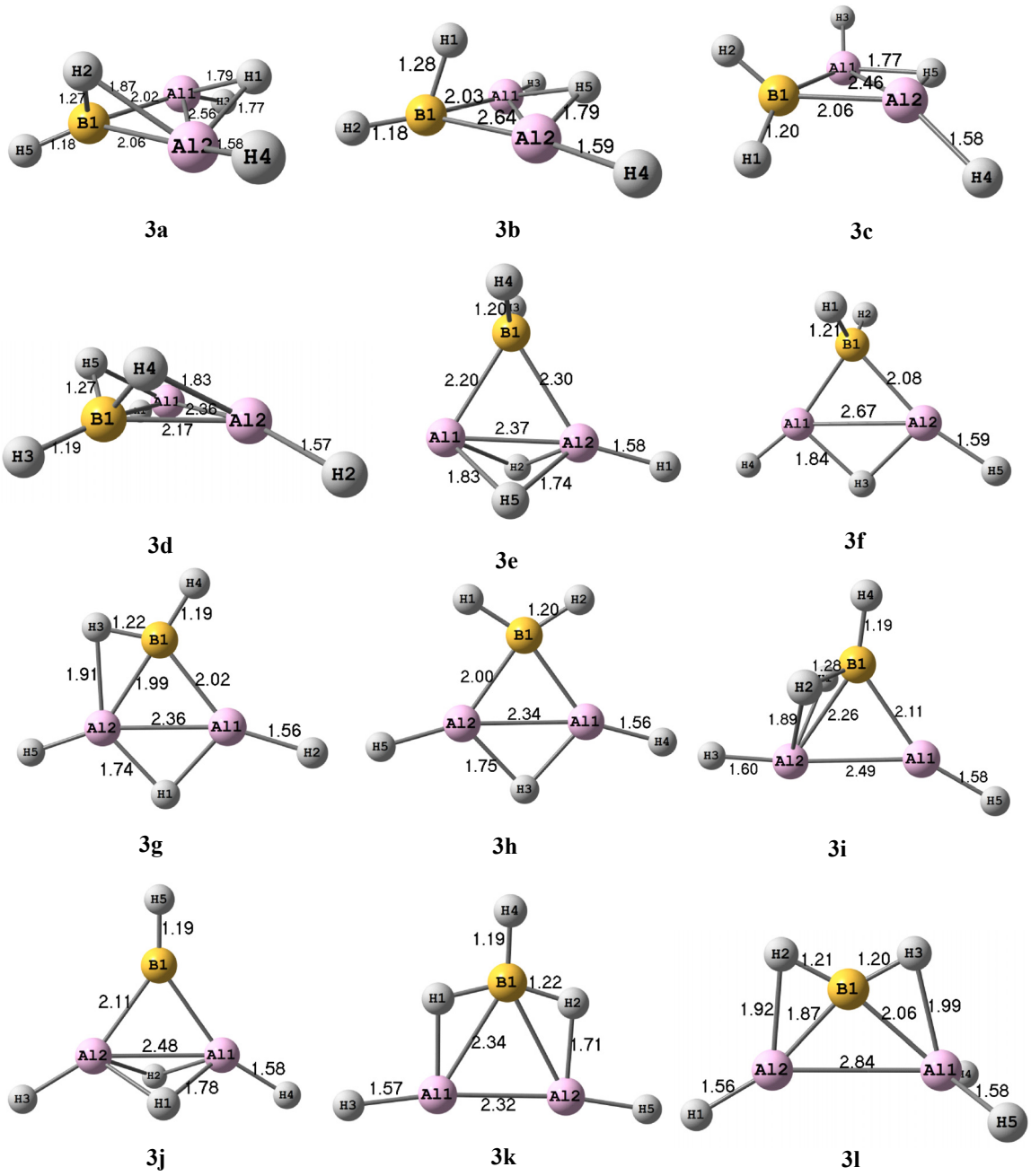

Figure 2.3: Optimized geometries and bond distances of BAl_2H_5 at B3LYP/6-311+G** level of theory.

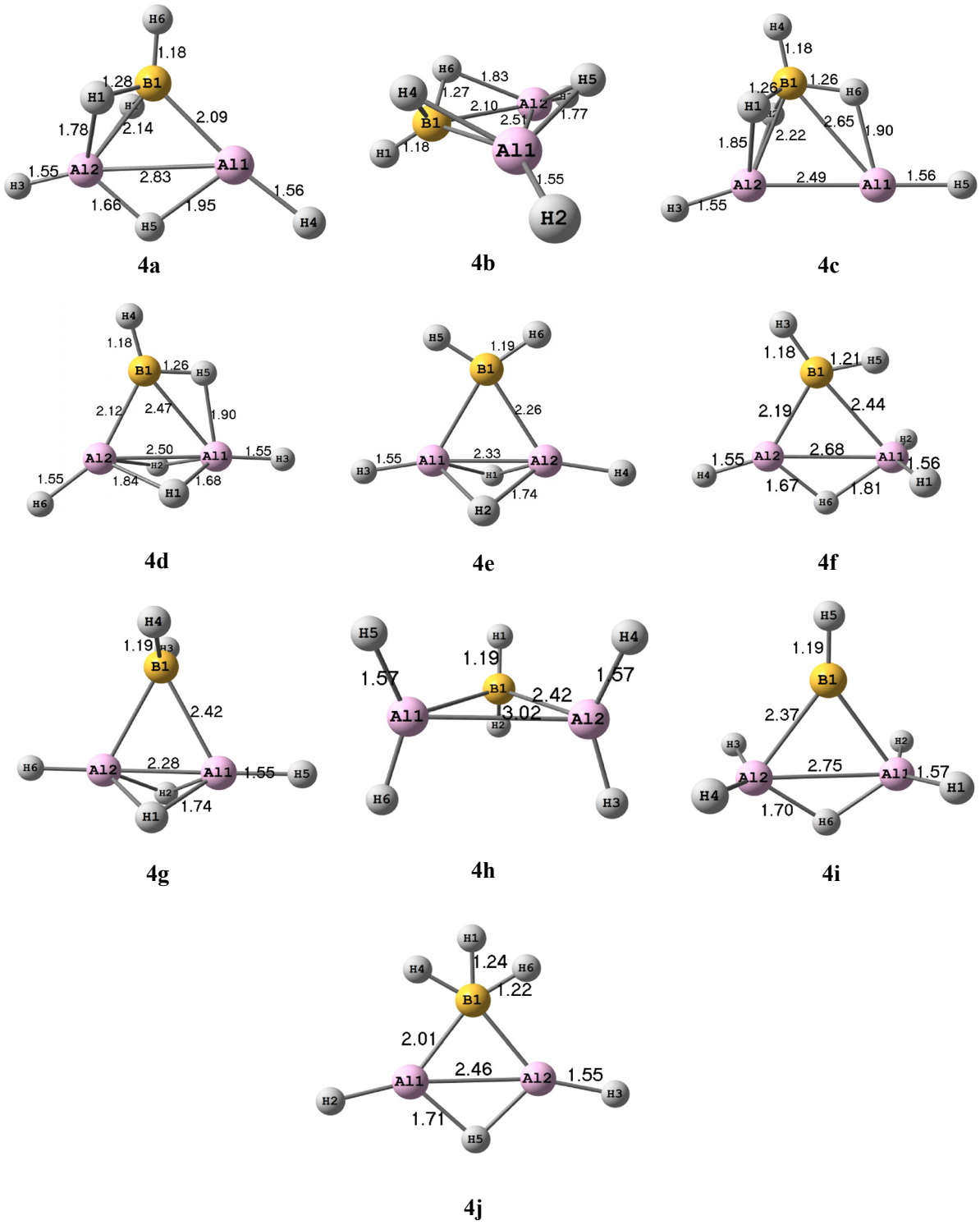

Figure 2.4: Optimized geometries and bond distances of $BAl_2H_6^+$ at B3LYP/6-311+G** level of theory.

The proton can be added to the more reactive nucleophilic centre of **1b**. These are the lone pairs on each aluminum atoms or bend π-MO of the Al-Al bond. The interaction of H^+ with lone pair on one of the aluminum atoms results in **2c**, with the terminal Al-H bond out of the ring plane. Similar structure is not observed for homocyclic boron or aluminum analogues. The addition of the H^+ to the bend π-MO of the Al-Al bond in **1b** results in **2a**, the cyclic global minimum structure of $BAl_2H_4^-$. Corresponding homocyclic aluminum analogue is 5.4kcal/mol (at B3LYP/6-31g*) higher in energy than its global minimum structure.[16] The structure **2c**, which has a lone pair one of the aluminum atoms, is 6.1kcal/mol higher in energy than **2a** which has lone pairs on each aluminum atom. There are no stable structures that results from the protonation of **2a**. It justifies that the more reactive nucleophilic centre is π-MO rather than the lone pair on aluminum atom.

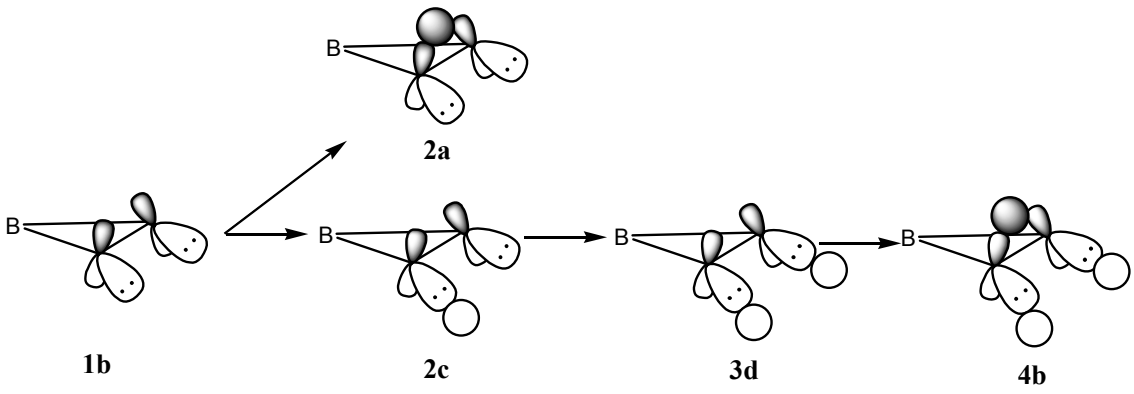

Scheme 2.10: Schematic molecular orbital representation for the protonation of **1b-(2a) 2c-3d-4b**. Some of the hydrogen atoms are left out for clarity. The structures are seen in schemes 2.2-2.5.

Addition of a proton to **2c** results in another terminal Al-H bond (**3d**). This terminal Al-H bond is also not in the ring plane. A structure similar to **3d** is the global minimum for homocyclic aluminum analogue, while its planar alternative is global minimum for homocyclic boron analogue. The addition of another proton on

3d results in bridging between two aluminum atoms (**4b**). Here, the three bridging hydrogens are on one side of the ring and the three terminal hydrogens on the other side. This structure is similar to the global minimum structure of $B_3H_6^+$.[16,17a] Here, the π-MO is stabilized further by mixing with the in-plane combination of the three s-orbitals of the bridging hydrogens. A similar structure is the third most stable among the isomers of $Al_3H_6^+$.[16] Planar alternative of **3d** is **3k**, which is a second order saddle point on the PES. Optimization in the direction of one of the imaginary vibrational frequency vector leads to the structure **3d**. Addition of H^+ to **3d** also results in **4c**, with three terminal and three bridging hydrogens. Two of the latter bridges the same B-Al bond. The third one bridges the next B-Al bond, and is in the BAl_2 plane.

The global minimum structures **1a** and **2a** do not have any protonation route that retains the same structural details. The higher order saddle point structures goes eventually to other structures. The structure **2b** is an unusual structure which has planar tetra-coordinate boron and aluminum atoms in the same structure. It can be obtained by the protonation at the lone pair on aluminum atom in **1c** (scheme 2.6a).

The structures **1d, 1e** and **1h** on protonation give the same product **2d**. **2d** is formed by the interaction of H^+ with lone pair on aluminum atom in **1d**, Al-Al in-plane sigma bond in **1e** and lone pair on boron atom in **1h**. This structure is minimum for homocyclic boron analogue and first order saddle point for aluminum analogue. The electronic structure of **2d** consists of one 2c-2e B-H, two Al-H and two B-Al bonds, a 3c-2e Al-H-Al bond and a delocalized π-MO. Protonation at B-Al in-plane sigma bond of **1e** results in **2f**. It is a transition state for the interconversion of **2e** and the energy barrier for the interconversion is 1.3kcal/mol.

In **2e**, all the terminal and bridging hydrogens are out of the plane of the three membered ring and tri-coordinated aluminum has pyramidal geometry. This is to be compared to the structure of $SiCBH_5$ with a pyramidal tri-coordinate boron[21] and its heavier analogues[16] in an unconstrained geometry. The classical structure **2j** which has two imaginary vibrational frequencies is considerably higher in energy. One of the imaginary vibrational frequency leads to **2j** where the p-orbitals of aluminum are brought to bonding. Though **2g** is a transition state, a structure similar to **2g** is a minimum in the PES of the homocyclic $Al_3H_3^{2-}$. Further twisting of BH_2 group in **2g** results in a bridging hydrogen atom at B-Al bond (**2e**). The energy difference between **2e** and **2g** are only 1.8kcal/mol at the B3LYP/6-311+G** level of theory. Anti van't Hoff structure **2h** is second order saddle point. Optimization in the direction of first imaginary vibrational frequency leads to **2f**, which is a transition state for the interconversion of **2e**.

2k and **2l** are first order stationary points. On optimization in the direction of the imaginary vector of **2l** leads to the structure, **2d**. The structure **2k** which has two bridging hydrogen atoms on Al-Al bond is a transition state which leads to **2b**.

The global minimum structure of BAl_2H_5, **3a** can be obtained by the protonation of **2d** and **2e**. All the terminal and bridging hydrogens are out of the plane of the three membered ring. Structures **3i** and **3j** are formed by the addition of two protons to the π-orbital at B-Al and Al-Al respectively in **1e**. The preference for hydrogen bridging at B-Al over Al-Al is reflected in the energy difference of 7.9 kcal/mol between **3i** and **3j**. Structure **3e** is an unusual structure, in that there is a tetrahedral co-ordination at boron, not seen in this series. The electronic structure of

3e consists of the two 2c-2e B-H bonds, one 2c-2e Al-H bond, one 2c-2e B-Al bond and two 3c-2e bonds between Al-Al-H and one 3c-2e bond between B-Al-Al.

Protonation of **2d** can also result in second order saddle point structures, **3f** (van't Hoff) and **3h** (anti van't Hoff). The first imaginary vibrational frequency of **3f** leads to the structure **3b**. This is a transition state for the shifting of bridging hydrogen atom between two B-Al bonds in **3a**. Similarly, the first imaginary vibrational frequency of **3h** leads to the structure **3c**. Optimization of the structure **3c** in the direction of the frequency vector leads to the structure **3a**. Structure **3g** is also a transition state for the out-of-plane distortion of hydrogen atoms in **3a**.

The global minimum structure, **3a**, on protonation gives three stable structures, **4a**, **4b** and **4d** depending on the position of protonation. Structures **4a**, **4c** and **4d** have two double bridged out-of-plane hydrogen atoms in one bond and one in-plane bridging hydrogen atom. All terminal hydrogen atoms are in the same plane of the ring. The significant molecular orbitals contributing to the bonding in **4a**, **4c** and **4d** are shown in the scheme 2.11. The preference for hydrogen bridging at B-Al over Al-Al explains the stability of **4a** and **4c** over **4d**. The higher stability of **4a** over **4c** is due to the preference of the in-plane bridging hydrogen at Al-Al rather than at B-Al bond. The energies of structures **2**, **3** and **4** were evaluated by single point calculation at QCISD(T)/6-311++G** using B3LYP/6-311+G** geometries. The relative energies (given in schemes 2.3, 2.4 and 2.5) did not change considerably.

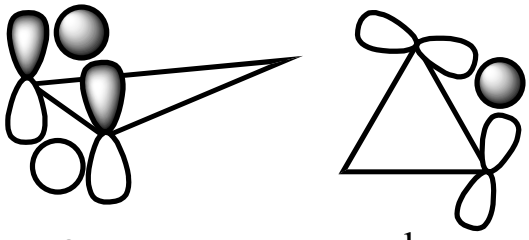

Scheme 2.11: Representations of (a) two out-of-plane bridging hydrogens and (b) an in-plane bridging hydrogen in **4a**, **4c** and **4d**.

Seven non-planar structures out of the 43 structures given in schemes 2.2-2.5 appear to have an option for a planar structure with all hydrogens remaining in the BAl_2 plane. Yet these seven are all non-planar, despite the fact that in the planar structures, there will be an undisturbed π-MO. Obviously significant stabilization is obtained by mixing the s-orbital of the bridging hydrogens and the in-plane p-orbitals with the π-orbital. The extent of this stabilizing effect is gauged by a correlation diagram (figure 2.5) connecting the π-MO energy at the planar geometry (middle of the plot, adjusted to zero) and the same MO in the non-planar geometry (left side). The relative energies correspond to twice the MO energy to reflect the occupancy of two electrons. As number of bridging hydrogen atoms increases the stabilization of the π-MO also increases. Maximum stabilization of the π-MO is seen for **4b** and **2a**, both having three bridging hydrogens. Structures with two bridging hydrogens **1b, 2c, 3a** and **3d** have less stabilizations of the π-MO on distortion from the planar structure. The least stabilization of the π-MO is calculated for the structure **2e** with one bridging hydrogen.

The extent of contribution of the π-MO to the stabilizing of non-planar structure is indicated by the parallel behavior of the total energy also plotted in figure 2.5, right hand side. However it is not only the stabilization of the π-MO that

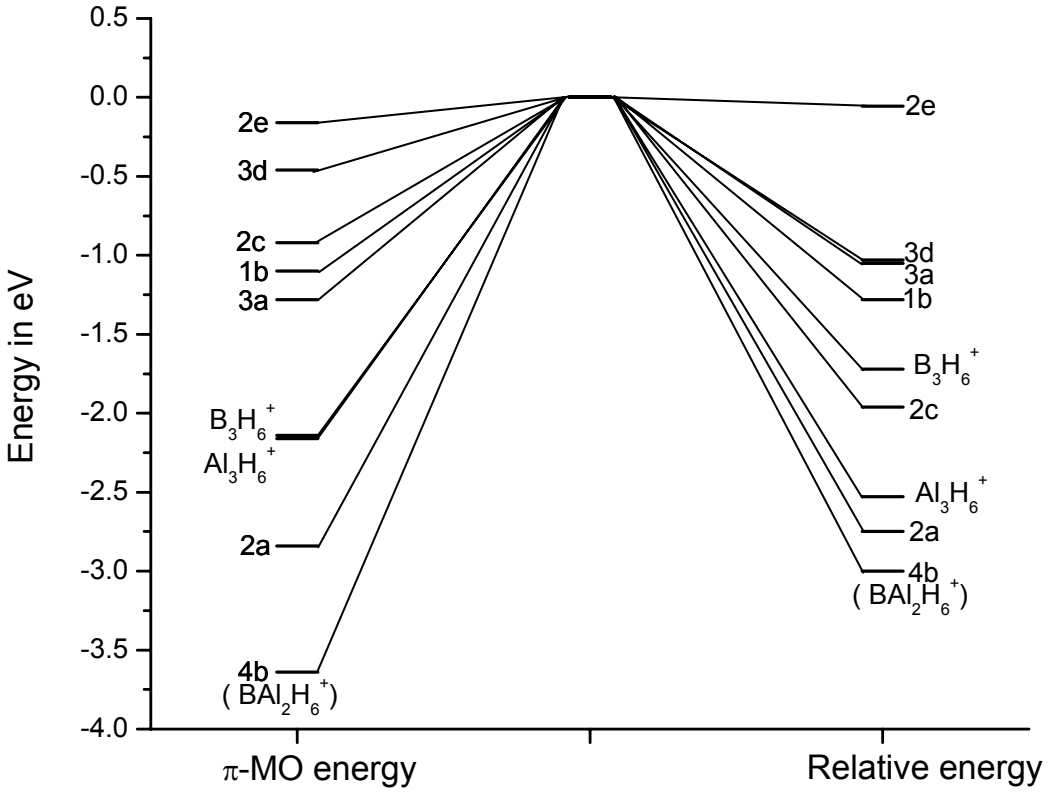

Figure 2.5: Stabilization of the π-MO of the structures having out-of-plane hydrogen bridges (left side) in comparison to corresponding planar structures. The relative energies of the structures in relation to the planar arrangement are shown on the right side. Relative π-MO and total energies of the homocyclic boron and aluminum analogues of structure **4b** are also shown.

controls the energetics. Another contribution to the decrease in energy of the non-planar structure is the H--H repulsion that exists in the planar structure. This is relieved in the non-planar structure. The steric repulsion is maximum when there are three bridging hydrogens in the planar structure, explaining the non-linear increase in energy with increasing number of bridging hydrogens. This is to be compared to the planar structures preferred for $B_3H_4^-$ (one bridging hydrogen) and B_3H_5 (two bridging hydrogens). Addition of the third bridging hydrogen as in $B_3H_6^+$ makes the structure non-planar, with the three bridging hydrogens pushed away from the B_3 plane and opposite to the three terminal B-H bonds. When the π-interactions in the planar arrangements are weak, the tendency for the non-planarity

increases. Thus, the structure with one bridging hydrogen ($Al_3H_4^-$) and two bridging hydrogens (Al_3H_5) are lowest in energy on their PES. Though a structure with three bridging hydrogens is a minimum in energy on the PES of $Al_3H_6^+$, the lowest energy isomer has four bridging hydrogens. This is not to say that there is no minimum energy structure with the in-plane bridging hydrogens. Structures **1d** and **2d** are planar structures with one bridging hydrogen each and show the delicate balance of the various factors that bestow stability to a structure.

The relative stabilization energy (RSE) for the minimum energy structures which contains π-delocalization is compared with corresponding homocyclic aluminum and boron analogues using the equations 1-7 (scheme 2.12). The sum of Al-Al, B-B and B-Al bond energies (equations 2.8, 2.9) would indicate that all reactions are endothermic by 17.7 kcal/mol. However, there are other factors involved. The high negative value of ΔE for **1a** is due to the more preferential position of lone pair on aluminum in comparison with boron atom. It has also contribution from the stronger B-H (≈93 kcal/mol) in comparison with the weaker Al-H bonds (≈69.2 kcal/mol). The positive value of **1e, 2d, 3a** and **3d** are the result of less π-delocalization through differential radial extension of p-orbital of aluminum and boron atoms. The stronger B-H-B bridge in relation to Al-H-Al bridge has also contributed to the endothermicity of **1h**, **2d**, **3a** and **3d**. The instability of lone pair on boron atoms leads to the high dramatic positive value for **1h**. The stabilization obtained by mixing of the π-MO with the in-plane σ-MO is larger for the structure **4b** than for the corresponding homocyclic boron and aluminum analogues (figure 2.5). This results in exothermicity of the equation 2.7 (scheme 2.12).

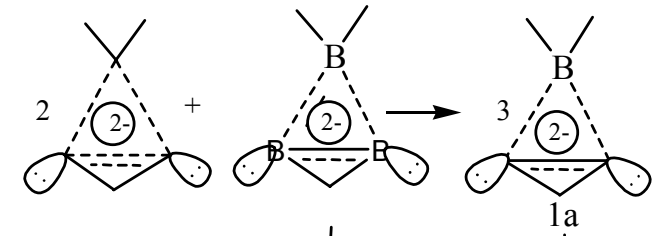

ΔE	Equation No.
−61.7 kcal/mol	(2.1)

1a

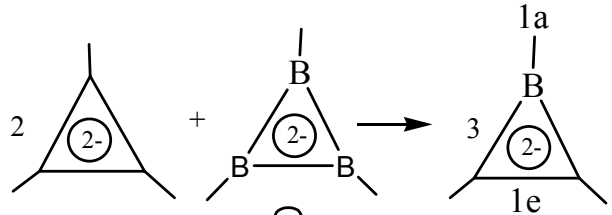

31.9 kcal/mol	(2.2)

1e

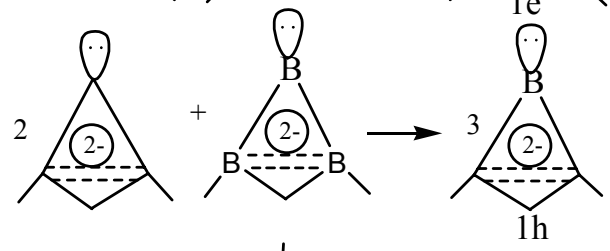

129.6 kcal/mol	(2.3)

1h

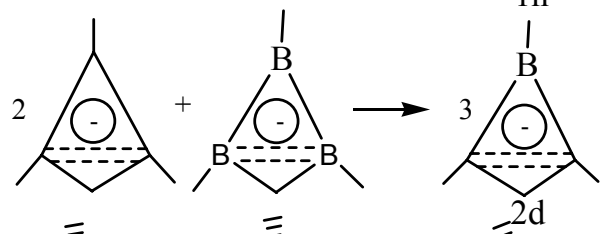

40.2 kcal/mol	(2.4)

2d

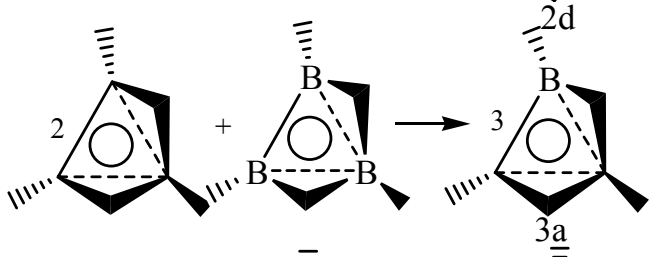

10.3 kcal/mol	(2.5)

3a

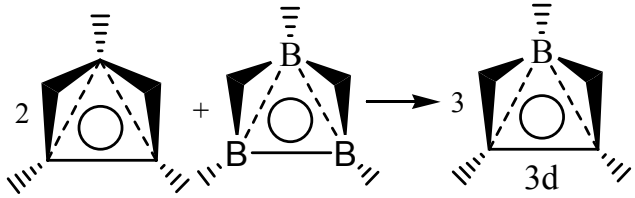

30.6 kcal/mol	(2.6)

3d

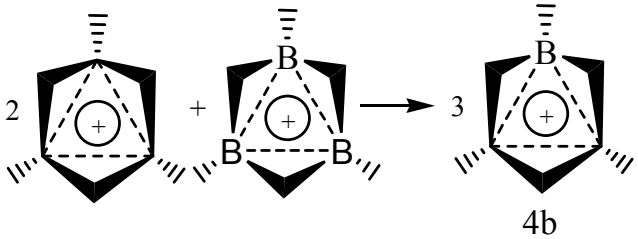

−18.9 kcal/mol	(2.7)

4b

5.8 kcal/mol	(2.8)

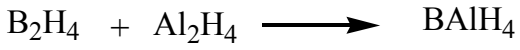

5.9 kcal/mol	(2.9)

Scheme 2.12

[2.4] Conclusions

The structure and bonding of $BAl_2H_n^m$ (n =3 - 6, m = -2 - +1) are compared with the corresponding homocyclic boron and aluminum analogues. Varying number of co-ordination mode is observed in these species. The $BAl_2H_3^{2-}$ shows similarities in geometrical and bonding pattern with BSi_2H_3. There are several unusual geometrical and bonding patterns such as planar tetra-coordinate boron and aluminum atoms in the same ring in $BAl_2H_4^-$ (**2b)** and divalent boron containing lone pair (**1h**) are common among them. Protonation route of $BAl_2H_3^{2-}$ to $BAl_2H_4^-$, BAl_2H_5 and $BAl_2H_6^+$ is also presented. Double hydrogen bridging is common in BAl_2H_5 and $BAl_2H_6^+$. The bridging hydrogen at the B-Al bond prefers to be out-side the plane of the three membered ring. The stabilization of the π-MO is a major contributor for the preference of non-planar structures with H-bridging. As number of bridging hydrogen atoms increases, the stabilization of the π-MO also increases. Most stable structures is the result of lower co-ordination of aluminum, higher co-ordination on boron and more bridging hydrogen atom between B-Al bonds. The relative stabilization energy (RSE) of $BAl_2H_n^m$ isomers depends on all these factors.

[2.5] References

(1) (a) Brown, H. C. *Boranes in Organic Chemistry*, Cornell University Press, Ithaca, 1972. (b) Brown, H.C.; Krishnamurthy, S. *Tetrahedron* **1979**, *35,* 567. (c) Pelter, A.; Smith, K.; Brown, H. C. *Borane Reagents (Best Synthetic Methods);* Academic Press: New York, 1988. (d) Cotton, F. A.; Wilkinson, G.; Murillo, C. A.; Bochmann, M. *Advanced Inorganic Chemistry,* 6th ed.; Wiley: New York, 1999. (e) Wehmschulte, R. J.; Power, P. P. *Polyhedron* **2000**, *19*, 1649. (f) Downs, A. J. *Coord. Chem. Rev.* **1999**, *189*, 59.

(2) (a) Burgess, K.; Ohlmeyer, M. J. *Chem. Rev.* **1991***, 91,* 1179. (b) Marks, T. J.; Kolb, J. R. *Chem. Rev.* **1977**, *77*, 263. (c) Barone, V.; Dolcetti, G.; Lelj, F.; Russo, N. *Inorg. Chem.* **1981***, 20,* 1687. (d) Ephritikhine, M. *Chem. Rev.* **1997**, *97*, 2193.

(3) (a) Sung, J.; Goedde, D. M.; Girolami, G. S.; Abelson, J. R. *J. Appl. Phys*. **2002**, *91*, 3904. (b) Jensen, J. A.; Gozum, J. E.; Pollina, D. M.; Girolami, G. S. *J. Am. Chem. Soc.* **1988**, *110*, 1643. (c) Wayda, A. L.; Schneemeyer, L. F.; Opila, R. L. *Appl. Phys. Lett.* **1988**, *53*, 361. (d) Tolle, J.; Roucka, R.; Tsong, I. S. T.; Ritter, C.; Crozier, P. A.; Chizmeshya, A. V. G.; Kouvetakis, J. *Appl. Phys. Lett.* **2003**, *82*, 2398. (e) Goedde, D. M.; Girolami, G. S. *J. Am. Chem. Soc.* **2004**, *126*, 12230.

(4) (a) Bogdanovic, B.; Schwickardi, M. *J. Alloys Compd.* **1997**, *253-254*, 1. (b) Grochala, W.; Edwards, P. P. *Chem. Rev.* **2004**, *104*, 1283. (c) Maltseva, N. N.; Golovanova, A. I. *Russ. J. Appl. Chem*. **2000**, *73*, 747. (d) Brinks, H. W.; Hauback, B. C.; Norby, P.; Fjellvåg, H. *J. Alloys Compd*. **2003**, *351*, 222. (e) Song, Y.; Singh, R.; Guo, Z. X. *J. Phys. Chem. B* **2006**, *110*, 6906. (f) Fu, Q.

J.; Ramirez-Cuesta, A. J.; Tsang, S. C**.** *J. Phys. Chem. B* **2006**, *110*, 711. (g) Vajeeston, P.; Ravindran, P.; Vidya, R.; Fjellvag, H.; Kjekshus, A. *Cryst. Growth Des.* **2004**, *4*, 471. (h) Dymova, T. N.; Konoplev, V. N.; Aleksandrov, D. P.; Sizareva, A. S.; Silina, T. A. *Russ. J. Coord. Chem*. **1995**, *21*, 165.

(5) (a) Marks, T. J.; Kennelly, W. J. *J. Am. Chem. Soc.* **1975**, *97*, 1439. (b) Beall, H.; Bushweller, C. H. *Chem. Rev.* **1973**, *73*, 465.

(6) (a) Power, P. P. *Chem. Rev.* **1999**, *99*, 3463. (b) Dill, J. D.; Schleyer, P. v. R.; Pople, J. A. *J. Am. Chem. Soc*. **1975**, *97*, 3402. (c) Knight, Jr., L. B.; Kerr, K.; Miller, P. K.; Arrington, C. A. *J. Phys. Chem*. **1995**, *99*, 16842. (d) Jouany, C.; Barthelat, J. C.; Daudey, J. P. *Chem. Phys. Lett*. **1987**, *136*, 52.

(7) (a) Yamaguchi, Y.; DeLeeuw, B. H.; Richards, Jr., C. A.; Schaefer, III, H. F.; Frenking, G. *J. Am. Chem. Soc.* **1994**, *116*, 11922. (b) Treboux, G.; Barthelat, J. C. *J. Am. Chem. Soc*. **1993**, *115*, 4870. (d) Armstrong, D. R. *Theor. Chim. Acta.* **1981**, *60*, 159. (e) McKee, M. L. *J. Phys. Chem.* **1991**, *95*, 6519. (f) Lammertsma, K.; Guener, O. F.; Drewes, R. M.; Reed, A. E.; Schleyer, P. v. R. *Inorg. Chem.* **1989**, *28*, 313.

(8) (a) Meller, A.; Maringgele, W. *Advances in Boron Chemistry* Siebert, W. Ed.; Royal Society of Chemistry Special Publication 201; 1997, p 224. (b) Maier, C. J.; Pritzkow, H.; Siebert, W. *Angew. Chem., Int. Ed. Engl.* **1999**, *38*, 1666.

(9) Chertihin, G. V.; Andrews, L. *J. Phys. Chem.* **1993**, *97*, 10295.

(10) (a) Mains, G. J.; Bock, C. W.; Trachtman, M.; Finley, J.; McNamara, K.; Fisher, M.; Wociki, L. *J. Phys. Chem.* **1990**, *94*, 6996.

(11) (a) Murrell, J. N.; Kroto, H. W.; Guest, M. F. *J. Chem. Soc., Chem. Commun.* **1977**, 619. (b) Hopkinson, A. C.; Lien, M. H. *J. Chem. Soc., Chem. Commun.*

1980, 107. (c) Gordon, M. S.; Koob, R. D. *J. Am. Chem. Soc.* **1981**, *103*, 2939. (d) Gordon, M. S.; Pople, J. A. *J. Am. Chem. Soc.* **1981**, *103*, 2945. (e) Gordon, M. S. *J. Am. Chem. Soc.* **1982**, *104*, 4352. (f) Hoffmann, M. R.; Yoshioka, Y.; Schaefer, III, H. F. *J. Am. Chem. Soc.* **1983**, *105*, 1084. (g) Hopkinson, A. C.; Lien, M. H.; Csizmadia, L. G. *Chem. Phys. Lett.* **1983**, *95*, 232. (h) Sherrill, C. D.; Schaefer, III, H. F. *J. Phys. Chem.* **1995**, *99*, 1949. (i) Nguyen, M. T.; Sengupta, D.; Vanquickenborne, L. G. *Chem. Phys. Lett.* **1995**, *244*, 83. (j) Stegmann, R.; Frenking, G. *J. Comput. Chem.* **1996**, *17*, 781. (k) Hilliard, R. K.; Grev, R. S. *J. Chem. Phys.* **1997**, *107*, 8823. (l) Apeloig, Y.; Karni, M. *Organometallics* **1997**, *16*, 310. (m) Stogner, S. M.; Grev, R. S. *J. Chem. Phys.* **1998**, *108*, 5458.

(12) Roseky, H. W. *Inorg. Chem.* **2004**, *43*, 7284.

(13) (a) Uhl, W. *Structure and Bonding*; Springer Verlag: Berlin, 2002; Vol. 105, pp 41-66. (b) Uhl, W.; Breher, F. *Eur. J. Inorg. Chem.* **2000**, 1. (c) Uhl, W.; Spies, T.; Koch, R.; Saak, W. *Organometallics* **1999**, *18*, 4598. (d) Cui, C.; Kopke, S.; Herbst-Irmer, R.; Roesky, H. W.; Noltemeyer, M.; Schmidt, H. -G.; Wrackmeyer, B. *J. Am. Chem. Soc.* **2001**, *123*, 9091.

(14) Cui, C.; Roesky, H. W.; Schmidt, H.-G.; Noltemeyer, M.; Hao, H.; Cimpoesu, F. *Angew. Chem., Int. Ed. Engl.* **2000**, *39*, 4274.

(15) (a) Himmel, H.–J. *Organometallics* **2003**, *22*, 2679. (b) Xie, Y.; Schaefer III, H. F. *J. Am. Chem. Soc.* **1990**, *112*, 5393.

(16) Srinivas, G. N.; Anoop, A.; Jemmis, E. D.; Hamilton, T. P.; Lammertsma, K.; Leszczynski, J.; Schaefer, III, H. F. *J. Am. Chem. Soc.* **2003**, *125*, 16397.

(17) (a) Jemmis, E. D.; Subramanian, G.; Srinivas, G. N. *J. Am. Chem. Soc.* **1992**, *114*, 7939. (b) Jemmis, E. D.; Subramanian, G. *Inorg. Chem.* **1995**, *34*, 6559. (c) Korkin, A. A.; Schleyer, P. v. R.; McKee, M. L. *Inorg. Chem.* **1995**, *34*, 961. (d) Schleyer, P. v. R.; Subramanian, G.; Dransfeld, A. *J. Am. Chem. Soc.* **1996**, *118*, 9988. (e) McKee, M. L.; Buehl, M.; Charkin, O. P.; Schleyer, P. v. R. *Inorg. Chem.* **1993**, *32*, 4549. (f) Krempp, M.; Damrauer, R.; DePuy, C. H.; Keheyan, Y. *J. Am. Chem. Soc.* **1994**, *116*, 3629. (g) Glukhovtsev, M. N.; Schleyer, P. v. R.; Hommes, N. J. R. v. E.; Carneiro J. W. d. M.; Koch, W. *J. Comput. Chem.* **1993**, *14*, 285. (h) McKee, M. L. *Inorg. Chem.* **1999**, *38*, 321. (i) McKee, M. L. *J. Am. Chem. Soc.* **1995**, *117*, 8001. (j) Skancke, A.; Liebman, J. F. *J. Mol. Struct. (THEOCHEM)* **1993**, *280*, 75.

(18) Subramanian, G.; Jemmis, E. D., Prasad, B.V. *Chem. Phys. Lett.* **1994**, *217*, 296.

(19) (a) Jemmis, E. D.; Prasad, B. V.; Tsuzuki, S.; Tanabe, K. *J. Phy. Chem.* **1990**, *94*, 5530. (b) Jemmis, E. D.; Prasad, B.V.; Prasad, P. V. A.; Tsuzuki, S.; Tanabe, K. *Proc. Ind. Acad. Sci.* (*Chem. Sci*.) **1990**, *102*, 107. (c) Subramanian, G.; Jemmis, E. D. *Chem. Phys. Lett.* **1992**, *200*, 567.

(20) Palagyi, Z.; Grev, R. S.; Schaefer, III, H. F. *J. Am. Chem. Soc*. **1993**, *115*, 1936.

(21) Giju, K. T.; Phukan, A. K.; Jemmis, E. D. *Angew. Chem., Int. Ed. Eng.* **2003**, *42*, 539.

(22) (a) Byun, Y. G.; Saebo, S.; Pittman, Jr., C. U. *J. Am. Chem. Soc.* **1991***, 113*, 3689. (b) Volpin, M. E.; Koreshkov, Y. D.; Dulova, V. G.; Kursanov, D. N. *Tetrahedron* **1962**, *18*, 107. (c) Pittman, Jr., C.U.; Kress, A.; Patterson, T. B.;

Walton. P.; Kispert, L. D. *J. Org. Chem.* **1974**, *39*, 373. (d) Krogh-Jespersen, K.; Cremer, D.; Dill, J. D.; Pople, J. A.; Schleyer, P. v. R. *J. Am. Chem. Soc*. **1981**, *103*, 2589. (e) van der Kerk, S. M.; Budzelaar, P. H. M.; Van Eekeren, A. H. M.; van der Kerk, G. J. M. *Polyhedron* **1984**, *3*, 271. (f) Eisch, J. J.; Shatii, B.; Rheingold, A. L.; *J. Am. Chem. Soc*. **1987**, *109*, 2526. (g) Eisch, J. J.; Shafii, B.; Odom, J. D.; Rheingold, A. L. *J. Am. Chem. Soc*. **1990**, *112*, 1847. (h) Bouhadir, G.; Bourissou, D. *Chem. Soc. Rev.* **2004**, *33*, 210. (i) Höfner, A.; Ziegler, B.; Hunold, R.; Willershausen, P.; Massa, W.; Berndt, A. *Angew. Chem., Int. Ed. Engl.* **1991**, *30*, 594. (j) Menzel, M.; Steiner, D.; Winkler, H.-J.; Schweikart, D.; Mehle, S.; Fau, S.; Frenking, G.; Massa, W.; Berndt, A. *Angew. Chem., Int. Ed. Engl.* **1995**, *34*, 327. (k) Korkin, A. A.; Schleyer, P. v. R.; Arx, U. V.; Keese, R. *Struct. Chem.* **1995**, *6*, 225.

(23) (a) Nakajima, A.; Kishi, T.; Sugioka, T.; Kaya, K. *Chem. Phys. Lett*. **1991**, *187*, 239. (b) Jiang, Z.-Y.; Yang, C. -J.; Li, S. -T. *J. Chem. Phys.* **2005**, *123*, 204315. (c) Kawamata, H.; Negishi, Y.; Nakajima, A.; Kaya, K. *Chem. Phys. Lett.* **2001**, *337*, 255.

(24) Kawamura, H.; Kumar, V.; Sun, Q.; Kawazoe, Y. *Phys. Rev. B.* **2001**, *65*, 045406.

(25) Hehre, W.; Radom, L.; Schleyer, P. v. R.; Pople, J. A. *Ab Initio Molecular Orbital Theory*; Wiley: New York, 1986.

(26) (a) Becke, A. D. *J. Chem. Phys.* **1993**, *98*, 5648. (b) Becke, A. D. *Phys. Rev. A* **1988**, *38*, 3098. (c) Lee, C.; Yang, W.; Parr, R. G. *Phys. Rev. B* **1988**, *37*, 785. (d) Vosko, S. H.; Wilk, L.; Nusair, M. *Can. J. Phys.* **1980**, *58*, 1200.

(27) Gaussian 03, Revision C.02, Frisch, M. J.; Trucks, G. W.; Schlegel, H. B.; Scuseria, G. E.; Robb, M. A.; Cheeseman, J. R.; Montgomery, Jr., J. A.; Vreven, T.; Kudin, K. N.; Burant, J. C.; Millam, J. M.; Iyengar, S. S.; Tomasi, J.; Barone, V.; Mennucci, B.; Cossi, M.; Scalmani, G.; Rega, N.; Petersson, G. A.; Nakatsuji, H.; Hada, M.; Ehara, M.; Toyota, K.; Fukuda, R.; Hasegawa, J.; Ishida, M.; Nakajima, T.; Honda, Y.; Kitao, O.; Nakai, H.; Klene, M.; Li, X.; Knox, J. E.; Hratchian, H. P.; Cross, J. B.; Bakken, V.; Adamo, C.; Jaramillo, J.; Gomperts, R.; Stratmann, R. E.; Yazyev, O.; Austin, A. J.; Cammi, R.; Pomelli, C.; Ochterski, J. W.; Ayala, P. Y.; Morokuma, K.; Voth, G. A.; Salvador, P.; Dannenberg, J. J.; Zakrzewski, V. G.; Dapprich, S.; Daniels, A. D.; Strain, M. C.; Farkas, O.; Malick, D. K.; Rabuck, A. D.; Raghavachari, K.; Foresman, J. B.; Ortiz, J. V.; Cui, Q.; Baboul, A. G.; Clifford, S.; Cioslowski, J.; Stefanov, B. B.; Liu, G.; Liashenko, A.; Piskorz, P.; Komaromi, I.; Martin, R. L.; Fox, D. J.; Keith, T.; Al-Laham, M. A.; Peng, C. Y.; Nanayakkara, A.; Challacombe, M.; Gill, P. M. W.; Johnson, B.; Chen, W.; Wong, M. W.; Gonzalez, C.; and Pople, J. A.; Gaussian, Inc., Wallingford CT, 2004.

(28) (a) Fujimoto, H.; Hoffmann, R. *J. Phys. Chem.* **1974**, *78*, 1167. (b) Hoffmann, R. *Angew. Chem., Int. Ed. Engl.* **1982**, *21*, 711.

(29) Reed, A. E.; Curtiss, L. A.; Weinhold, F. *Chem. Rev.* **1988**, *88*, 899.

(30) (a) Jemmis, E. D.; Srinivas, G. N.; Leszczynski, J.; Kapp, J.; Korkin, A. A.; Schleyer, P. v. R. *J. Am. Chem. Soc.* **1995**, *117*, 11361. (b) Srinivas, G. N.; Jemmis, E. D.; Korkin, A. A.; Schleyer, P. v. R. *J. Phys. Chem. A.* **1999**, *103*, 11034. (c) So, S. P. *Chem. Phys. Lett.* **1998**, *291*, 523.

(31) Jemmis, E. D.; Pathak, B.; King, R. B.; Schaefer, III, H. F. *Chem. Commun.* ***2*****006**, 2164.

(32) (a) Wang, Z.-X.; Schleyer, P. v. R. *J. Am. Chem. Soc.* **2001**, *123*, 994. (b) Rasmussen, D. R.; Radom, L. *Angew. Chem., Int. Ed. Engl.* **1999**, *38*, 2875. (c) Röttger, D.; Erker, G. *Angew. Chem., Int. Ed. Engl.* **1997**, *36*, 813. (d) Collins, J. B.; Dill, J. D.; Jemmis, E. D.; Apeloig, Y.; Schleyer, P. v. R.; Seeger, R.; Pople, J. A. *J. Am. Chem. Soc.* **1976**, *98*, 5419. (e) Hoffmann, R.; Alder, R. W.; Wilcox, Jr.,C. F. *J. Am. Chem. Soc.* **1970**, *92*, 4992.

CHAPTER 3

THE EFFECT OF METAL COMPLEXATION ON RING OPENING OF BOWL SHAPED HYDROCARBONS: A THEORETICAL STUDY

[3.0] Abstract

DFT study on benzenoid and tris-acetylenic structure of fullerene and its fragments shows that tris-acetylenic model structures lead to benzenoid model structure, due to the proximity of π-orbitals in the former. The tris–acetylenic model structures are stabilized on metal complexation in comparison to the parent benzene-acetylene equilibrium. In going from Cr to Co, the acetylenic metal complex becomes more stabilized than benzene-metal complex. The curved surface of the tris-acetylenic fullerene fragments causes one set of π-orbital of the tris-acetylenic groups to rehybridize so as to bend more towards the metal fragments than found in the parent acetylene complexes. This leads to the increased overlap between metal fragments and tris-acetylenic model structures. The benzenoid and tris-acetylenic model complexes of $C_{12}H_6$ and $C_{12}H_{12}$ where five membered rings are replaced with more strained four membered rings are also studied.

[3.1] Introduction

The contiguous unsaturation of fullerene C_{60} and bowl shaped hydrocarbons has led to fascinating organometallic chemistry.[1,2] Synthesis of the organometallic complex, η^2-$C_{60}Pt(PPh_3)_2$ started the exohedral orgnometallic chemistry of fullerenes.[3] Several fullerene transition metal complexes have been reported since then.[2] Most of them are η^2-complexes and the major driving force for their formation is the release of strain energy.[4]

Equally intriguing is the endohedral complexes of fullerenes.[5] In fact fullerenes with one or more metals inside heralded the metal chemistry of fullerenes.[5] One of the concerns in the recent years has been to find ways to open the cluster.[6] In addition to the obvious possibilities for functionalization, this may provide a way to condense fullerenes to form nanotubes[7] with or without constrictions. One of the possibilities to open up a fullerene is to dismantle a six-membered ring (figure 3.1). The product of the retro-cycloaddition of a benzenoid ring, the tris-acetylenic structure, is so high in energy that theoretically no stationary point is obtained for this using any SCF method. Attempts have been made to compare this with the benzene-acetylene reaction and find ways in which the tris-acetylenic structures can be stabilized.[8] The ring opening of C_{60} and its fragments is compared with the reverse process of the well-known catalytic conversion of acetylene into benzene.[9] In our attempt to find a system where tris-acetylenic side is more stable than the benzenoid, we tried varying the metal fragments and the environment around tris-acetylenic unit. It is desirable to try metal fragments with differing capabilities to bind with the open and closed structures so that these could

be stabilized at the extremes. The steric and orbital requirements can be changed by going to smaller hydrocarbon models with lower curvature.

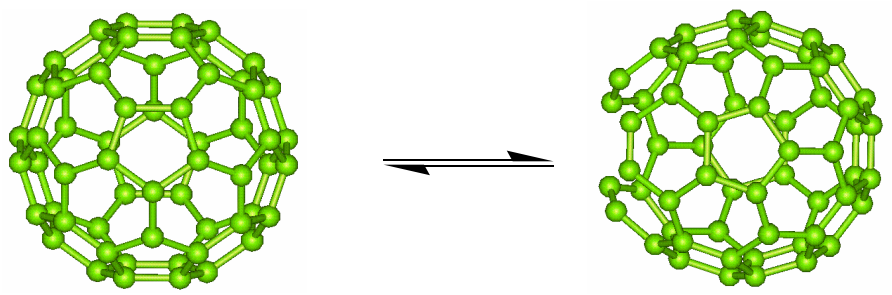

(3.1)

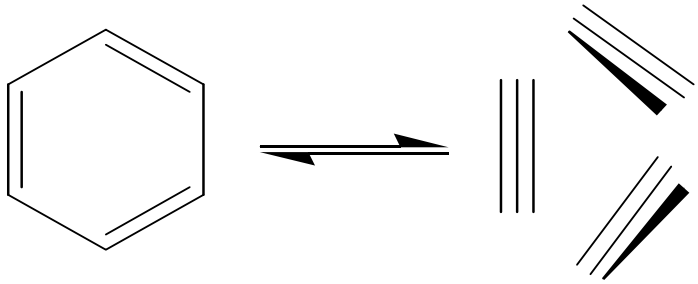

Figure 3.1: Benzene-acetylene equilibrium and benzeniod and tris-acetylenic structure of fullerene.

Our group had previously studied both these approaches in a limited way using semi-empirical SCF-MO calculations. Those studies on the structure and energetics of exohedral η^5-and η^6-transition metal organometallic complexes of C_{60} and C_{70} showed that suitable transition metal fragment (ML) such as C_3H_3Co and C_4H_4Fe could overcome to a large extent the unfavorable interaction[10] arising from the splayed out π-orbital of the five and six membered rings of C_{60} and C_{70} on complexation.[11] Studies on sumanene (single point Hartree-Fock and hybrid density functional theory calculation on PM3 optimized geometry) and C_6H_6ML (C_6H_6 constrained geometry) had also suggested similar possibilities.[11] It was also showed that the acetylenic bonds of the ring-opened structure of C_{60} and C_{70} can be stabilized

by the transition metal fragments of the form C_nH_nM, where n=3 to 6 and M=Cr, Mn, Fe, Co, and Rh.[8] While these are encouraging, more reliable results at better levels of theory are clearly needed in this area. The current attempt is to study these problems by Density Functional Theory (DFT), expanding the substrates as well. It is also necessary to seek more strained models so that stable ring-opened structures are more favorable. Our results on complexes of C_6H_6, $C_{21}H_{12}$, $C_{36}H_{12}$, C_{60} and highly strained hydrocarbons, $C_{12}H_6$ and $C_{12}H_{12}$, where five membered rings are replaced with more strained four membered rings are detailed in this chapter.

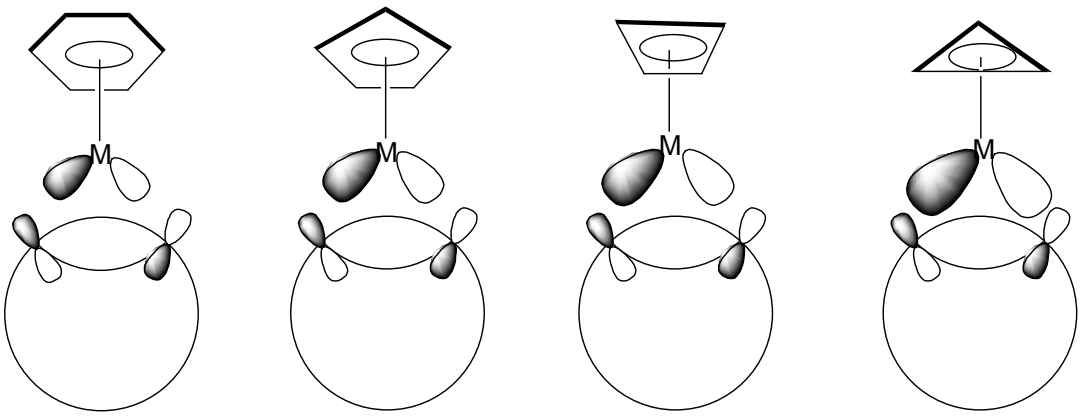

Scheme 3.1: Schematic representation for the diffuse nature of the different metal fragments.

It has been established that the fragment molecular orbitals of C_nH_nM become more diffuse with decreasing value of n (scheme 3.1).[11] The additional way of increasing the size of the orbital is to use heavier metals. Thus we selected CrC_6H_6, MnC_5H_5, FeC_4H_4, CoC_3H_3 and RhC_3H_3 as metal fragments so that the fragment molecular orbitals become progressively more diffuse. This can be compared with the recent experimental observation on $(C_{60}Me_5)FeC_5H_5$.[12] In any such fullerene fragment-ML combination, the electron count around the metal has to be carefully controlled. All complexes considered here have 18 electrons around the

metal. The C-C bonds in the 6-membered rings of C_{60} and its fragments are of two kinds, one that is a part of 6-membered rings and the other which is a part of 5-membered rings. The C-C bonds of former kind are shorter than the latter. It must be easier to cleave the longer C-C bonds. Thus the resulting tris-acetylenic structures should have three disconnected 6-membered rings capped by a transition metal fragment.

[3.2] Computational Details

All calculations are carried out using ADF (Amsterdam Density Functional) package.[13] The total bonding energy of each molecule is calculated using the generalized gradient approximation at Becke-Perdew level. This includes the Becke's non-local correction[14] to the local exchange energy expression and the Perdew's non-local correction[15] to the local expression of the correlation energy. Within ADF program Slater Type Orbital (STO) basis set with double ζ quality without polarization functions are employed. Inner shells are treated within the frozen core approximation (1s for C and up to 3p for Cr-Co and Rh). The total bonding energy of ring opened and closed structure with and without metal complexation is shown in table 3.1. The optimized geometries are shown in figure 3.2.

Table 3.1: Total bonding energy (in kcal/mol) of benzenoid and tris-acetylene model structures (open) of fullerene C_{60} and its fragments with and without metal complexation.

C_nH_m	Total energy	Total energy for metal complexation	
		FeC_4H_4	CoC_3H_3
C_6H_6	-1669.8	-2904.4	-2581.8
C_2H_2	-504.2	-2749.7	-2433.5
$C_{21}H_9$	-4733.0	a	-5635.9
$C_{21}H_9$-open	a	a	-5505.7
$C_{36}H_{12}$	-7911.1	-8805.6	-8811.3
$C_{36}H_{12}$-open	a	-8722.6	-8705.6
C_{60}	-11363.6	-12588.7	-12265.3
C_{60}-open	a	-12503.6	-12174.2
$C_{12}H_6$	-2645.9	-3870.8	-3558.4
$C_{12}H_6$- open	-2678.6	-3916.0	-3602.2
$C_{12}H_{12}$	-3264.9	-4504.4	-4180.6
$C_{12}H_{12}$-open	-3215.4	-4455.3	-4142.2

'a' indicates that the specific structure is not a stationary point.

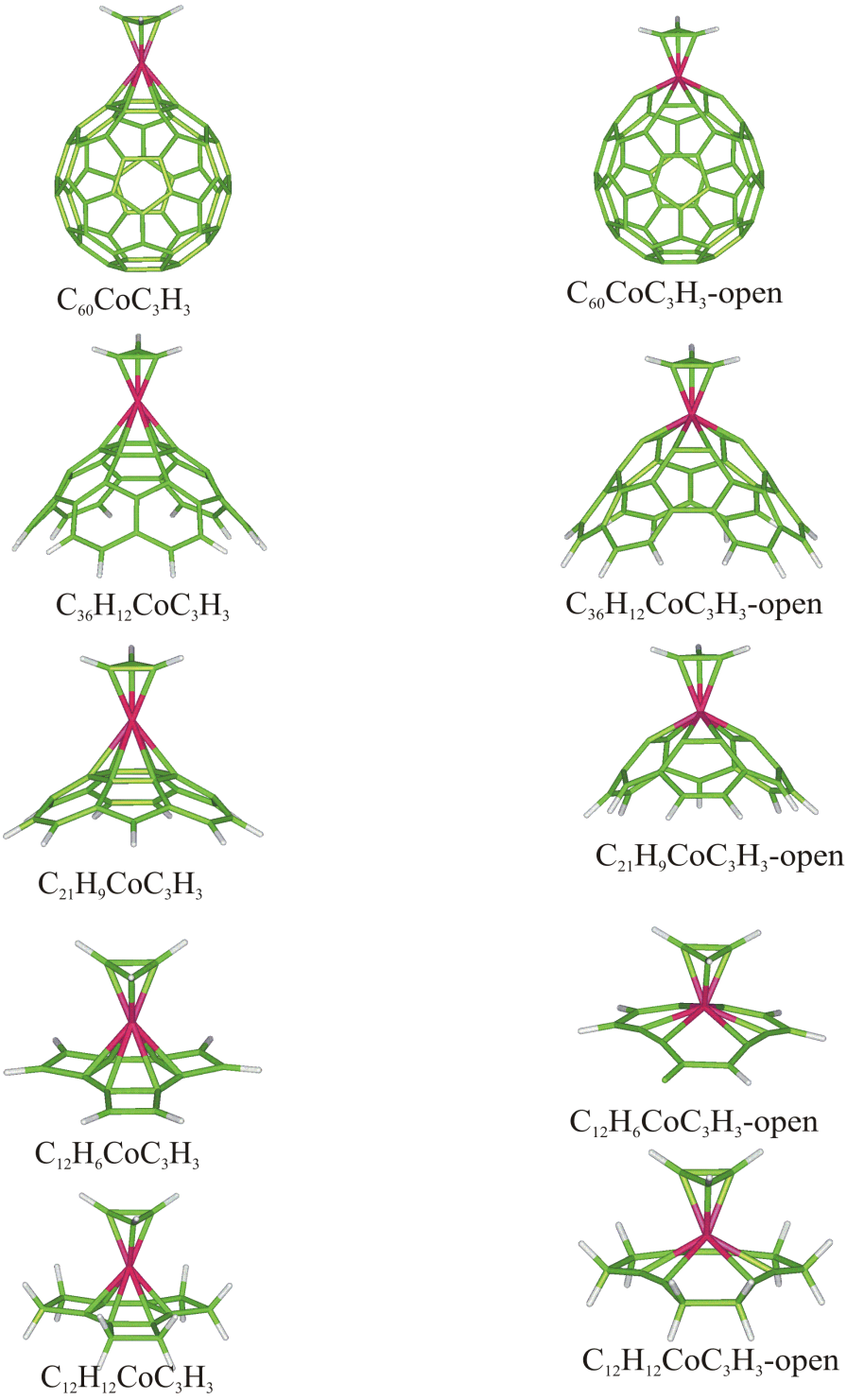

Figure 3.2: Optimized geometries of benzenoid and tris-acetylenic model metal complexes of fullerene and its fragments.

[3.3] Results and Discussion

The molecules studied are C_{60}, $C_{36}H_{12}$, $C_{21}H_9$, $C_{12}H_6$ and $C_{12}H_{12}$. Benzenoid and tris-acetylenic structure of fullerene and its fragments can be compared with benzene-acetylene equilibrium (equation 3.1, figure 3.1).

The reaction energy of the benzene-acetylene equilibrium obtained by DFT method is found to be endothermic by 157.2 kcal/mol, higher than the value obtained at PM3 (128.6 kcal/mol) (table 3.2). At PM3 level, the tris-acetylenic structure (open structure) of C_{60} is calculated to be less stable than the benzenoid structure (closed structure) by 255.4 kcal/mol. All the tris-acetylenic structures without metal complexation collapse to the benzenoid structure on optimization at the DFT level.

Table 3.2: The reaction energy (kcal/mol) obtained from equation 3.2 for different metal complexations on benzene-acetylene equilibrium. ΔE (DFT) and ΔE (PM3) are the reaction energy from DFT and PM3 calculation. Non-bonded distance (in Å) is the distance between the nearest carbon atoms of two different acetylene molecules on DFT optimized geometry.

Metal fragment	ΔE (DFT)	ΔE (PM3)	Non-bonded distance
CrC_6H_6	166.1	93.4	2.439
MnC_5H_5	155.8	68.9	2.501
FeC_4H_4	154.8	68.2	2.537
CoC_3H_3	148.4	48.3	2.715
RhC_3H_3	152.2	49.7	3.129

[3.3.1] Complexation of Metal Fragments (CrC_6H_6, MnC_5H_5, FeC_4H_4, CoC_3H_3 and RhC_3H_3) on Benzene and Tris-acetylenes

On complexation with metal fragments, CrC_6H_6, MnC_5H_5, FeC_4H_4, CoC_3H_3 and RhC_3H_3, the reaction energy of benzene-acetylene equilibrium is changed to 166.1, 155.8, 154.8, 148.4 and 152.2 kcal/mol respectively (equation 3.2, table 3.2). A similar trend is observed for the endothermicity of the reaction in going from CrC_6H_6 to RhC_3H_3 at PM3 level as well (table 3.2).

$$C_6H_6ML \rightleftharpoons (C_2H_2)_3ML \qquad (3.2)$$

Complexation with metal reduces the endothermicity of reaction compared to benzene-acetylenic equilibrium, except for Cr. This higher reaction energy, when ML=CrC_6H_6 may be due to the less diffused orbitals of Cr. In all other cases (ML= MnC_5H_5, FeC_4H_4, CoC_3H_3 and RhC_3H_3) the reaction energy is lower than that of benzene-acetylene equilibrium and is minimum for CoC_3H_3. The magnitude of the reduction in the endothermicity is very much less than that calculated previously by PM3 method.[10] Acetylene has two π-orbitals which are perpendicular to each other and one of them is better oriented compared to the π-orbitals of benzene, towards the metal fragment (scheme 3.2). This leads to increased overlap of the metal fragments with acetylene units in comparison to benzene. From table 3.2, it is clear that on complexation the distance between the nearest carbon atoms of two different acetylene molecules increases on going from CrC_6H_6 to RhC_3H_3.

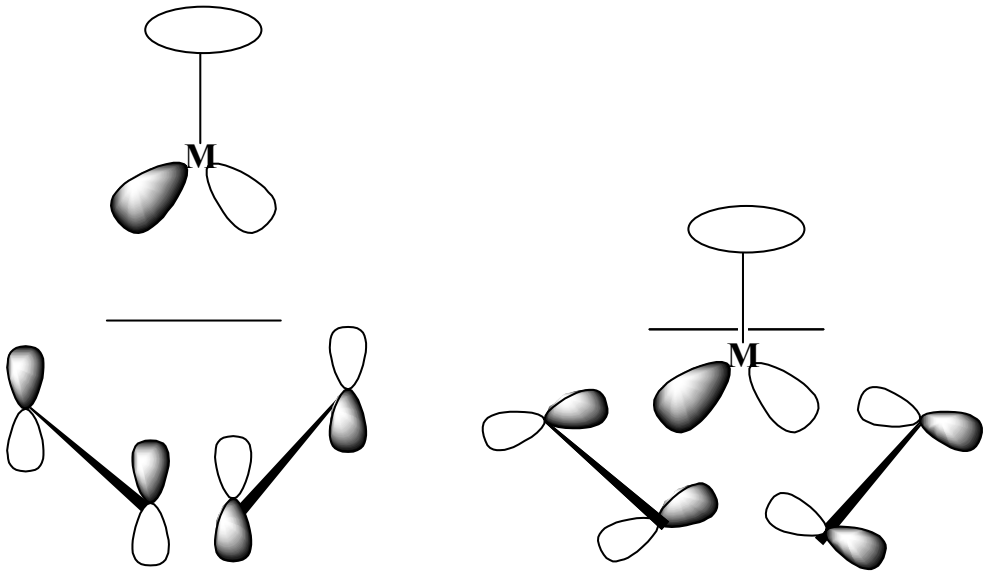

Scheme 3.2: Schematic representation of the interaction of metal orbital with two types of π-orbital of acetylenes

[3.3.2] Benzenoid and Tris-acetylenic Model Metal Complexes (FeC_4H_4, CoC_3H_3) of Fullerene and Its Fragments (C_{60}, $C_{36}H_{12}$, $C_{21}H_9$, $C_{12}H_6$ and $C_{12}H_{12}$)

The difference in energy between the FeC_4H_4 and CoC_3H_3 complexes of benzenoid and tris-acetylenic model structures of C_{60} are 85.0 and 91.1 kcal/mol from DFT study (table 3.3) and 8.3 and 23.5 kcal/mol from PM3 study (equation 3.3). Even though metal complexation with benzenoid model is more favorable than corresponding tris-acetylenic model, the tris-acetylenic model structures get more stabilized on going from C_6H_6 to C_{60}.

$$C_nH_mML \rightleftharpoons \text{open-}C_nH_mML \qquad (3.3)$$

Table 3.3: The difference in total bonding energy (kcal/mol) between metal complexes of benzenoid and tris-acetylenic model structures of fullerene C_{60} and its fragments from equation 3.3.

	FeC_4H_4	CoC_3H_3
C_6H_6	154.8	148.4
$C_{21}H_9$	a	130.3
$C_{36}H_{12}$	83.1	105.7
C_{60}	85.0	91.1
$C_{12}H_6$	-45.2	-43.8
$C_{12}H_{12}$	49.0	38.5

'a' indicates that the specific structure is not a stationary point.

The difference between total bonding energy of the tris-acetylenic model and benzenoid model structures for CoC_3H_3 complexation is reduced from 148.4 to 91.1 kcal/mol for C_6H_6 and C_{60} respectively (equation 3.3, table 3.3). Similar trend is obtained for FeC_4H_4 also. The plot of the difference in total bonding energy between the benzenoid and tris-acetylenic model structure of various fullerene fragments (equation 3.3) for CoC_3H_3 complexation and their curvature θ as defined in figure 3.3 are shown in figure 3.4.

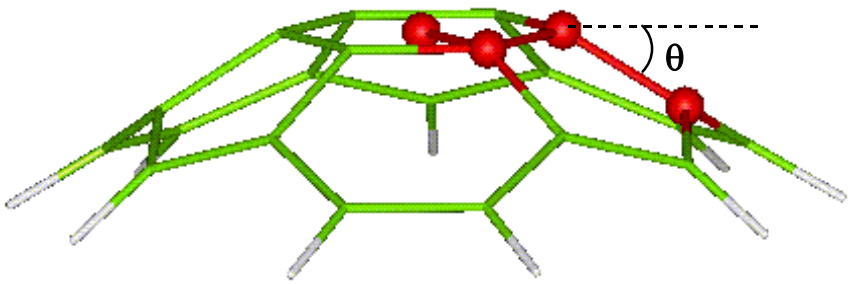

Figure 3.3: θ is the curvature of fullerene fragment

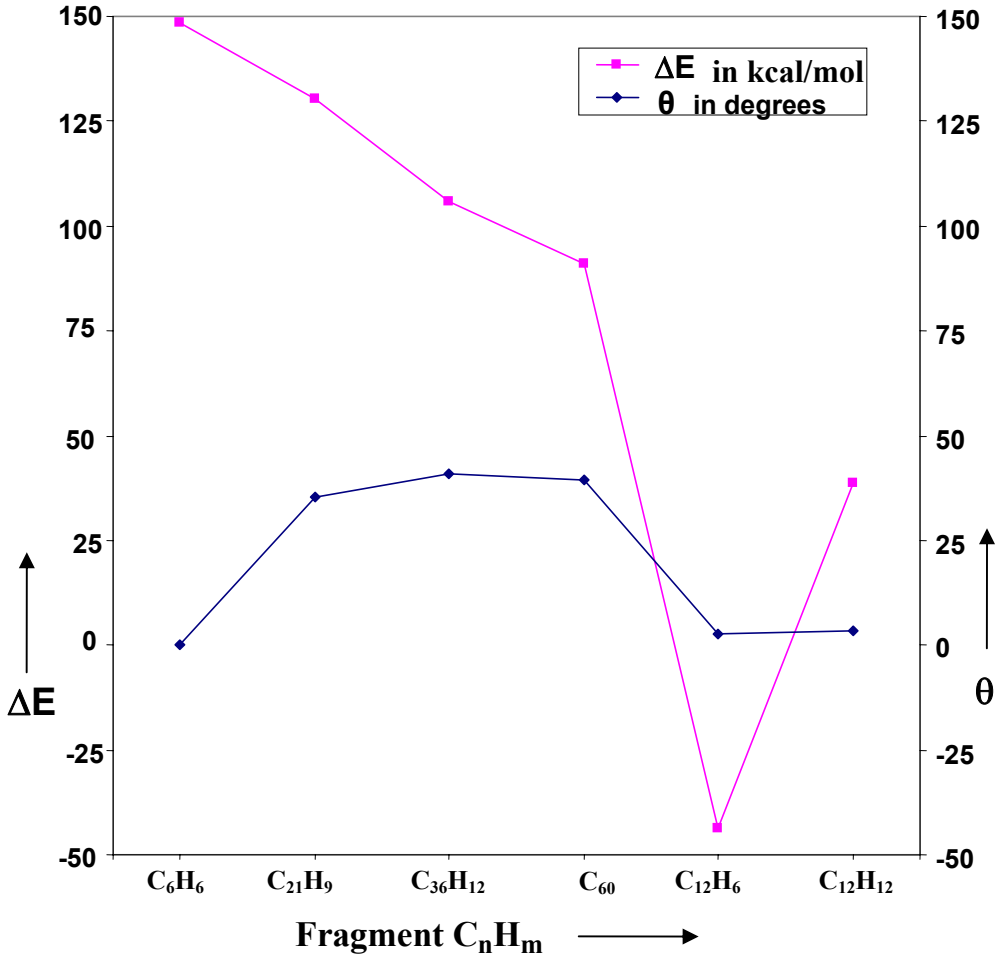

Figure 3.4: ΔE (kcal/mol) for different fullerene fragments for CoC_3H_3 complexation as well as their curvature θ (in degree) as a function of fullerene fragments, C_nH_m.

The curved surfaces of the ring opened fullerene fragments cause one set of π-orbital of the tris-acetylenic groups to rehybridize so as to bend more towards the metal fragments than found in parent acetylene complex (scheme 3.3). On the other hand the π-orbital in the benzenoid structures is inclined away from the metal atoms. This reduces the bonding interaction between the metal fragment and the benzenoid structure. The curvature increases from benzene to $C_{36}H_{12}$; C_{60} lies in between. An estimate of this can be obtained from dihedral angle involving the centre of the six membered ring, two adjacent carbon atoms on the rings and one

carbon atom connected to it externally (figure 3.3). This constraint is released in the acetylenic structure and leads to increased stabilization of the metal complex. But in the tris-acetylenic model structure without the metal fragment, the π-orbitals are too close and lead to the benzenoid arrangements on optimization.

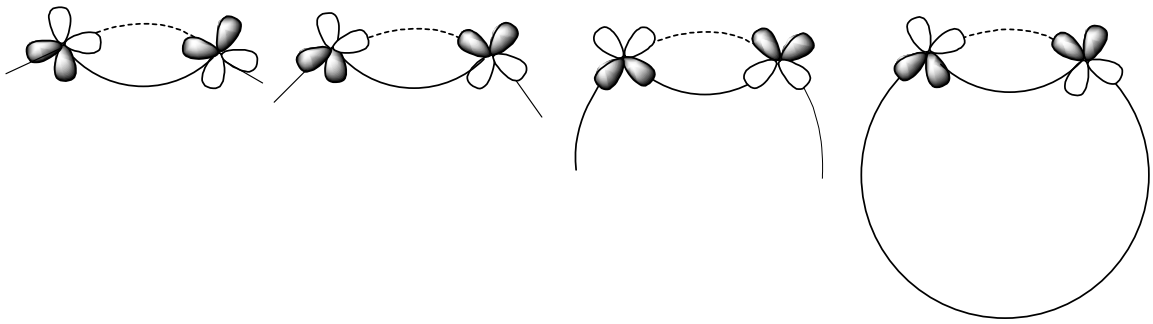

Scheme 3.3: Schematic representation of the inclinations of π-orbitals of six membered rings in bowl shaped hydrocarbons as a function of curvature.

[3.3.3] Relative Stability of Benzene and Tris-acetylenic Model Metal Complexes

Using equation 3.4, we can estimate the stabilization of open fullerene fragment by complexation, on going from small bowl shaped hydrocarbon to higher ones compared to benzene-acetylene equilibrium (table 3.4).

$$C_nH_mML + 3C_2H_2 \longrightarrow \text{open-}C_nH_mML + C_6H_6 \qquad (3.4)$$

From table 3.4, it is clear that on going from benzene to C_{60}, the reaction becomes more exothermic for the CoC_3H_3 metal fragment complex. $C_{12}H_6$, which contains a benzene ring surrounded by three cyclobutadienes, is a very strained molecule. The high strain predisposes the benzenoid structure to tris-acetylenic structure, but aromaticity of benzene ring prevents it.

Table 3.4: The reaction energy (kcal/mol) obtained from the equation 3.4 for CoC_3H_3 and FeC_4H_4 complexation on different fullerene fragments. The curvature, θ (in degree) calculated as per figure 3.3 is also given.

	CoC_3H_3	FeC_4H_4	Dihedral angle	Curvature, θ
C_6H_6	-8.8	-2.4	180.0	0.0
$C_{21}H_9$	-26.9	a	144.7	35.3
$C_{36}H_{12}$	-51.0	-74.1	139.0	41.0
C_{60}	-66.0	-72.1	140.4	39.6
$C_{12}H_6$	-201.0	-202.3	177.2	2.8
$C_{12}H_{12}$	-118.7	-108.1	176.6	3.4

'a' indicates that the specific structure is not a stationary point.

The tris-acetylenic structures without metal complexation are more stable than the benzenoid structures. The stabilization of tris-acetylenic model with metal complexation is more than that of benzenoid complex. The reaction energy obtained from the isodesmic equation (equation 3.4) reveals this factor. In $C_{12}H_{12}$, the benzenoid model structure is more stable than tris-acetylenic model structure by 49.5 kcal/mol. This is due to the increased delocalization in the closed structure even though the geometry is highly strained. This delocalization breaks down when it opens. But on complexation, the total bonding energy differences come down to 49.0 and 38.4 kcal/mol for FeC_4H_4 and CoC_3H_3 respectively. While these highly strained systems are only models, attempts to bring similar strained fragments on to fullerene cluster may be worthwhile.

[3.4] Conclusions

The tris-acetylenic model structure of the fullerene fragments cyclises to the benzenoid form due to the strain in the open structure. The closeness of π-orbitals in the tris-acetylenic model helps in the formation of the benzenoid arrangements. Metal complexes of tris-acetylenic model structures are preferentially stabilized over their benzenoid isomers in going from smaller fragments to higher ones. The curved surface of the ring opened fullerene fragments causes one set of π-orbital of the tris-acetylenic groups to rehybridize so as to bend more towards the metal fragments than found in parent acetylene complex. This leads to increased overlap of metal fragments with tris-acetylenic model structure than benzenoid structure. The metal complex of tris-acetylenic $C_{12}H_6$ is more favorable than benzenoid complex due to the release of strain energy.

[3.5] References

(1) Billups, W. E.; Liufolin, M. A. *Buckminsterfullerene*; VCH Publishers: 1993.

(2) (a) Balch, A. L.; Olmstead, M. M. *Chem. Rev.* **1998**, *98*, 2123. (b) Balch, A. L.; Hao, L.; Olmstead, M. M. *Angew. Chem., Int. Ed. Engl.* **1996**, *35*, 188. (c) Fagan, P. J.; Calabrese, J. C.; Malone, B. *Acc. Chem. Res.* **1992**, *25*, 134. (d) Balch, A. L.; Catalano, V. J.; Lee, J. W.; Olmstead, M. M. *J. Am. Chem. Soc.* **1992**, *114*, 5455. (e) Bahsilov, V. V.; Petrovskii, P. V.; Sokolov, V. I.; Lindeman, S. V.; Guzey, I. A.; Struchkov, Y. T. *Organometallics*. **1993**, *12*, 991. (f) Balch, A. L.; Lee, J. W.; Noll, B. C.; Olmstead, M. M. *Inorg. Chem*. **1993**, *32*, 3577. (g) Schreiner, S.; Gallaher, T. N.; Parsons, H. K. *Inorg. Chem*. **1994**, *33*, 3021. (h) Park, J. T.; Cho, J.; Song, H. *Chem. Commun*. **1995**, 15. (i) Mavunkal, I. J.; Chi Y.; Peng, S.; Lee, G. *Organometallics* **1995**, *14*, 4454. (j) Hsu, H.; Shapley, J. R. *J. Am. Chem. Soc.* **1996**, *118*, 9192. (k) Lee, K.; Hsu, H.; Shapley, J. R. *Organometallics* **1997**, *16*, 3876. (l) Chernega, A. N.; Green, M. L. H.; Haggitt, J.; Stephens, A. H. H. *J. Chem. Soc. Dalton Trans.* **1998**, 755. (m) Park, J. T.; Song, H.; Cho, J.; Chung, M.; Lee, J.; Suh, I. *Organometallics* **1998**, *17*, 227. (n) Maggini, M.; Guldi, D. M.; Mondini, S.; Scorrano, G.; Paolucci, F.; Ceroni, P.; Roffia, S. *Chem. Eur. J*. **1998**, *4*, 1992. (o) Frash, M. V.; Hopkinson, A. C.; Bohme, D. K. *J. Am. Chem. Soc.* **2001**, *123*, 6687.

(3) Fagan, P. J.; Calabrese, J. C.; Malone, B. *Science* **1991**, *252*, 1160.

(4) (a) Koga, N.; Morokuma, K. *Chem. Phys. Lett.* **1993**, *202*, 330. (b) Haddon, R. C. *J. Comput. Chem.* **98**, *19*, 139. (c) Fowler, P. W.; Ceulemans, A. *J. Phys. Chem.* **1995**, *99*, 508.

(5) (a) Saunders, M.; Jiménez-Vázquez, H. A.; Cross, R. J.; Poreda, R. J. *Science* **1993**, *259*, 1428. (b) Saunders, M.; Jiménez-Vázquez, H. A.; Cross, R. J.; Mroczkowski, S.; Freedberg, D. I.; Anet, F. A. L. *Nature* **1994**, *367*, 256. (c) Wieske, T.; Böhme, D. K.; Hrušák, J.; Krätschmer, W.; Schwarz, H. *Angew. Chem., Int. Ed. Engl.* **1991**, *30*, 884. (d) Caldwell, K. A.; Giblin, D. E.; Hsu, C. S.; Cox, D.; Gross, M. L. *J. Am. Chem. Soc.* **1991**, *113*, 8519. (e) Shimshi, R.; Cross, R. J.; Saunders, M. *J. Am. Chem. Soc.* **1997**, *119*, 1163.

(6) (a) Arce. M.; Viado. A. L; An, Y.; Khan, S. I.; Rubin, Y. *J. Am. Chem. Soc.* **1996**, *118*, 3775. (b) Rubin, Y.; Ganapathi, P. S.; Franz, A.; An, Y.; Qian, W.; Neier, R. *Chem. Eur. J.* **1999**, *5*, 3162. (c) Schick. G.; Jarrosson. T.; Rubin, Y. *Angew. Chem. Int. Ed. Engl.* **1999**, *38*, 2360.

(7) Saito, R.; Dresselhaus, G.; Dresselhaus, M. S. *Physcial Properties of Nanotubes*; Imperial College Press: London, 1998.

(8) Jemmis, E. D.; Sharma, P. K. *J. Mol. Graphics Mod.* **2001**, *19*, 256.

(9) (a) Finar, I. L. *Organic Chemistry;* English Language Book Society and Longmans, Green and Co Ltd: London, 1967, Vol. I. (b) Maitlis, P. M. *J. Organomet. Chem.* **1980**, *200*, 161. (c) Reppe, W.; Schweckendiek, W. J. *Liebigs Ann. Chem.* **1948**, *560*, 104.

(10) Rogers, J. R.; Marynick, D. S. *Chem. Phys. Lett.* **1993**, *205*, 197.

(11) (a) Jemmis, E. D.; Manoharan M. *Curr. Sci.* **1999**, *76*, 1122. (b) Jemmis, E. D.; Manoharan, M.; Sharma, P. K. *Organometallics* **2000**, *19*, 1879.

(12) Sawamura, M.; Kuninobu, Y.; Toganoh, M.; Matsuo, Y.; Yamanaka, M.; Nakamura, E. *J. Am. Chem. Soc.* **2002**, *124*, 9354.

(13) (a) ADF2002.03, SCM, *Theoretical Chemistry*, Vrije Universiteit, Amsterdam, The Netherlands, http://www.scm.com (b) Baerends, E. J.; Ellis, D. E.; Ros, P. *Chem. Phys.* **1973**, *2*, 41. (c) Boerrigter, P. M.; Velde, G.; Baerends, E. J. *Int. J. Quant. Chem.* **1988**, *33*, 87. (d) te Velde, G.; Baerends, E. J. *J. Comput. Phys*. **1992**, *99*, 84.

(14) Becke, A. D. *Phys. Rev. A* **1988**, *38,* 3098.

(15) Perdew, J. P. *Phys. Rev. B* **1986**, *33*, 8822.

CHAPTER 4

BINUCLEAR ORGANOMETALLIC COMPOUNDS CONTAINING PLANAR TETRA-COORDINATED CARBON ATOMS: THEORETICAL STUDY ON GEOMETRICAL AND BONDING PATTERNS

[4.0] Abstract

Structure and bonding in the binuclear complex, **1**, the metallacyclocumulene, **2** and the metal-acetylene complex, **3**, are studied using Density Functional Theory. The C-C bond lengths in metal-acetylene complex mainly depend on the diffuseness of the orbitals of the metal atom. Since the C1-C2-C3 angle in **2** changes to get effective overlap as the size of the metal is changed, the central C-C bond length of the cumulene remains nearly constant. In many ways, the ML_2 fragments in **2** dictate the bond angles C1-C2-C3 and C4-C3-C2 and the distance C2-C3 to have effective overlap with the C_4H_2 frame. Four in-plane delocalized molecular orbitals and two π-molecular orbitals perpendicular to the MC_4M' plane contribute to the stability of the planar tetra-coordination around the two central carbon atoms. At the B3LYP/LANL2DZ levels, the stability of the complex **1**, increases with decrease in the size of the M′.

[4.1] Introduction

Transition metal binuclear heterometallic complexes are important in stoichiometric and catalytic reactions.[1] The synergetic effect of the two metals plays a key role in their reactivity such as insertion of polar molecules into metal-metal bonds and the Cannizzaro disproportionation reaction with aryl aldehydes.[2] The complexation of one ligand to two electron poor transition metals is rare.[3] Such combinations are found to be useful in organometallic chemical vapour deposition (OMCVD) to give ceramic thin films.[4] Rosenthal and co-workers reported [5] the binuclear complex $(PPh_3)_2Ni(\mu\text{-}\eta^2\text{:}\ \eta^4\text{–butadiyne})MCp_2$, **1a,b**, where M=Zr, Ti from the reaction of $(PPh_3)_2Ni(\eta^2\text{–PhCCCCPh})$ with Cp_2Ti or Cp_2Zr. They suggested a metallacyclocumulene species **2**, as an intermediate (scheme 4.1). Recently, Choukroun and co-workers reported another such complex $Cp_2V(\mu\text{-}\eta^2\text{:}\ \eta^4\text{–butadiyne})Zr(C_5H_4t\text{-}Bu)_2$, **1c**, synthesized by the reaction of Cp_2V with $(C_5H_4t\text{-}Bu)_2Zr(CCPh)_2$ and its structure was established by X-ray Diffraction.[6] Over the years several complexes of this variety have been synthesized. The length of the middle C-C bond of **1** varies with the metal M′: 1.410Å (**1a**); 1.419Å (**1b**); 1.432Å (**1c**) and 1.447Å (**1d**).

One of the striking features of **1** is two planar tetra-coordinate carbons adjacent to each other. While there have been several examples of structures with single planar tetra-coordinated carbon atom,[7] structures with two of them adjacent to each other are not common. The success in the stabilization of tetra-coordinated planar carbon depends on the ability of the substituents to stabilize the in-plane multicentre orbitals around carbon and to delocalize the lone pair of electrons

perpendicular to the plane. It would be interesting to see the ways in which the two metals on the opposite sides of the C-C bond achieve this.

Scheme 4.1: Schematic diagram of the binuclear complex (**1**), the metallacyclocumulene (**2**) and the metal-acetylene complex (**3**). The lines here meant to imply the nature of bonding in the ligands and do not represent the numbering of bonds. Experimental geometrical parameters of these complexes are shown in the table below. C-C bond length is C2-C3, C2-C3 and C1-C2 bond lengths in **1**, **2** and **3** respectively. As there are more than 42 structures of the type **3**, only a limited set of structures are indicated.

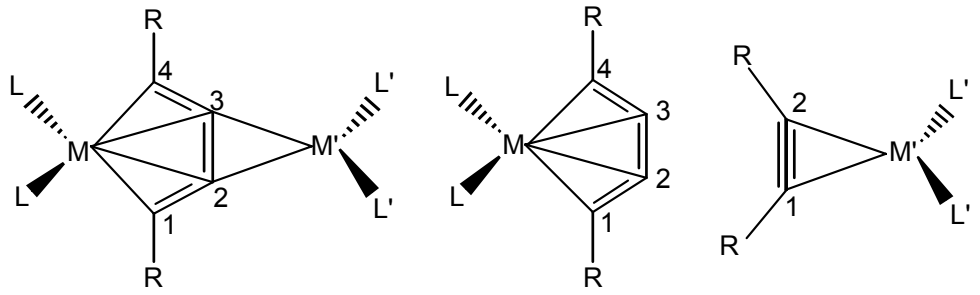

1 **2** **3**

Str. No.	M	M′	R	L	L′	C-C bond length (Å)	Ref.
1a	Zr	Ni	H	Cp	PPh_3	1.410	5
1b	Ti	Ni	H	Cp	PPh_3	1.419	5
1c	Zr	V	Ph	C_5H_4t-Bu	Cp	1.432	6a
1d	Zr	V	H	$C_5H_4SiMe_3$	Cp	1.447	6b
2a	Zr		t-Bu	Cp		1.310	16a
2b	Zr		Ph	Cp*		1.327	16b
2c	Ti		t-Bu	Cp		1.338	17
2d	Zr		$SiMe_3$	Cp*		1.337	16b
3a		Zr	$SiMe_3$		Cp	1.302	11
3b		Ti	t-Bu, $SiMe_3$		Cp	1.280	12
3c		V	CO_2Me		Cp	1.287	13
3d		Ni	Ph, $SiMe_3$		PPh_3	1.273	14

The complex **1** can be considered in-part as a metallacyclocumulene, **2**, and also as a metal-acetylene complex, **3**. Another point of interest is the variation of the central C-C bond length from 1.45Å to1.27Å in structures **1**-**3**.

[4.2] Computational Details

All structures were optimized using the hybrid HF-DFT method, B3LYP/LANL2DZ, based on Becke's three-parameter functional[8a] including Hartree-Fock exchange contribution with a non-local correction for the exchange potential proposed by Becke[8b] together with the non-local correction for the correlation energy suggested by Lee et al.[8c] The LANL2DZ basis set uses the effective core potentials (ECP) of Hay and Wadt.[9] The nature of the stationary points was characterized by vibrational frequency calculations. The Gaussian 94 programme package was used for all calculations.[10] Structures of the binuclear complexes are numbered by **1** with the small letters **a-d** corresponding to the experimentally characterized structures (scheme 4.1). The metal atom symbols are added after the number to indicate the structures calculated. The metal fragments involved are Cp_2Zr, Cp_2Ti, Cp_2V and $(PH_3)_2Ni$. The metallacyclocumulenes are given number, **2**, and the metal-acetylene complexes, **3**.

[4.3] Results and Discussion

The binuclear complex **1** has readily recognizable structural parts such as the metallacyclocumulene, **2**, and the acetylene complex **3**. The variations in the structural parameters of the smaller complexes are discussed first.

[4.3.1] Metal-acetylene complexes, (3Zr, 3Ti, 3V and 3Ni)

The complexes of acetylene with electron poor and electron rich metal fragments such as Cp_2Zr, Cp_2Ti, Cp_2V and $(PH_3)_2Ni$ (scheme 4.1) provide direct comparisons to the binuclear cumulene complex, **1**. The computed geometrical parameters of acetylene-metal complex are compared to the experimental values (table 4.1).[11-14]

Table 4.1: Geometrical parameters (Distances in Angstroms and bond angles in degrees) of the acetylene-metal complex calculated at B3LYP/LANL2DZ level of theory. Experimental values for specific structures are given in parenthesis.

Structure No.	Molecule	Bond lengths in Å		Bond angles in degrees	
		C-C	M-C	C-C-H	C-M-C
3Zr	$C_2H_2ZrCp_2$	1.345 (1.302)[a]	2.181 (2.204)[a]	133.3	35.9 (33.9)[a]
3Ti	$C_2H_2TiCp_2$	1.319 (1.280)[b]	2.052 (2.018)[b]	139.6	37.5 (35.6)[b]
3V	$C_2H_2VCp_2$	1.301 (1.287)[c]	2.058 (2.084)[c]	144.7	36.9 (35.8)[c]
3Ni	$C_2H_2Ni(PH_3)_2$	1.297 (1.273)[d]	1.919 (1.826)[d]	147.3	39.5 (39.0)[d]

Experimental data of [a]$Cp_2(thf)Zr(SiMe_3CCSiMe_3)$[11], [b]$Cp_2Ti(SiMe_3CC(t\text{-}Bu))$[12], [c]$(Cp_2)V(MeO_2CCCCO_2Me)$[13], and [d]$(PPh_3)Ni(PhCCSiMe_3)$[14]

As expected, the C-C bond length in acetylene, 1.220Å (B3LYP/LANL2DZ level) increases on complexation with metal fragments (table 4.1). The diffuseness of the metal orbitals controls the C-C distance and the C-C-H bond angles (table 4.1). The C-H bending maximizes overlap with orbitals of the metal atoms. The nickel exhibits traditional planar coordination and the ligands are in the plane of the ring.

The interaction between the metal fragment and acetylene can be described in terms of the traditional Dewar-Chatt-Duncansan (DCD) model[15] of ligand to metal donation and metal to ligand back donation. In principle, the back donation process should be stronger for electron rich metals than the electron poor ones. But a closer look at the C-C bond lengths given in table 4.1 reveals that the electron poor metal Zr accounts for the longer C-C bond in the series **3Zr**, **3Ti**, **3V** and **3Ni**. The donor levels of the electron poor Cp_2Zr and Cp_2Ti fragments are closer in energy to the π^* levels of acetylene, leading to better back bonding and longer C-C distances. In addition the size of the metal atoms also contributes to this; Zr leads to a complex with longer C-C distances. This is shown diagrammatically in scheme 4.2.

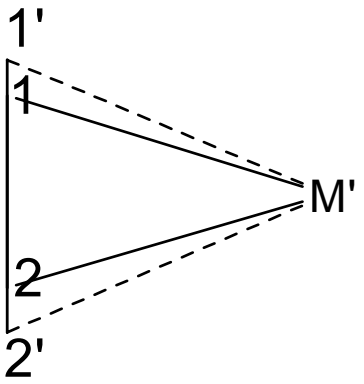

Scheme 4.2: The dependence of the size of the metal atom on the C-C bond length in acetylene-metal complex. The dotted line corresponds to **3Zr** and thick line to **3Ni**.

[4.3.2] Metallacyclocumulenic complexes, (2Zr, 2Ti, 2V and 2Ni)

Several derivatives of metallacyclocumulenes, **2**, $Cp_2MC_4H_2$ (M=Zr, Ti) are known experimentally.[16-17] The parent structures are calculated to be minima on their potential energy surfaces. The nickellacyclocumulenic complex, **2Ni**, on

optimization, rearranges to the cyclopropene complex, a derivative of which was synthesized by Rosenthal and co-workers.[18]

Table 4.2: Geometrical parameters (Distances in Angstroms and bond angles in degrees) of the cumulene-metal complex calculated at B3LYP/LANL2DZ level of theory. Experimental values for specific structures are given in parenthesis.

Structure No.	Molecule	Bond lengths in Å				Bond angles in degrees	
		C1-C2	C2-C3	M-C1	M-C2	C1-C2-C3	M-C1-C2
2Zr	$C_4H_2ZrCp_2$	1.316	1.342	2.353	2.373	146.6	74.7
		(1.280)[a]	(1.310)[a]	(2.357)[a]	(2.303)[a]	(150.0)[a]	
2Ti	$C_4H_2TiCp_2$	1.302	1.344	2.242	2.259	145.1	73.9
		(1.277)[b]	(1.338)[b]	(2.252)[b]	(2.210)[b]	(147.6)[b]	
2V	$C_4H_2VCp_2$	1.296	1.349	2.191	2.217	144.1	74.0

Experimental data of [a] $Cp_2ZrC_4(t\text{-}Bu)_2$[16], [b] $Cp_2TiC_4(t\text{-}Bu)_2$[17]

The theoretical and experimental geometrical parameters of all structures represented by **2** are given in table 4.2. The C2-C3 bond lengths in all of them are of comparable magnitude, indicating a similarity in the electronic structure as well. The electronic structure of metallacyclocumulene is best analyzed from fragment molecular orbital approach.[19,20] The metal in the Cp_2M fragment is in the formal oxidation state of +2 with two valence electrons (three electrons in Cp_2V). The three frontier orbitals of Cp_2M are in the MC_4 plane. The in-plane frontier orbitals of the HCCCCH fragment are formed from the two in-plane p-orbitals on the two middle carbon atoms and the sp-hybrid orbitals on the end carbon atoms, C1 and C4. These form four linear combinations, similar to the π-orbitals of butadiene. The lowest two orbitals among these are filled. The next MO, the LUMO of the C_4H_2

fragment, corresponds to the in-plane equivalent of the LUMO of the butadiene π-orbitals and is bonding between C2 and C3.

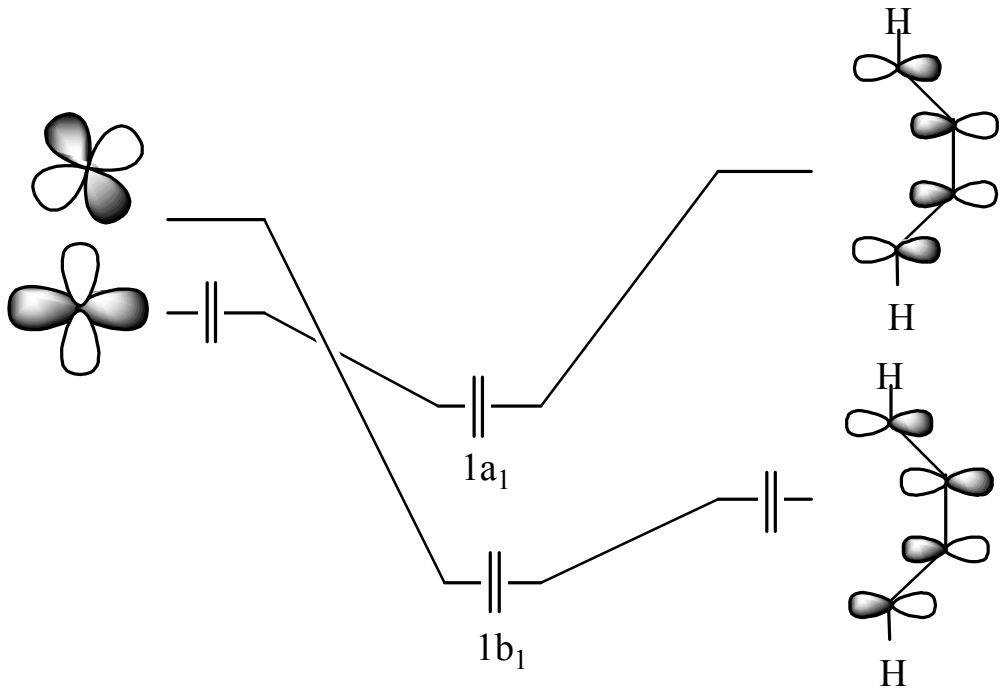

Scheme 4.3: Interaction diagram between the cumulene and metal fragment.

The strongest stabilizing interaction is between this LUMO of C_4H_2 and the HOMO of Cp_2M ($1a_1$). This interaction stabilizes the C2-C3 bond (scheme 4.3). This is in contrast with the familiar Dewar-Chatt-Duncanson model of metal to π^* back-bonding, which decreases C2-C3 bonding, lengthening the C2-C3 bond. The consequence of this bonding is tempered by the two π-MOs perpendicular to the MC4 plane, typical of butadiene. Another interaction is the donation of electrons from the HOMO of C_4H_2 to the empty d orbital of the metal atom ($1b_1$). The variation in the C1-C2-C3 angle with the metal is small, but the decrease from 146.6°, 145.1° to 144.1° corresponds to the decrease in the size of the metal atoms. The LUMO of the metallacyclocumulene is a nonbonding metal orbital. The extra electron in vanadocyclocumulene, **2V**, in comparison to **2Zr** and **2Ti**, occupies this

nonbonding metal orbital. The frontier molecular orbitals of $Cp_2MC_4H_2$ on the side of C4 away from the metal are ideally suited for further reactions. These are analyzed in the next section.

[4.3.3] Organobimetallic Compounds Containing Planar Tetra-coordinated Carbon Atoms, (1Zr-Zr, 1Zr-Ti, 1Zr-V, 1Zr-Ni, 1Ti-Zr, 1Ti-Ti, 1Ti-V and 1Ti-Ni)

We studied molecules of the type $L'_2M'(\mu\text{-}\eta^2\text{:}\ \eta^4\text{-butadiyne})ML_2$, where ML_2=$ZrCp_2$ and $TiCp_2$ and $M'L'_2$= $ZrCp_2$, $TiCp_2$, VCp_2 and $Ni(PH_3)_2$. The C1-C2 and C2-C3 bond distances are longer than those in the cumulenic complexes (table 4.3). But the elongation of the C2-C3 bond distance is much more than that of C1-C2. It is as if the $M'L'_2$ fragment molecular orbitals dictate the C4 unit to adopt geometries suitable for best overlap with changes in the C1-C2-C3 and C4-C3-C2 bond angles and C2-C3 bond distance (scheme 4.4, table 4.3). The M-C2 bond distances are higher than that in the cumulenic complex, but are within the distances found, in general, for similar structures.

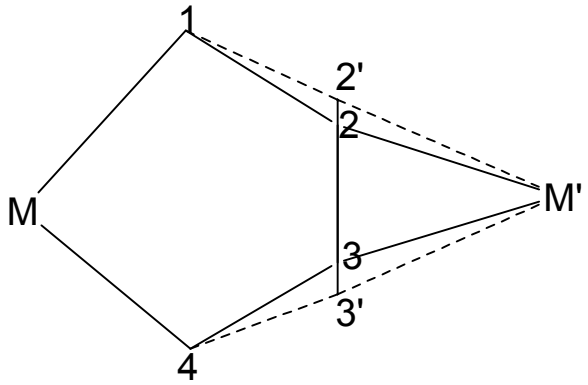

Scheme 4.4: The dependence of the size of the metal atom (M′) on C2-C3 bond length and C1-C2-C3 bond angle. The dotted line corresponds to $Cp_2MC_4H_2ZrCp_2$ and thick line $Cp_2MC_4H_2Ni(PH_3)_2$.

Table 4.3: Geometrical parameters (Distances in Angstroms and bond angles in degrees) of the binuclear organometallic complex calculated at B3LYP/LANL2DZ level of theory. Experimental values for specific structures are given in parenthesis. First and second metal symbols in structure number correspond to η^4 and η^2 coordination respectively.

Structure No.	Molecule $Cp_2MC_4H_2M'L'_2$	Bond lengths in Å					Bond angles in degrees	
		C1-C2	C2-C3	M-C1	M-C2	M′-C2	C1-C2-C3	C2-M′-C3
1Zr-Zr	$Cp_2ZrC_4H_2ZrCp_2$	1.355	1.540	2.223	2.584	2.211	132.1	40.8
1Zr-Ti	$Cp_2ZrC_4H_2TiCp_2$	1.350	1.491	2.232	2.539	2.086	134.2	41.9
1Zr-V	$Cp_2ZrC_4H_2VCp_2$	1.346	1.465	2.240	2.512	2.089	135.7	41.1
		(1.334)[a]	(1.432)[a]	(2.240)[a]	(2.462)[a]	(2.133)[a]	(137.6)[a]	(39.5)[a]
1Zr-Ni	$Cp_2ZrC_4H_2Ni(PH_3)_2$	1.346	1.450	2.248	2.480	1.910	137.2	44.6
		(1.322)[b]	(1.410)[b]	(2.239)[b]	(2.389)[b]	(1.911)[b]	(139.4)[b]	(43.1)[b]
1Ti-Zr	$Cp_2TiC_4H_2ZrCp_2$	1.347	1.561	2.087	2.547	2.188	127.1	41.8
1Ti-Ti	$Cp_2TiC_4H_2TiCp_2$	1.342	1.499	2.095	2.476	2.067	130.2	42.5
1Ti-V	$Cp_2TiC_4H_2VCp_2$	1.337	1.464	2.100	2.425	2.078	132.3	41.3
1Ti-Ni	$Cp_2TiC_4H_2Ni(PH_3)_2$	1.335	1.449	2.109	2.380	1.909	134.1	44.6
		(1.333)[c]	(1.419)[c]	(2.118)[c]	(2.340)[c]	(1.907)[c]	(133.3)[c]	(40.6)[c]

Experimental data of [a] $(C_5H_4t\text{-}Bu)_2ZrC_4(Ph)_2VCp_2$[6], [b] $Cp_2ZrC_4H_2Ni(PPh_3)_2$[5], [c] $Cp_2TiC_4H_2Ni(PPh_3)_2$[5]

A major point of interest in this structure is the two planar tetra-coordinate carbons adjacent to each other. The molecular orbitals of **1**, where M=Zr and M′ =Zr, Ti (**1Zr-Zr**, **1Zr-Ti**) are shown in scheme 4.5.

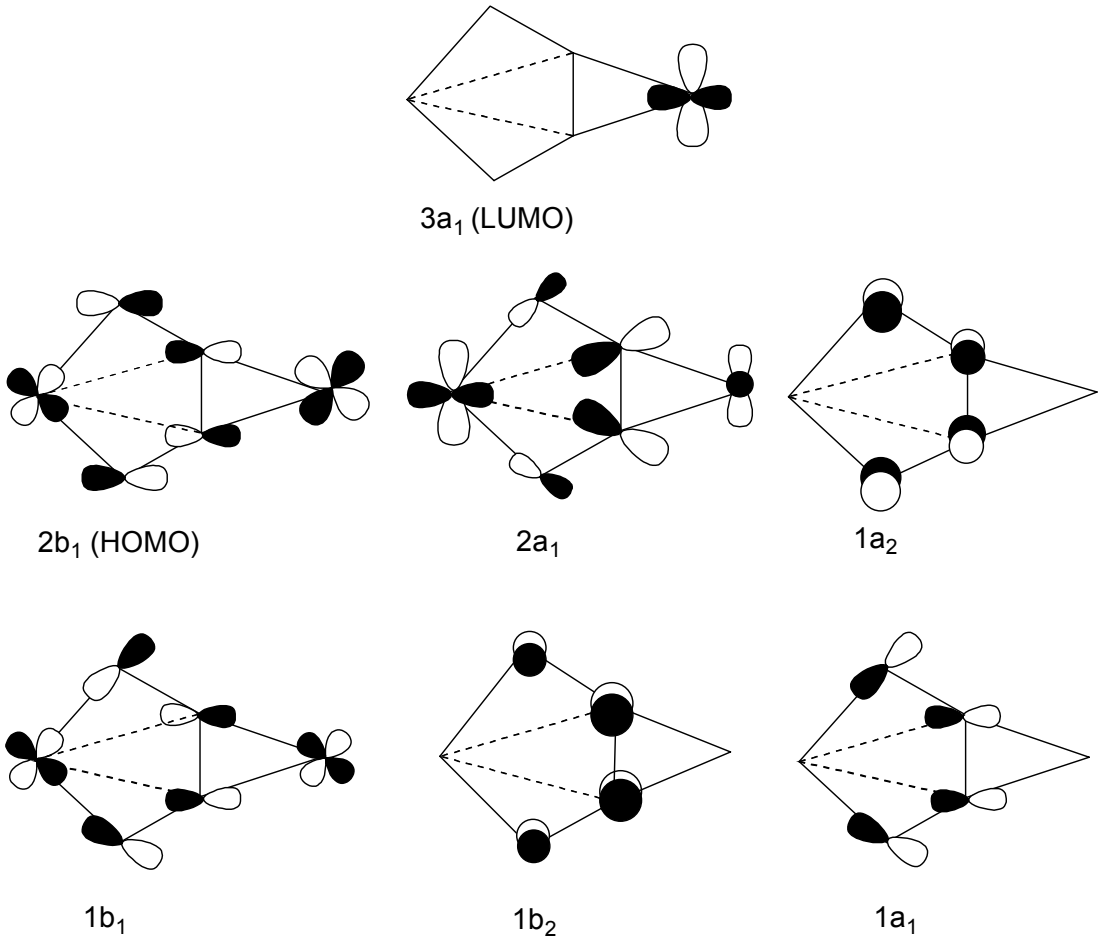

Scheme 4.5: Molecular orbitals of **1** ($L_2MC_4H_2M'L'_2$)

Bonding can be understood by taking HCCCCH as a tetra anion and the metals in the +4 oxidation state. The π-molecular orbitals ($1b_2$ and $1a_2$) perpendicular to the MC_4M' plane do not interact substantially with the metals. As an approximation, these four electrons can be considered as lone pairs of the two tetra-coordinate planar carbon atoms. It is stabilized through the delocalization over

all the four carbon atoms. The molecular orbitals, $1a_1$, $1b_1$, $2a_1$ and $2b_1$ are delocalized across the two metals. These account for the remaining eight valence electrons ensuring the planarity of the M_2C_4 unit. In **1Zr-V** (M′ =V), the LUMO of **1Zr-Zr**, **1Zr-Ti** becomes the SOMO, which has negligible interaction with the orbitals on the C4 skeleton. The important bonding molecular orbitals of **1Zr-Ni** (M′ =Ni) are almost the same, except in the relative ordering of energy.

The $2a_1$ molecular orbital can be considered as formed by the donation of electrons from the filled HOMO of the metallacyclocumulene to the empty d-orbital of the metal (M′). This reduces the C2-C3 bonding interaction. The HOMO ($2b_1$) represents the back donation from the filled metal orbital (M′) to the empty LUMO of the metallacyclocumulene. This leads to an increase in the antibonding interaction between the C2-C3 bonds. Both of these interaction leads to the elongation in the C2-C3 bond. The analysis remains nearly the same in all complexes even with M′=Ni. The stability of these complexes can be judged from the following isodesmic equations (table 4.4).

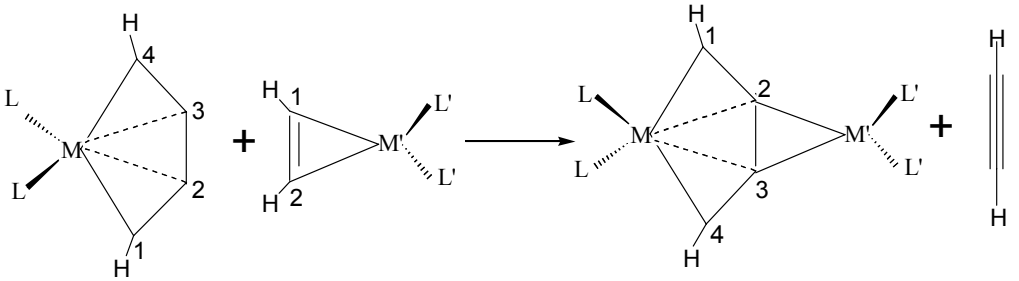

(4.1)

When M=Ti and M′ varies form Zr to Ni, (**1Ti-Zr** to **1Ti-Ni**), the exothermicity (ΔE_{Ti}) of the reaction increases. It is clear from table 4.4 that when C-C-H bond angles in **3** are closer to C1-C2-C3 bond angle of **2**, the exothermicity of the reaction and hence the stability of the complex increases. Similarly when M=Zr,

and, M′ varies form Zr to Ni, (**1Zr-Zr** to **1Zr-Ni**), the exothermicity (ΔE_{Zr}) of the reaction increases. Binuclear complexes with M=Zr, Ti; M′=Ni (**1a**, **1b**) and M=Zr; M′=V (**1c, 1d**) are known experimentally and these are shown to be more favorable from the equation 4.1 (table 4.4).

Table 4.4: ΔE_{zr} and ΔE_{Ti} are the energies obtained from isodesmic equation 4.1. C-C-H is the angle of $C_2H_2ML_2$, **3**. C1-C2-C3 angles of **2Zr** and **2Ti** are146.6 and 144.1.

$C_2H_2M'L_2$	C-C-H Angle	ΔE_{zr} (kcal/mol)	ΔE_{Ti} (kcal/mol)
3Zr	133.3	-1.8	-4.8
3Ti	139.6	-6.0	-6.9
3V	144.7	-8.0	-8.5
3Ni	147.3	-9.3	-9.1

[4.4] Conclusions

We compared the structure and bonding in the binuclear complex **1**, the metallacyclocumulene, **2** and the metal-acetylene complex, **3**. The diffuseness of the orbitals of the metal atom and the extent of back bonding are the main reasons for the elongation on the C-C bond length in metal-acetylene complexes. The central C-C bond length in **2** is almost same for all the metals, because the C1-C2-C3 bond angles in **2** change to get effective overlap as the size of the metal changes. The central C-C bond length in **1** increases with an increase in the size of the metal M′ as in the case of metal-acetylene complex, **3**. The planar tetra-coordinate arrangements around two adjacent carbons are stabilized through the four in-plane

delocalized molecular orbitals resulting from the interaction with the metal fragment orbitals and two π-molecular orbitals perpendicular to the MC_4M' plane. When the C1-C2-C3 bond angle of **2** comes closer to the C-C-H bond angle of **3**, the stability of the complex, **1**, increases.

[4.5] References

(1) (a) Roberts, D. A.; Geoffroy, G. L., *In Comprehensive Organometallic Chemistr*y, Wilkinson, G.; Stone, F. G. A.; Abel E. W., Eds., Pergamon: Oxford 1982, Vol. 6, Chapter 40. (b) Ferguson, G. S.; Wolczanski, P. T. *Organometallics* **1985,** *4*, 1601. (c) Bullock, R. M.; Casey, C. P. Acc. *Chem. Res.* **1987**, *20*, 167. (d) Stephan, D. W. *Coord. Chem. Rev.* **1989**, *95*, 41. (e) Baker R. T.; Fultz W. C.; Morder, T. B.; Williams, I. D. *Organometallics* **1990**, *9*, 2357., and references therein. (f) Graham, T. W.; Llamazares, A.; McDonald, R.; Cowie, M. *Organometallics* **1999**, *18*, 3490; 3502.

(2) Gade, L. H.; Memmler, H.; Kauper, U.; Schneider, A.; Fabre, S.; Bezougli, I.; Lutz, M.; Galka, C.; Scowen, I. J.; McPartlin, M. *Chem. Eur. J.* **2000**, *6*, 692.

(3) (a) Mazzanti, M.; Floriani, C.; Chiesi-Villa, A.; Guastini, C. *Inorg.Chem.* **1986**, *25*, 4158. (b) Friebel, C.; Scherfise, K. D.; Willing, W.; Mueller, U.; Dehnicke, K. *Z. Anorg. Allg. Chem.* **1987***, 546*, 21. (c) Elschenbroich, C.; Schmidt, E.; Metz, B.; Harms, K. *Organometallics* **1995**, *14*, 4043. (d) Burlakov, V. V.; Ohff, A.; Lefeber, C.; Tillack, A.; Baumann, W.; Kempe, R.; Rosenthal, U. *Chem. Ber.* **1995**, *128*, 967. (e) Schottek, J.; Erker, G.; and Frohlich, R. *Eur. J. Inorg. Chem.* **1998**, 551.

(4) (a) Fischer, R. A.; Behm, J.; Priermeier, T.; Sherer, W. *Angew. Chem., Int. Ed. Engl.* **1993***, 32*, 746. (b) Fischer, R. A. *In Material Research Society Symposium Proceedings*, Abernathy, C. R.; Bates, J. C. W.; Bohling, D. A.; Hobson, W. S., Eds., Materials Research Society: Pittsburgh, 1993, pp 267. (c) Fischer, R. A.; Kleine, M.; Lehmann, O.; Stuke, M. *Chem. Mater.* **1995**, *7*, 1863. (d) Danjoy, C., *Ph.D. Thesis*, Institut National Polytechnique de

Toulouse, France, 1996, No 1197. (e) Valade, L.; Choukroun, R.; Danjoy, C.; Chansou, B.; De Caro, D.; Cassoux, P. *Ann. Chim. Sci. Mater.* **1998**, *23,* 721.

(5) Pulst, S.; Arndt, P.; Heller, B.; Baumann, W.; Kempe, R.; Rosenthal, U. *Angew. Chem., Int. Ed. Engl.* **1996**, *35*, 1112.

(6) (a) Choukroun, R.; Donnadieu, B.; Zhao, J.; Cassoux, P.; Lepetit, C.; Silvi, B. *Organometallics* **2000**, *19,* 1901. (b) Danjoy, C.; Zhao, J.; Donnadieu, B.; Legros, J. P.; Valade, L.; Choukroun, R.; Zwick, A.; Cassoux, P. *Chem. Eur. J.* **1998**, *4*, 1100.

(7) (a) Seidel, W.; Kreisel, G.; Mennenga, H. *Z. Chem.* **1976**, *16*, 492. (b) Cotton, F. A.; Millar, F. *J. Am. Chem. Soc.* **1977**, *99*, 7886. (c) Erker, G. *Comments Inorg. Chem.* **1992**, *13*, 111. (d) Albrecht, M.; Erker, G.; Kruger, C. *Synlett.* **1993**, 441. (e) Pellny, P. M.; Peulecke, N.; Burlakov, V. V.; Tillack, A.; Baumann, W.; Spannenberg, A.; Kempe, R.; Rosenthal, U. *Angew. Chem., Int. Ed. Engl.* **1997**, *36*, 2615. (f) Jones, W. M.; Klosin, J. *Adv. Organomet. Chem.* **1998**, *42*, 147. (g) Pulst. S.; Kirchbauer, F. G.; Heller, B.; Baumann, W.; Rosenthal, U. *Angew. Chem., Int. Ed. Engl.* **1998**, *37*, 1925. (f) Jemmis, E. D.; Giju, K. T. *J. Am. Chem. Soc.* **1998**, *120*, 6952. (g) Rottger, D.; Erker, G. *Angew. Chem., Int. Ed. Engl.* **1997**, *36*, 812. (h) Erker, G.; Rottger, D. *Angew. Chem., Int. Ed. Engl.* **1993**, *32*, 1623. (i) Rottger, D.; Erker, G.; Frohlich, R.; Grehl, M.; Silverio, S. J.; Hyla-Kryspin, I.; Gleiter, R. *J. Am. Chem. Soc.* **1995**, *117*, 10503. (j) Rottger, D.; Erker, G.; Frohlich, R.; Kotila, S. *Chem. Ber.* **1996**, *129*, 1.

(8) (a) Becke, A. D. *J. Chem. Phys.* **1993**, *98*, 5648. (b) Becke, A. D. *Phys. Rev. A* **1988**, *38*, 2398. (c) Lee, C.; Yang, W.; Parr, R. G. *Phys. Rev. B* **1988**, *37*, 785.

(9) (a) Hay, P. J.; Wadt, W. R. *J. Chem. Phys.* **1985**, *82*, 270. (b) Wadt, W. R.; Hay, P. J. *J. Chem. Phys.* **1985**, *82*, 284. (c) Hay, P. J.; Wadt, W. R. *J. Chem. Phys.* **1985**, *82*, 299.

(10) Frisch, M. J.; Trucks, G. W.; Schlegel, H. B.; Gill, P. M. W.; Johnson, B. G.; Robb, M. A.; Cheeseman, J. R.; Keith, T.; Petersson, G. A.; Montgomery, J. A.; Raghavachari, K.; Al-Laham, M. A.; Zakrzewski, V. G.; Ortiz, J. V.; Foresman, J. B.; Cioslowski, J., W.; Wong, M. W.; Andres, J. L.; Replogle, E. S.; Gomperts, R.; Martin, R. L.; Fox, D. J.; Binkley, J. S.; Defrees, D. J.; Baker, J.; Stewart, J. P.; Head-Gordon, M.; Gonzalez, C.; Pople, J. A., *Gaussian 9*4, Gaussian, Inc.: Pittsburgh, PA, 1995.

(11) Rosenthal, U.; Ohiff, A.; Michalik, M.; Gorls, H.; Burlakov, V. V.; Sghur, V.B. *Angew. Chem., Int. Ed. Engl.* **1993**, *32*, 1193.

(12) Lefeber, C.; Ohff, A.; Tillack, A.; Baumann, W.; Kempe, R.; Burlakov, V. V.; Rosenthal, U.; Gorls, H. *J. Organomet. Chem.* **1995**, *501*, 189.

(13) Fachinetti, G.; Floriani, C.; Chiesi-villa, A.; Guastini, C. *Inorg. Chem.* **1979**, *18,* 2282.

(14) Bartlk, T.; Happ, B.; Iglewsky, M.; Bandmann, H.; Boese, R.; Heimbacht P.; Hoffmann, T.; Wenschuh, E. *Organometallics* **1992**, *11*, 1235.

(15) (a) Dewar, M. J. S. *Bull. Soc. Chim. Fr.* **1951**, C71-C79. (b) Chatt, J.; Duncanson, L. A. *J. Chem. Soc.* **1953**, 2939.

(16) (a) Rosenthal, U.; Ohiff, A.; Baumann, W.; Kempe, R.; Tillack. A.; Burlakov, V. V. *Angew. Chem., Int. Ed. Engl.* **1994**, *33*, 1605. (b) Pellny, P. M.; Kirchbauer, F. G.; Burlakov, V. V.; Baumann, W.; Spannenberg, A.; Rosenthal, U. *J. Am. Chem. Soc.* **1999**, *121*, 8313.

(17) Burlakov, V. V.; Ohff, A.; Lefeber, C.; Tillack, A.; Baumann, W.; Kempe, R.; Rosenthal, U. *Chem. Ber.* **1995**, *128*, 967.

(18) (a) Rosenthal, U.; Pulst, S.; Arndt, P.; Baumann, W.; Tillack, A.; Kempe, R. *Z. Naturforsch. B.* **1995**, *50,* 377. (b) Rosenthal, U.; Pulst, S.; Arndt, P.; Baumann, W.; Tillack, A.; Kempe, R. *Z. Naturforsch. B.* **1995**, *50,* 368.

(19) (a) Hoffmann, R. *J. Chem. Phys.* **1963***, 39*, 1397. (b) Hoffmann, R.; Lipscomb, W. N. *J. Chem. Phys.* **1962**, *36*, 2179. (c) Fujimoto, H.; Hoffmann, R. *J. Phys. Chem.* **1974**, *78*, 1167. (d) Hoffmann, R. *J. Phys. Chem.* **1974**, *78*, 1167.

(20) Jemmis , E. D.; Phukan, A. K.; Giju, K. T. *Organometallics* **2002,** *21*, 2254.

CHAPTER 5

THEORETICAL STUDY ON THE INSERTION OF HETEROALLENES (CO_2, COS AND CS_2) INTO METAL-METAL POLAR BOND OF EARLY-LATE BIMETALLIC COMPLEXES

[5.0] Abstract

The mechanism of the insertion of heteroallenes, XCY (CO_2, COS, and CS_2,) into metal-metal polar bond of early-late heterobimetallic (ELHB) complexes, $(NH_2)_3M\text{-}M'(CO)_2Cp$ (where M=Ti, Zr and M′=Fe, Ru) is studied using Density Functional Theory. The reactions of CO_2 and COS with M-M′ bond of ELHB complexes (**9p**) give the initial intermediates, **10pq** which undergo isomerization to the four membered metallacycles, **12pq** through transition states, **11pq**. The synergetic effect of both transition metals plays a key role in the reactivity towards the heteroallenes. The greater strain arising from the smaller size of titanium and oxygen rules out the formation of the metallacycles, **12aa** and **12ba**. On the other hand, larger size of sulphur averts the formation of **10pc**. The first row late transition metal has more effective interaction with LUMO of XCY and the greater population in LUMO induces the XCY bending to generate bonding interaction. This stabilizes the bimetallic complexes, **10pq** and **12pq**. The isomerization of the complexes, **10ab** and **10bb** to **12ab** and **12bb** have relatively high energy barrier and is endothermic. The larger size of the zirconium atom results in the greater stability of bimetallic complexes, **12cb** and **12db** than the titanium complexes, **12ab** and **12bb**.

[5.1] Introduction

Early-late heterobimetallic (ELHB) complexes have widespread interest in catalytic reactions,[1] synthetic organometallic chemistry[2,3] and materials science.[4] Interest in these complexes arises from the possibility of utilizing the complementary reactivities of the electron-poor early transition metal and the electron-rich late transition metal in reactions with organic substrates. The synergetic effect of the two metals plays a key role in their reactivity such as insertion of polar substrate into metal-metal bonds, Cannizzaro disproportionation reaction with aryl aldehydes etc.[2]

Even though numerous theoretical studies are available to understand the polarity of the metal-metal bond in ELHB complexes,[5,6] the complete mechanistic study to understand its cooperative reactivity is lacking. Here, we discuss the process of insertion of heteroallenes such as CO_2, COS and CS_2 into metal-metal bonded systems. Since these heteroallenes are most abundant source of C_1 chemistry, the activation and functionalization of these molecules through transition metal complexes have received much attention. The bonding of heteroallenes such as CO_2 and CS_2 to transition-metal fragments and its fluxional behaviour in coordination complexes have been investigated in the literature.[7] There are mainly three types of coordination possible for the interaction of metal fragment with heteroallenes (scheme 5.1) and all of them are found experimentally.[8] It is interesting to explicate a general trend for the variation in the coordinative properties when heteroallenes undergo reaction with early-late bimetallic complexes.

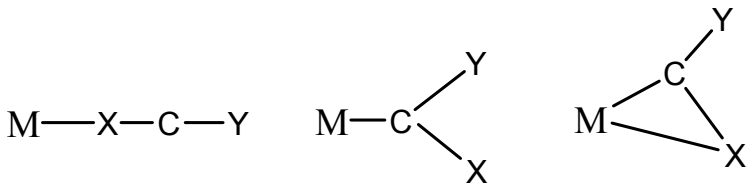

1 **2** **3**

Scheme 5.1: End-on, C-on and side-on coordination of metal-XCY complexes

Several insertion reactions of heteroallenes into metal-metal bond are also known experimentally. Gade and co-workers had reported the insertion reaction of heteroallenes such as CO_2, CS_2 and RCN into metal-metal bond of ELHB complexes (scheme 5.2, **4, 5**).[2a] In this type of reaction, the early transition metal centre undergoes electrophilic attack to the more Lewis basic part of the polar substrate and the late transition metal centre undergoes nucleophilic attack to the more Lewis acidic part of the polar substrate. Bergman and co-workers reported a similar reaction of CO_2 with $Cp_2Zr(\mu\text{-}N^{t\text{-}}Bu)IrCp^*$ (scheme 5.2, **6**)[9] where one C=O bond of CO_2 undergoes direct addition to Zr-Ir bond (scheme 5.2, **7**). On the other hand, the addition of allene to **6** gives **8** which is similar to structure, **5**.[9]

In view of the divergent coordination products encountered by varying the metals of ELHB and heteroallenes, we have studied the possible mechanism for the insertion of heteroallenes into metal-metal polar bonds. We have chosen the model bimetallic complexes as $(NH_2)_3M\text{-}M'(CO)_2Cp$ where M= Ti, Zr; M′= Fe, Ru, and heteroallenes as XCY (CO_2, COS and CS_2). The structure and bonding of various intermediates and transition states are also presented.

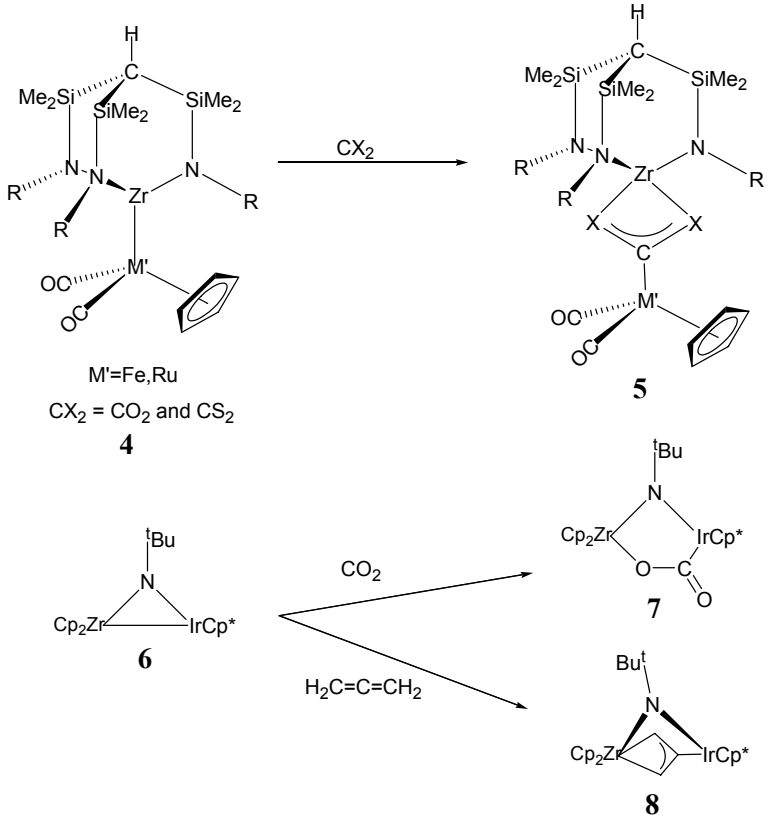

Scheme 5.2: Experimentally known reactions of heteroallenes with ELHB complexes.

[5.2] Computational Details

All structures were optimized using the hybrid HF-DFT method, B3LYP/LANL2DZ, based on Becke's three-parameter functional[10a] including Hartree-Fock exchange contribution with a non-local correction for the exchange potential proposed by Becke[10b] together with the non-local correction for the correlation energy suggested by Lee et. al.[10c] The LANL2DZ basis set uses the effective core potentials (ECP) of Hay and Wadt.[11] The nature of the stationary points was characterized by vibrational frequency calculations. The Gaussian 03 programme package[12] was used for all calculations. In view of the large number of structures, the following labeling scheme is used (figure 5.1). A number followed

by one letter is used to indicate the initial ELHB complexes. Thus, **9a** corresponds to the complex with M=Ti and M′=Fe. A second letter is added to this to represent the complex with XCY. Thus, **10aa** would correspond to the adduct structure, **10pq** with M=Ti and M′=Fe and XCY=CO_2. The generic letters **p** and **q** are used to represent to the complete set. Thus, **11pq** corresponds to all the structures of the type **11** considered in this paper (**p=a-d, q=a-c**).

[5.3] Results and Discussion

The insertion of heteroallenes (XCY) such as CO_2, COS and CS_2 into ELHB complexes, **9p** gives the inserted bimetallic complexes, **10pq** and **12pq** and the transition states for their interconversion, **11pq** (figure 5.1). The reaction of CO_2 and COS with M-M′ bond of ELHB complexes, **9p** results in the formation of the initial intermediates, **10pa** and **10pb** which undergo isomerization to the final products, **12pa** and **12pb** through their respective transition states, **11pa** and **11pb**. On the other hand, CS_2 gives direct insertion products, **12pc** without forming the initial intermediates, **10pc**. The initial complexes, **10aa** and **10ba** are more stable than **12aa** and **12ba** and do not isomerize. A detailed analysis of the geometrical and bonding pattern of each complex is given in the following sections.

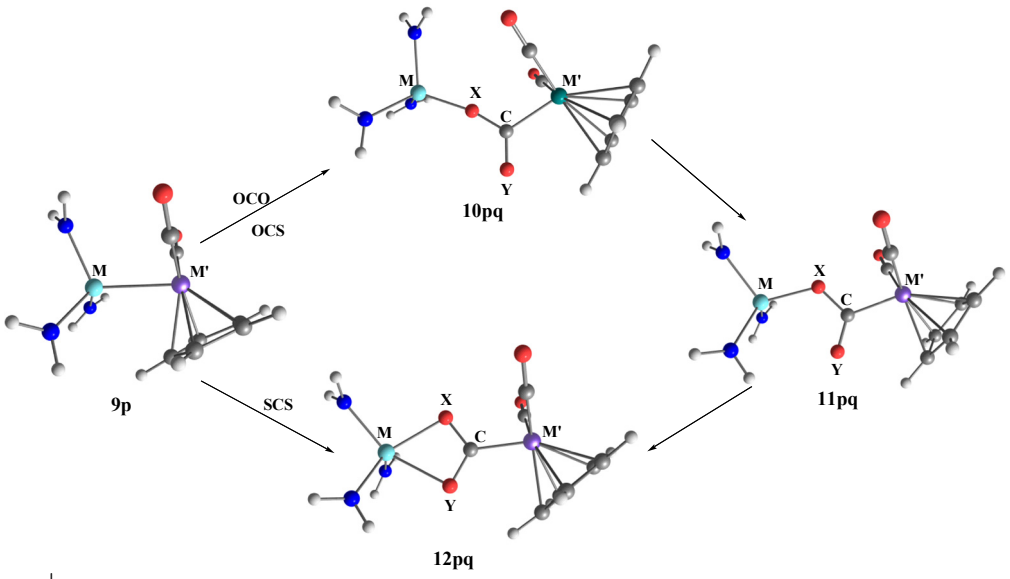

pq	aa	ab	ac	ba	bb	bc	ca	cb	cc	da	db	dc
M	Ti	Ti	Ti	Ti	Ti	Ti	Zr	Zr	Zr	Zr	Zr	Zr
M'	Fe	Fe	Fe	Ru	Ru	Ru	Fe	Fe	Fe	Ru	Ru	Ru
XCY	OCO	OCS	SCS	OCO	OCS	SCS	OCO	OCS	SCS	OCO	OCS	SCS

Figure 5.1: Mechanistic scheme for the insertion of heteroallenes (**XCY**) into ELHB complexes, **9p**. **10pq** and **12pq** are the complexes resulting from XCY insertions and **11pq** is the transition state for the interconversions. Here, **p** stands for **a-d** indicating the M-M′ complexes and **q** for **a-c** indicating the heteroallenes, XCY.

[5.3.1] Bimetallic Complexes (9p) and Heteroallenes (XCY)

An analysis of the structure and bonding of ELHB complexes, **9p (**M= Ti, Zr and M′= Fe, Ru) helps to understand the structure, bonding and its reactions with heteroallenes, XCY. The geometrical parameters and charges on each metal of the bimetallic complexes are given in the table 5.1. The experimental bond lengths are in agreement with the theoretically calculated bond lengths.

The polar nature of the M-M′ bond of the ELHB complexes can be understood from the Mülliken charge analysis, which shows positive charge on early transition metal (M) and negative charge on late transition metal (M′). The positive charge on early transition metal, M is more when it is connected to the first row late

transition metal (M′=Fe) in comparison to second row (M′=Ru). On the other hand, the negative charge on the late transition metal, M′ is more when it is connected to the second row early transition metal (M=Zr) in comparison to the first row (M=Ti). The charge difference between M and M′ shows that the polarity decreases in the order **9c**>**9a** >**9d**> **9b**. The polarity of the M-M′ bond based on the electronegativity difference is in the order **9d** > **9b** >**9c** >**9a** (table 5.1).

Table 5.1: Metal-metal bond lengths of the model complexes in Å (experimental values are given in parentheses) and Mülliken charges on each metal of the ELHB complexes (**9p**) at B3LYP/LANL2DZ level of theory. The charge and electronegativity differences are also shown.

Structure No.	Bond length M-M´	Mülliken charge on		Charge diff. between M and M´	Electronegativity diff. between M and M´
		M	M´		
9a	2.482 (2.460)[a]	1.064	-0.511	1.575	0.29
9b	2.590 (2.561)[b]	1.025	-0.046	1.071	0.66
9c	2.648 (2.605)[c]	1.484	-0.707	2.191	0.50
9d	2.756 (2.828)[d]	1.381	-0.173	1.554	0.87

Experimental data of [a]$MeSi\{SiMe_2N(C_6H_4Me)\}_3Ti$-$FeCp(CO)_2$,[2c] [b]$(Me_2N)_3Ti$-$RuCp(CO)_2$,[6l] [c]$MeSi\{SiMe_2N(C_6H_4Me)\}_3Zr$-$FeCp(CO)_2$[2b] and [d]$(CH_2)(CH_2NSiMe_3)_2(Cp)Zr$-$RuCp(CO)_2$ [2i]

The HOMO and the HOMO-1 are mainly concentrated on M′ and slightly antibonding between M and M′. The LUMO of the ELHB complexes, **9p** is mainly concentrated on M and it is antibonding between the metals (figure 5.2a). The LUMO of the ELHB complexes is likely to interact with the nucleophilic part of the substrate and HOMO and HOMO-1 with electrophilic part. In other words, the late

transition metal M' has nucleophilic and early transition metal M has electrophilic character.

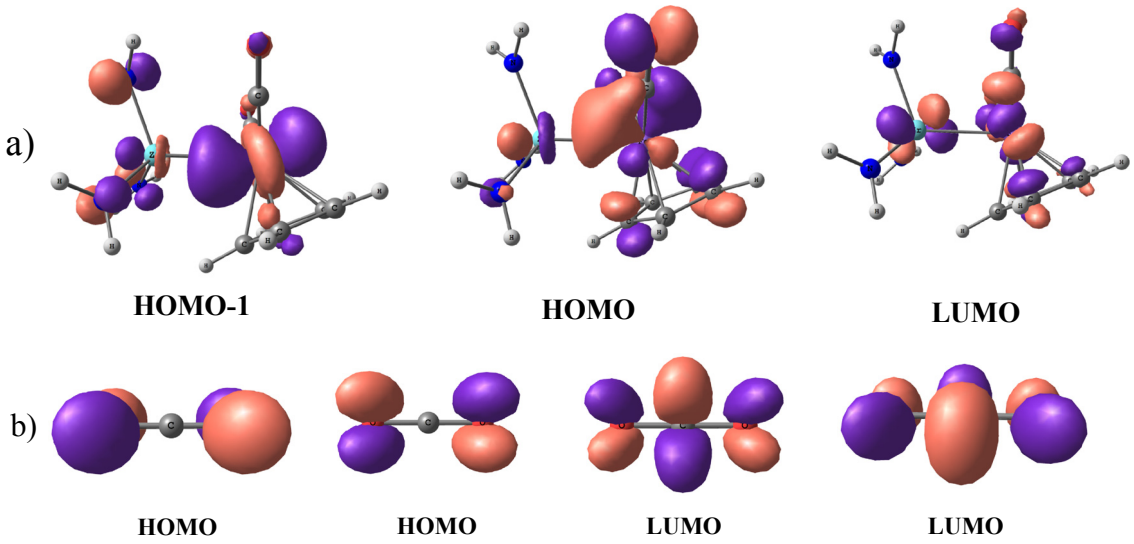

Figure 5.2: Important molecular orbitals of a) **9p** and b) XCY. The molecular orbitals are almost the same for similar type of structures, except in the relative ordering of energy.

The geometrical parameters and Mülliken charge on each element of the heteroallenes are shown in the table 5.2. Here, the carbon atom is sp hybridized. Mülliken charge analysis shows that the electron density on X (or Y) reduces on going from CO_2 to CS_2. The degenerate HOMO corresponds to the lone pairs on X and Y (figure 5.2b). The LUMO has antibonding character between all the elements and is mainly located on carbon. Hence, the nucleophilic centers in XCY are X and Y, and electrophilic centre is carbon atom.

Table 5.2: Geometrical parameters and Mülliken charges on each element of XCY at B3LYP/LANL2DZ level of theory.

XCY	Bond length (Å)		Mülliken charges on		
	C-X	C-Y	X	C	Y
O=C=O	1.193	1.193	-0.178	0.356	-0.178
O=C=S	1.189	1.611	-0.089	-0.031	0.118
S=C=S	1.601	1.601	0.157	-0.314	0.157

[5.3.2] Bimetallic Complexes (10pq)

The possible coordination modes of the interaction of heteroallenes with transition metal fragments are shown in the scheme 5.1.[5] The end-on coordination mode (scheme 5.1, **1**) results from the nucelophilic attack of X in XCY to the early transition metal. On the other hand, the electrophilic attack of carbon in XCY to the late transition metal leads to the second type of coordination mode (scheme 5.1, **2**). The synergic effect of the both early and late transition metals results in the insertion of X-C bond of XCY into the M-M′ bond in **9p** and gives bimetallic complexes, **10pq**. Insertion of XCY to M-M′ bond results in the cleavage of M-M′ bond and the formation of M′-C and M-X bonds. Here, the C-X bond undergoes insertion in which carbon is attached to late transition metal and X to the early transition metal. The insertion of C-O bond of CO_2 and COS into M-M′ bond in **9p** results in the complexes, **10pa** and **10pb**, while the insertion of C-S bond of CS_2 converts **10pc** into **12pc**.

The geometrical parameters and Mülliken charges on each metal of the bimetallic complexes, **10pq** are given in the table 5.3. The hybridization on carbon has changed to nearly sp^2 in **10pq**. This results in the elongation of both C-X and C-Y bonds in **10pq**. All the C-X bond lengths are close to single bond lengths and the C-Y bond lengths are close to localized double bond lengths (table 5.3). As expected the electron density on CO_2 and COS is mostly concentrated on oxygen (table 5.2). This results in the nucleophilic attack of oxygen in **XCY** to the electron poor early transition metal (M) of the ELHB complexes. Even though there is lone pair on sulphur in COS, the positive charge on the sulphur prevents its coordination to M. As a result the bimetallic complexes of type **10pq** in which sulphur is

coordinated to early transition metal are not stationary points on the potential energy surface. On the other hand higher diffused orbital on two sulphur atoms in CS_2 preclude the formation of **10pc**, but it directly gives **12pc**. Since the M-X and M'-C bonds are more polar than the M-M′ bond, the positive charge on M increases and the negative charge on M′ decreases in the complexes, **10pq** as compared to **9p** (tables 5.1 and 5.3).

Table 5.3: Geometrical parameters (bond lengths in Å and angles in degree) and Mülliken charges on each metal of bimetallic complexes (**10pq**) at B3LYP/LANL2DZ level of theory. ΔH (ΔG) (kcal/mol) is the reaction energy from the equation 5.1.

Structure No.	M-X	C-X	C-Y	M′-C	X-C-Y	Mülliken charge on		ΔH (ΔG)
						M	M′	**9p→10pq**
10aa	1.848	1.383	1.245	1.968	119.6	1.256	-0.442	-28.0 (-20.1)
10ba	1.840	1.369	1.243	2.084	121.0	1.275	0.110	-25.3 (-16.6)
10ca	2.015	1.377	1.245	1.975	119.9	1.505	-0.451	-26.0 (-18.1)
10da	2.014	1.365	1.244	2.089	121.3	1.520	0.108	-24.0 (-15.1)
10ab	1.872	1.348	1.721	1.971	119.3	1.262	-0.290	-20.2 (-11.0)
10bb	1.871	1.342	1.720	2.079	119.9	1.267	0.250	-18.1 (-8.7)
10cb	2.198	1.324	1.777	1.947	119.5	1.331	-0.248	-20.0 (-9.9)
10db	2.031	1.339	1.715	2.085	120.5	1.518	0.245	-16.5 (-6.8)
10pc	Converging to **12pc** on optimization.							

The interaction of XCY with the M-M' bond in **10pq** is shown in the interaction diagram (figure 5.3). The HOMO (1a') of XCY donates its electrons to

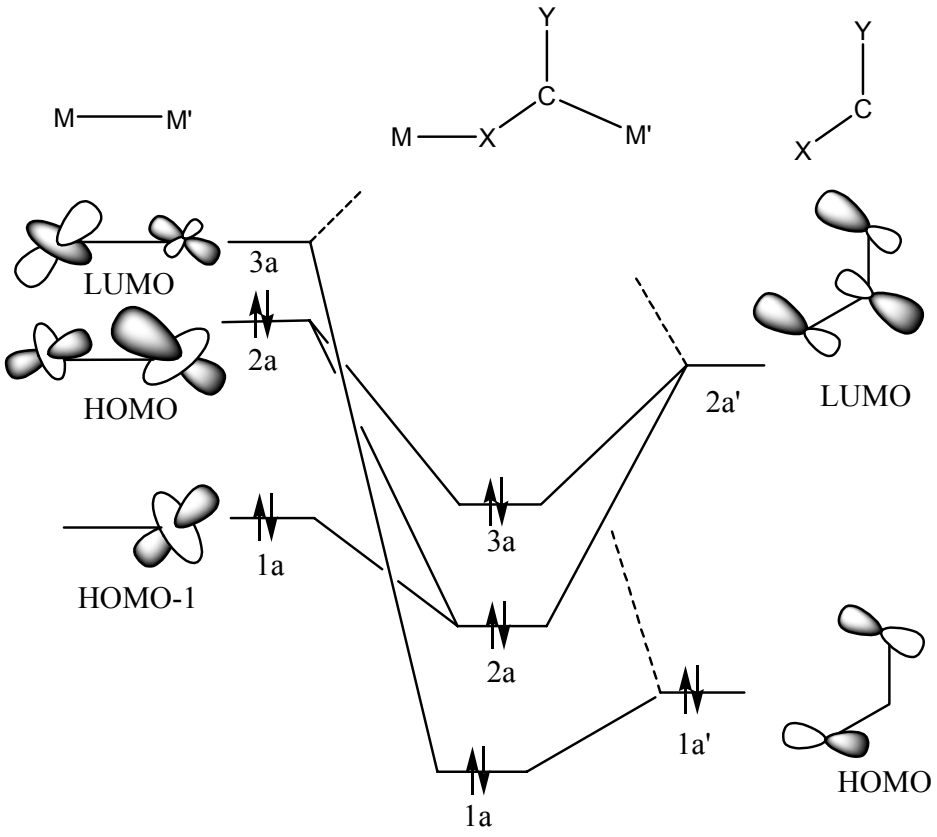

Figure 5.3: Interaction diagram between **XCY** and bimetallic complexes (**9p**) to form the complexes, **10pq**.

LUMO (3a) of the bimetallic complexes, **9p** which is antibonding between M-M′ and mainly localized on M. Since Zr is more electropositive than Ti, LUMO of the **9a** and **9b** is closer in energy to HOMO of the XCY. Hence, the donation is more effective when XCY forms complexes with Ti (**10aq** and **10bq**). This results in the cleavage of M-M′ bond and the formation of M-X bond. The second interaction is the back donation of electron from HOMO (2a) and HOMO-1 (1a) of the complexes, **9p** which is mainly concentrated on M′ to the LUMO (2a') of XCY. Since Ru is more electronegative than Fe, the HOMO and HOMO-1 of the complexes, **9b** and **9d** are more stabilized than **9a** and **9c**. This results in the effective interaction of HOMO and HOMO-1 of the complexes, **9a** and **9c** with LUMO of the XCY, which are closer in energy. This interaction elongates C-X and

C-Y bonds. The bending of XCY enhances the bonding interaction and stabilizes the LUMO. Hence, the occupation of electrons in the LUMO (figure 5.2b and 5.3) favors the bending of XCY. Since first row late transition metal is more electron rich than second row transition metal, former donates more effectively to LUMO of the XCY. As a result the bending of XCY is more when it is connected to first row late transition metal (table 5.3). The important molecular orbitals are shown in the figure 5.4.

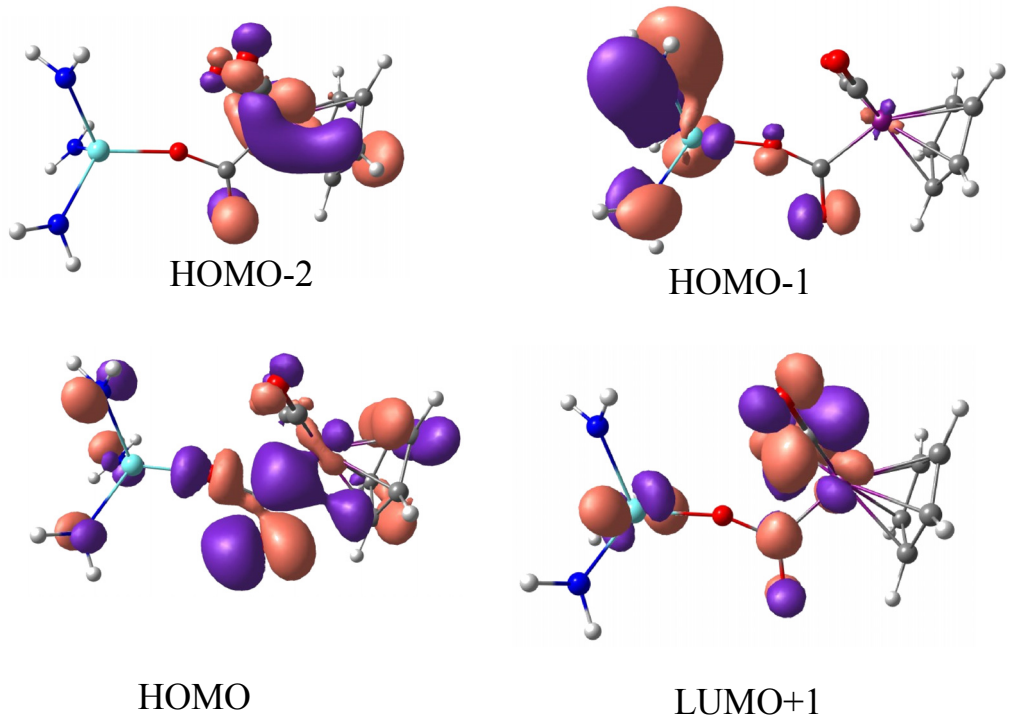

Figure 5.4: Important molecular orbitals of the complexes, **10pq**. The molecular orbitals are almost the same, except in the relative ordering of energy.

Hence, the acceptance of the electrons from the HOMO and the donation to LUMO of the XCY is more pronounced when the early and late transitions metals are from the first row. This is reflected in the stability order of the complexes, **10pq** which can be analyzed by the following equation.

$$9p + XCY \longrightarrow 10pq \qquad (5.1)$$

The ΔH and ΔG obtained from the equation (5.1) shows that the stability of the complex for CO_2 insertion is in the order **10aa** > **10ca** > **10ba** > **10da** (table 5.3). The same order is retained for the COS inserted complexes, but the magnitude of the stabilization energy is less than that for the complexes resulting from CO_2 insertion. This may be due to the greater electron density on oxygen in CO_2 than that in COS. It is interesting to note that the stability order is not in accordance with the polarity order either based on Mülliken charges or electronegativity differences.

[5.3.3] Bimetallic Complexes (12pq)

The first inserted complexes, (**10pa** and **10pb**) of CO_2 and COS can isomerize to a four membered metallacycles, **12pq** by coordinating the free end of XCY to the early transition metal, M. The insertion of CS_2 directly leads to the complexes, **12pc** without forming the initial intermediates, **10pc**. **12aa** and **12ba** are not stable in the PES and converged into **10aa** and **10ba** respectively on geometry optimization. Since Ti has less diffused orbital than Zr, OCO has to bend more for getting effective overlap to form the complexes, **12aa** and **12ba**. It leads to increase strain which prevents the formation of **12aa** and **12ba**. On the other hand, the higher diffused orbital on Zr reduces the strain in the OCO angle and stabilizes the bimetallic complexes, **12ca** and **12da**. Our group has studied the similar size effect for the stability of metallacyclocumulene and metallacyclopropene.[14] The metallacyclopropene is reported to be more stable for Ti and metallacyclocumulene for Zr. The geometrical parameters and charges on each metal atom of the bimetallic complexes, **12pq** are given in the table 5.4.

The complexes, **12pq** have the shorter C-X bond and longer C-Y bond in comparison to those in **10pq** and these bond lengths are with in the range of distances observed in delocalized systems. The XCY bond angle (table 5.4) is lower for **12aq** and **12bq** in comparison to **12cq** and **12dq**. Since the titanium has less diffused orbital in comparison to zirconium, the XCY has to bend more to get effective overlap in **12aq** and **12bq**. Similar to the initial intermediates, **10pq** the first row late transition metal is more electron rich than the second row. This helps the first row late transition metal to donate more effectively to LUMO of the XCY than the latter. As a result the XCY angle is less when it is connected to first row late transition metal (tables 5.3 and 5.4). The bending of XCY increases the s-orbital contribution on carbon and leads to the reduction of M′-C bond length in comparison to that in **10pq**. It is interesting to note that both positive charge on M and negative charge on M′ decreases in **12pq** in comparison to **10pq**. It is in contrast to the increase in positive charge on M and decreases in negative charge on M′ of the complexes **10pq** in comparison to **9p**. Since the total energy and free energy differences between the complexes, **10pq** and **12pq** are very low, the feasibility for their interconversions is also more (table 5.5). Since all the complexes, **10pc** are converged to **12pc**, the energetic for the direct formation of the complexes, **12pc** from **9p** can be calculated by the equation (5.2) (table 5.4).

$$9p + SCS \longrightarrow 12pc \qquad (5.2)$$

The stability order is **12cc** > **12dc** > **12ac** > **12bc**. The reduced strain in the XCY bond angle due to larger size of Zr stabilizes the complexes, **12cc** and **12dc** more than the titanium complexes, **12ac** and **12bc**. Stability of **12pc** is more when

Table 5.4: Geometrical parameters (bond lengths in Å, angle in degree and experimental values in parenthesis) and Mülliken charges on each metal of bimetallic complexes (**12pq**) at B3LYP/LANL2DZ level of theory. ΔH (ΔG) are from the equation (5.2).

Structure No.	M-X	M-Y	X-C	C-Y	M′-C	X-C-Y	Mülliken charge on		ΔH (ΔG) **9p→12pc** kcal/mol
							M	M′	
12aa **12ba**	Converging to **10aa** and **10ba** on optimization								
12ca	2.226 (2.148)[a]	2.404 (2.152)	1.341 (1.308)	1.305 (1.303)	1.938 (1.895)	113.6 (111.9)	1.359	0.355	
12da	2.233 (2.222)[b]	2.408 (2.255)	1.334 1.294	1.305 (1.275)	2.048 (2.087)	114.4 (116.3)	1.377	0.285	
12ab	2.144	2.671	1.296	1.812	1.941	112.7	1.015	-0.270	
12bb	2.156	2.665	1.296	1.804	2.053	113.5	1.026	0.305	
12cb	2.311	2.792	1.297	1.821	1.942	113.8	1.255	-0.260	
12db	2.316	2.794	1.297	1.812	2.054	114.5	1.272	0.310	
12ac	2.819	2.583	1.744	1.783	1.944	117.0	0.877	-0.202	-10.6 (0.4)
12bc	2.580	2.827	1.781	1.741	2.057	117.6	0.886	0.408	-7.3 (3.0)
12cc	2.764 (2.632)[c]	2.901 (2.643)	1.783 (1.745)	1.753 (1.745)	1.942 (1.935)	118.2 (116.1)	1.138	-0.189	-14.9 (-4.6)
12dc	2.913	2.767	1.750	1.780	2.055	118.6	1.145	0.415	-12.0 (-2.7)

Experimental data of [a]$HC\{SiMe_2N(2,3,4\text{-}F_3C_6H_2)\}_3Zr(\mu\text{-}O_2C)FeCp(CO)(C_3Ph_2)$,[2h] [b]$MeSi(SiMe_2NTol)_3Zr\{OSMe_2\}(\mu\text{-}O_2C)RuCp(CO)\{S(Me_2)\}$[2g] and [c]$HC(SiMe_2NC_6H_4\text{-}F\text{-}2)_3Zr(\mu\text{-}S_2C)Fe(Cp_2)(CO)_2$[2f]

the late transition metal is from the first row. This is the result of the increased population of LUMO of the XCY (figure 5.2b) which favours the bending when the late transition metal is from the first row. Some of the important molecular orbitals of the complexes, **12pq** are shown in figure 5.5. HOMO-3 and HOMO-6 contribute to M′-C bond and HOMO-5 corresponds to M-X and M-Y bonds. These are formed by intramolecular interaction of filled HOMO of **10pq** which is largely localized on Y with LUMO+1 which is mainly localized on M (figure 5.4). As a result the M-Y bond forms and C-Y bond elongates in comparison to those in **10pq**. The resulting bimetallic complexes, **12pq** have shorter XCY bond angle. The bending of XCY increases the bonding interaction between these three atoms. Hence, the C-X bond lengths are shorter in the complexes, **12pq** than those in **10pq**.

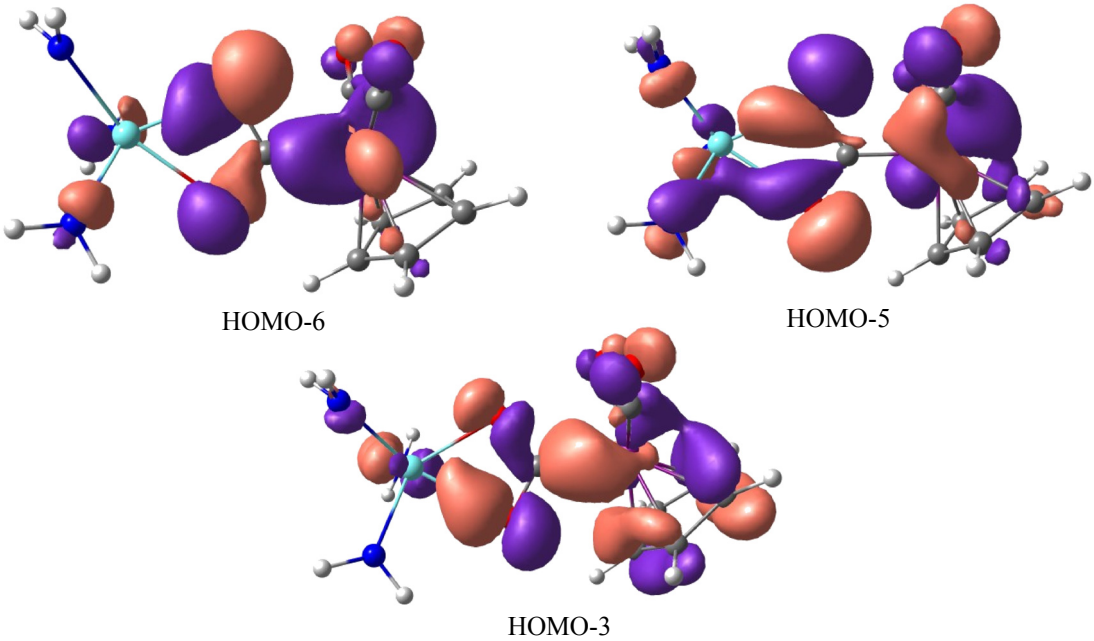

Figure 5.5: Important molecular orbitals of the complexes, **12pq**. The molecular orbitals are almost the same for all the structures, except in the relative ordering of energy.

[5.3.4] Transition States (11pq)

The complexes, **10pq** and **12pq** are stable only for M=Zr; M′=Fe, Ru and XCY=CO_2 and M=Ti, Zr; M′=Fe, Ru and XCY=COS. The geometrical parameters of the transition states, energy barrier and the isomerization energy between the complexes, **10pq** and **12pq** are shown in the table 5.5. All the M-Y bond distances are longer than that in **12pq** and are within Van der Waals distances. The X-C, C-Y, M′-C bond distances, X-C-Y bond angles and Mülliken charges are in between the complexes, **10pq** and **12pq**. The energy difference and energy barrier for isomerization is very low except for the titanium complexes, **11ab** and **11bb**. It indicates that the zirconium complexes (**10cq** and **10dq**) undergo easy isomerization reaction compared to the titanium complexes (**10aq** and **10bq**).

The potential energy diagram (by plotting ΔG) for the insertion reaction of the heteroallenes into the M-M′ bond of ELHB complexes, **9p** is shown in the figure 5.6. It is important to note that the titanium complexes resulting from the CO_2 insertion, **10aa** and **10ba** are the stable initial intermediates and do not isomerize to **12aa** and **12ba** (not shown in the diagram). The zirconium complexes resulting from the CO_2 insertion (**10ca** and **10da**) have lower barrier for isomerization to **12ca** and **12da**. The initial intermediates resulting from the COS insertion (**10pb**) is less stable than those resulting from the CO_2 insertion. Out of these COS inserted complexes, the titanium complexes, **10ab** and **10bb** have relatively high energy barrier for the interconversion to **12ab** and **12bb** and its isomerization is endothermic. On the other hand, the zirconium complexes, **10cb** and **10db** have low energy barrier for interconversion and relative energy differences for their interconversion are also very low.

Table 5.5: Important geometrical parameters and Mülliken charges on each metal of the complexes, **11pq** and the isomerization energy ΔH (ΔG) for **10pq→12pq** and their energy barriers ΔH_a (ΔG_a) at B3LYP/LANL2DZ level of theory.

Structure No.	Bond lengths (Å)						Mülliken charges		ΔH (ΔG) **10pq→12pq** kcal/mol	ΔH_a (ΔG_a) **10pq→11pq** kcal/mol
	M-X	M-Y	X-C	C-Y	M′-C	X-C-Y	M	M′		
11ca	2.008	3.150	1.376	1.261	1.958	117.9	1.432	-0.410	-1.3 (0.4)	0.6 (2.4)
11da	2.090	3.114	1.366	1.263	2.067	118.6	1.429	0.197	-0.8 (-0.13)	1.0 (2.3)
11ab	1.901	3.280	1.348	1.754	1.956	116.3	2.107	-0.280	4.7 (5.4)	11.1 (12.4)
11bb	1.908	3.267	1.340	1.753	2.064	117.6	1.097	0.275	4.5 (5.2)	10.8 (11.4)
11cb	2.231	3.174	1.338	1.753	1.964	118.0	1.341	-0.336	0.08 (-0.26)	3.4 (3.8)
11db	2.125	3.168	1.337	1.755	2.069	118.9	1.336	0.287	-0.92 (1.3)	4.1 (4.3)

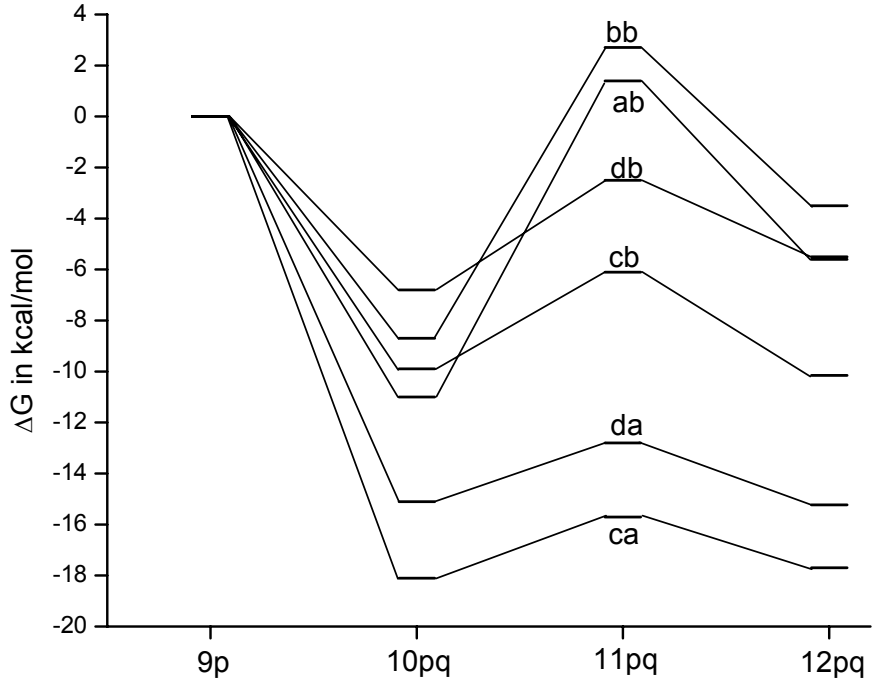

Figure 5.6: Potential energy diagram for the insertion of heteroallenes to metal-metal polar bond of ELHB complexes, **9p**.

The complexes resulting from the CS_2 insertion, **10pc** are not a stationary point on the potential energy surface and converge into **12pc** on geometry optimization (not shown in the diagram). More strain in TiOCO ring due to smaller size of titanium and oxygen prevent the formation of **12aa** and **12ba**. Conversely smaller size of titanium averts the formation of **10ac** and **10bc**. The optimal size of COS leads to the formation of both bimetallic complexes **10pb** and **12pb**. The larger size of Zr and hence less strain in the OCS bond angle stabilize **12cb** and **12db** more than the corresponding titanium complexes. The energy barrier for the isomerization of COS complexes are high compared to CO_2 complexes. This may be due to the greater electron density on oxygen than sulphur for the second coordination.

[5.4] Conclusions

The mechanism for the insertion of heteroallenes, XCY (CO_2, COS, and CS_2) into metal-metal polar bond (M- M′) of ELHB complexes $(NH_2)_3M\text{-}M'(CO)_2Cp$; (where M= Ti, Zr and M′= Fe, Ru) are studied. The insertion of CO_2 and COS into the complexes, **9p** forms the intermediates, **10pq** which undergo isomerization to the final products, **12pq** through transition states, **11pq**. The size of the early transition metal and electron donating capacity of late transition metal have major role in the stabilization of the complexes, **10pq** and **12pq**. The titanium prefers to form more stable complexes, **10pq**, while zirconium prefers to **12pq**. It reflects in the high stability of the complexes, **10aa** and **10ba** which do not undergo isomerization to **12aa** and **12ba**. On the other hand, the complexes, **10pc** is not stable and converted into the complexes, **12pc** on optimization. The first row late transition metal stabilizes the LUMO of XCY which favors the bending more effectively than the second row. This reflects in the more stability of the complexes, **10pq** which have the late transition metal from the first row. The smaller atomic size of Ti and hence more strain in the OCS angle destabilize the complexes, **12ab** and **12bb** more than **10ab** and **10bb**.

[5.5] References

(1) (a) Roberts, D. A., Geoffroy, G. L., In *Comprehensive Organometallic Chemistr*y, Wilkinson, G., Stone, F. G. A., Abel E. W., Eds., (Pergamon: Oxford) Vol. 6, Chapter 40, 1995. (b) Wheatley, N.; Kalck, P. *Chem. Rev.* **1999**, *99*, 3379. (c) Stephan, D. W. *Coord. Chem. Rev.* **1989**, *95*, 41. (d) Ferguson, G. S.; Wolczanski, P. T. *Organometallics* **1985**, *4*, 1601. (e) Bullock, R. M.; Casey, C. P. *Acc. Chem. Res.* **1987**, *20*, 167. (f) Baker, R. T.; Fultz, W. C.; Marder, T. B.; Williams, I. D. *Organometallics* **1990**, *9*, 2357. (g) Graham, T. W.; Llamazares, A.; McDonald, R.; Cowie, M. *Organometallics* **1999**, *18*, 3490; 3502.

(2) (a) Gade, L. H.; Memmler, H.; Kauper, U.;, Schneider, A.; Fabre, S.; Bezougli, I.; Lutz, M.; Galka, C.; Scowen, I. J.; McPartlin, M. *Chem. Eur. J.* **2000**, *6*, 692. (b) Findeis, B.; Schubart, M.; Platzek, C.; Gade, L. H.; Scowen, I. J.; McPartlin, M. *Chem. Commun.* **1996**, 219. (c) Gade, L. H.; Schubart, M.; Findeis, B.; Fabre, S.; Bezougli, I.; Lutz, M.; Scowen, I. J.; McPartlin, M. *Inorg. Chem.* **1999**, *38*, 5282. (d) Pinkes, J. R.; Steffey, B. D.; Vites, J. C.; Cutler, A. R. *Organometallics* **1994**, *113,* 21. (e) Butler, I. S.; Fenster, A. E. *J. Organomet. Chem.* **1974***, 66,* 161. (f) Memmler, H.; Kauper, U.; Gade, L. H.; Scowen, I. J.; McPartlin, M. *Chem. Commun.* **1996**, 1751. (g) Fabre, S.; Findeis, B.; Trösch, D. J. M.; Gade, L. H.; Scowen, I. J.; McPartlin, M. *Chem. Commun.* **1999**, 577. (h) Lutz, M.; Haukka, M.; Pakkanen, T. A.; Gade, L. H. *Organometallics* **2001**, *20*, 2631. (i) Gade, L. H.; Friedrich, S.; Trösch, D. J. M.; Scowen, I. J.; McPartlin, M. *Inorg. Chem*. **1999**, *38*, 5295.

(3) (a) Johansson, R.; Jarenmark, M.; Wendt. O. F. *Organometallics* **2005**, *24,* 4500. (b) Pandey, K. K. *Coord. Chem. Rev.* **1995**, *140*, 37. (c) Darensbourg, D. J.; Hankel, K. R.; Bauch, C. G.; Pala, M.; Simmons, D.; White, J. N. *J. Am. Chem. Soc.* **1985**, *107*, 7463. (d) Darensbourg, D. J.; Groetsch, G.; Wiegreffe, P.; Rheingold, A. L. *Inorg. Chem.* **1987**, *26*, 3827. (e) Mankad, N. P.; Gray, T. G.; Laitar, D. S.; Sadighi, J. P. *Organometallics* **2004**, *23*, 1191. (f) Yin, X.; Moss, J. R. *Coord. Chem. Rev.* **1999**, *181*, 27.

(4) (a) Fischer, R. A.; Behm, J.; Priermeier, T.; Sherer, W. *Angew. Chem., Int. Ed. Engl.* **1993***, 32*, 746. (b) Fischer, R. A. In *Material Research Society Symposium Proceedings*, Abernathy, C. R.; Bates, J. C. W.; Bohling, D. A.; Hobson, W. S.; Eds., (Materials Research Society: Pittsburgh), pp 267, 1993. (c) Fischer, R. A.; Scherer, W.; Kleine, M.; Lehmann, O.; Stuke, M. *Chem. Mater.* **1995**, *7*, 1863. (d) Valade, L.; Choukroun, R.; Danjoy, C.; Chansou, B.; De-Caro, D.; Cassoux, P. *Ann. Chim. Sci. Mater.* **1998**, *23,* 721. (e) Albertin, G.; Antoniutti, S.; Roveda, G. *Inorg. Chim. Acta.* **2005***, 358, 3093.*

(5) (a) Bursten, B. E.; Strittmatter, R. J. *Angew. Chem., Int. Ed. Engl.* **1991**, *30*, 1069. (b) Bursten, B. E.; Novo-Gradac, K. J. *J. Am. Chem. Soc.* **1987***, 109,* 904. (c) Ferguson, G. S.; Wolczanski, P. T.; Parkanyi, L.; Zonnevylle, M. C. *Organometallics* **1988***, 7,* 1967. (d) Selent, D.; Ramm, M.; Janiak, C. *J. Organomet. Chem.* **1995***, 501,* 235. (e) Jansen, G.; Schubart, M.; Findeis, B.; Gade, L. H.; Scowen, I. J.; McPartlin, M. *J. Am. Chem. Soc.* **1998***, 120,* 7239.

(6) (a) Gade, L. H. *Angew. Chem., Int. Ed. Engl.* **2000**, *39*, 2658. (b) Sartain, W. S.; Selegue, J. P. *Organometallics* **1987***, 6*, 1812. (c) Sartain, W. S.; Selegue, J. P. *Organometallics* **1989**, *8,* 2153. (d) Casey, C. P.; Jordan, R. F. Rheingold,

A. L. *J. Am. Chem. Soc.* **1983***, 105,* 665. (e) Casey, C. P.; Jordan, R. F. Rheingold, A. L. *Organometallics* **1984**, *3,* 504. (f) Casey, C. P.; Palermo, R. E.; Jordan, R. F.; Rheingold, A. L. *J. Am. Chem. Soc.* **1985***, 107,* 4597. (g) Selent, D.; Beckhaus, R.; Pickardt, J. *Organometallics* **1993**, *12,* 2857. (h) Friedrich, S.; Memmler, H.; Gade, L. H.; Li, W. –S.; McPartlin, M. *Angew. Chem., Int. Ed. Engl.* **1994**, *33*, 676. (i) Friedrich, S.; Memmler, H.; Gade, L. H.; Li, W. –S.; Scowen, I. J.; McPartlin, M.; Housecroft, C. E. *Inorg. Chem.* **1996**, *35*, 2433. (j) Friedrich, S.; Gade, L. H.; Scowen, I. J.; McPartlin, M. *Organometallics* **1995**, *14,* 5344. (k) Galakhov, M.; Martin, A.; Mena, M.; Yelamos, C. *J. Organomet. Chem.* **1995**, *496*, 217. (l) Sartain, W. S.; Selegue, J. P. *J. Am. Chem. Soc.* **1985***, 107,* 5818.

(7) (a) Mealli, C.; Hoffmann, R.; Stockis, A. *Inorg. Chem.* **1984**, *23*, 56. (b) Sakaki, S.; Kitaura, K.; Morokuma, K. *Inorg. Chem.* **1982**, *21*, 760. (c) Behr, A**.** *Angew. Chem., Int. Ed. Engl.* **1988**, *27*, 661.

(8) (a) Leitner, W. *Coord. Chem. Rev*. **1996**, *153,* 257. (b) Pandey, K. K. *Coord. Chem. Rev*. **1995**, *140,* 37. (c) Tanaka, K. *Adv. Inorg. Chem*. **1995**, *43,* 409. (c) Field, L. D.; Shaw, W. J.; Turner, P. *Organometallics* **2001**, *20,* 3491. (d) Field, L. D.; Lawrenz, E. T.; Shaw, W. J.; Turner, P. *Inorg. Chem*. **2000**, *39,* 5632. (e) Gandhi, T.; Nethaji, M.; Jagirdar, B. R. *Inorg. Chem.* **2003**, *42*, 4798. (f) Gandhi, T.; Nethaji, M.; Jagirdar, B. R. *Inorg. Chem.* **2003**, *42*, 667. (g) Whittlesey, M. K.; Perutz, R. N.; Moore, M. H. *Organometallics* **1996**, *15,* 5166. (h) Tai, C. -C.; Chang, T.; Roller, B.; Jessop, P. G. *Inorg. Chem.* **2003**, *42*, 7340. (i) Munshi, P.; Main, A. D.; Linehan, J.; Tai, C. -C.; Jessop, P. G. *J. Am. Chem. Soc.* **2002**, *124,* 7963. (j) Yin, X.; Moss, J. R. *Coord. Chem. Rev.*

1999, *181,* 27. (k) Kim, Y.; Deng, H.; Gallucci, J. C.; Wojcicki, A. *Inorg. Chem.* **1996**, *35,* 7166.

(9) (a) Hanna, T. A.; Baranger, A. M.; Bergman, R. G. *J. Am. Chem. Soc.* **1995**, *117*, 11363. (b) Baranger, A. M.; Bergman, R. G. *J. Am. Chem. Soc.* **1994**, *116*, 3822.

(10) (a) Becke, A. D. *J. Chem. Phys.* **1993**, *98*, 5648. (b) Becke, A. D. *Phys. Rev. A,* **1988**, *38*, 2398. (c) Lee, C.; Yang, W.; Parr, R. G. *Phys. Rev. B.* **1988**, *37*, 785.

(11) (a) Hay, P. J.; Wadt, W. R. *J. Chem. Phys.* **1985**, *82*, 270. (b) Wadt, W. R.; Hay, P. J. *J. Chem. Phys.* **1985**, *82*, 284. (c) Hay, P. J.; Wadt, W. R. *J. Chem. Phys.* **1985**, *82*, 299.

(12) Gaussian 03, Revision C.02, Frisch, M. J.; Trucks, G. W.; Schlegel, H. B.; Scuseria, G. E.; Robb, M. A.; Cheeseman, J. R.; Montgomery, Jr., J. A.; Vreven, T.; Kudin, K. N.; Burant, J. C.; Millam, J. M.; Iyengar, S. S.; Tomasi, J.; Barone, V.; Mennucci, B.; Cossi, M.; Scalmani, G.; Rega, N.; Petersson, G. A.; Nakatsuji, H.; Hada, M.; Ehara, M.; Toyota, K.; Fukuda, R.; Hasegawa, J.; Ishida, M.; Nakajima, T.; Honda, Y.; Kitao, O.; Nakai, H.; Klene, M.; Li, X.; Knox, J. E.; Hratchian, H. P.; Cross, J. B.; Bakken, V.; Adamo, C.; Jaramillo, J.; Gomperts, R.; Stratmann, R. E.; Yazyev, O.; Austin, A. J.; Cammi, R.; Pomelli, C.; Ochterski, J. W.; Ayala, P. Y.; Morokuma, K.; Voth, G. A.; Salvador, P.; Dannenberg, J. J.; Zakrzewski, V. G.; Dapprich, S.; Daniels, A. D.; Strain, M. C.; Farkas, O.; Malick, D. K.; Rabuck, A. D.; Raghavachari, K.; Foresman, J. B.; Ortiz, J. V.; Cui, Q.; Baboul, A. G.; Clifford, S.; Cioslowski, J.; Stefanov, B. B.; Liu, G.; Liashenko, A.; Piskorz, P.; Komaromi, I.; Martin, R. L.; Fox, D. J.; Keith, T.; Al-Laham, M. A.; Peng, C. Y.; Nanayakkara, A.;

Challacombe, M.; Gill, P. M. W.; Johnson, B.; Chen, W.; Wong, M. W.; Gonzalez, C.; Pople, J. A. Gaussian, Inc., Wallingford CT, 2004.

(13) (a) Gade, L. H. *Angew. Chem., Int. Ed. Engl.* **2000***, 39,* 2658. (b) Schubart, M.; Mitchell, G.; Kottke, T.; Gade, L. H.; Scowen*,* I. J.; McPartlin, M. *Chem. Commun.* **1999**, 233.

(14) (a) Jemmis, E. D.; Phukan, A. K.; Giju, K. T. *Organometallics* **2002**, *21*, 2254. (b) Jemmis, E. D.; Phukan, A. K.; Jiao, H.; Rosenthal, U. *Organometallics* **2003**, *22*, 4958. (c) Jemmis, E. D.; Parameswaran, P.; Phukan, A. K. *Molecular Physics* **2005**, *103*, 897.

List of Publications

1. "The Effect of Metal Complexation on Ring Opening of Bowl Shaped Hydrocarbons: A Theoretical Study" Jemmis, E. D.; **Parameswaran, P**.; Anoop, A. *Int. J. Quan. Chem.* **2003**, *95*, 810.
2. "Reduction of 1,4-dichlorobut-2-yne by Titanocene to a 1,2,3-butatriene: Formation of a 1-titanacyclopent-3-yne and a 2,5-dititanabicyclo[2.2.0]hex-1(4)-ene" Burlakov, V. V.; Arndt, P.; Baumann, W.; Spannenberg, A.; Rosenthal, U.; **Parameswaran, P**.; Jemmis, E. D. *Chem. Comm.* **2004**, 2074**.**
3. "Binuclear Organometallic Compounds Containing Planar Tetra-coordinated Carbon Atoms: Theoretical Study on Structure and Bonding" Jemmis, E. D.; **Parameswaran, P.**; Phukan, A. K. *Molecular Physics* **2005**, *103*, 897.
4. "Hypercarbons in Polyhedral Structures" Jemmis, E. D.; Jayasree, E. G.; **Parameswaran, P.** *Chem. Soc. Rev***. 2006**, *35***,** 157 (with a cover page).
5. "Structure and Bonding in Cyclic Isomers of $BAl_2H_n^m$ (n = 3 - 6, m = -2 - +1): Preference for Planar Tetra-coordination, Pyramidal Tri-coordination and Divalency" Jemmis, E. D.; **Parameswaran, P.** (Submitted to *Chem. Eur. J*)
6. "Theoretical Study on the Insertion of Heteroallenes (CO_2, COS and CS_2) into Metal-Metal Polar Bond of Early-Late Bimetallic Complexes" Jemmis, E. D.; **Parameswaran P.** (Manuscript under Preparation)
7. "The Unusual Pyramidalization on Boron and Aluminum Atoms in a Three Membered Ring: A Theoretical Study" Jemmis, E. D.; **Parameswaran P.** (Manuscript under Preparation)

8. "Comparative Study on Binuclear Complexes of Five Membered Metallacyclocumulenes and Metallacyclopentynes" Bach, M. A.; **Parameswaran, P.**; Rosenthal, U.; Jemmis, E. D. (Manuscript under Preparation)
9. "Heterolytic Activation of the H-X (X = H, C, B and Si) Bonds Using a Highly Electrophilic Ruthenium Complex $[Ru(dppe)_2(P(OH)_3)]^{2+}$: An Experimental and Theoretical Investigation" Nagaraja, C. M.; **Parameswaran, P**.; Jemmis, E. D.; Jagirdar, B. R. (Manuscript under Preparation)